USING SHALLOW GEOPHYSICAL METHODS TO LOCATE A BURIED STREAM CHANNEL AT A STREAM RESTORATION SITE IN THE BURD RUN WATERHED, SHIPPENSBURG, PA

By Neal P. Kerrigan

A Thesis Submitted to the Department of Geography and Earth Science and the Graduate Council in partial fulfillment of the requirements for the degree of Masters of Science of Geoenvironmental Studies

SHIPPENSBURG UNIVERSITY

Shippensburg, PA

December, 2013

SHIPPENSBURG UNIVERSITY

Shippensburg, Pennsylvania

This thesis submitted by Neal P. Kerrigan has been approved as meeting the research requirements for the Masters of Science in Geoenvironmental Studies degree.

_____	_____
Date	Dr. Joseph T. Zume Chairperson of Thesis Committee Associate Professor of Geography and Earth Science
_____	_____
Date	Dr. Thomas P. Feeney Professor of Geography and Earth Science
_____	_____
Date	Dr. Sean R. Cornell Associate Professor of Geography and Earth Science

TABLE OF CONTENTS

List of Figures

List of Figures in the Appendix

List of Tables

Acknowledgements

The research for this thesis would not be possible without the help of various institutions, organizations, and people who dedicated their time and efforts to this study. First and foremost, I would like to thank Shippensburg University and the Department of Geography and Earth Science. Included in the Geography and Earth Science Department faculty are my Advisor Dr. Joseph Zume, and the members of my thesis committee, Dr. Thomas Feeney and Dr. Sean Cornell. From this same department, I'd also like to thank Dr. Paul Marr for his guidance in using of the EMP400. Shippensburg University's Graduate Research Grant Program provided me the opportunity to attend the Geological Society of America Northeast Section Conference in Hartford, CT where my initial research was presented. Dana Heston was a tireless field assistant and Dana Kerrigan helped proofread drafts of my thesis. Finally, I hope that this work benefits the scientific community and that there is continued success in geophysical research at Shippensburg University due to the efforts of its students, faculty, and the National Science Foundation Grant that supplied this geophysical equipment.

Abstract

This study used a multi-method geophysical approach, including electrical resistivity, electromagnetic induction, and ground penetrating radar, to image a known buried stream channel in the Burn Run watershed near Shippensburg University campus in Pennsylvania. The buried stream channel was filled-in during a stream restoration project in 2001. Prior to the in-filling, the stream channel was mapped and characterized. Silt loams mixed with a variety of organics, minor cobble materials from the restored stream channel, and topsoil were used to fill the channel and build it up to grade for the development of a recreational field.

This study was performed along five transects oriented perpendicular to the long-axis of the buried stream channel. Before embarking on the geophysical investigation, the study site was mapped with a total station to establish surface topography to aid geophysical interpretation. Soil auger samples were also taken for the verification of geophysical anomalies. The analyses and interpretation of data acquired in the geophysical investigation yielded anomalies that are consistent with the known dimensions of the buried stream channel. Interpretation of the data revealed layers of fill and alluvial deposits above underlying residual clay. When GPR and ER profiles were overlayed, the locations of anomalies were verified.

Chapter I

INTRODUCTION

1.1 Background

Excavation of a plot of land is the most definitive way to determine what is beneath the surface. However, once a site is excavated, the terrain can rarely be effectively reassembled to its original condition. Excavation is simply environmentally unfriendly. An alternative to excavation is found in geophysical methods. Geophysical methods can remotely locate both natural and anthropogenic features that are buried underground without unearthing the site. This study aims to use geophysics to investigate an area of Burd Run where an old channel segment was buried after relocation to the present course. The former channel was filled during a stream restoration project in 2001.

Anthropogenic alteration of land surfaces can change rates of subsurface weathering, especially if such alterations expose the bedrock to more weathering. A stream restoration project, for example, relocates the path of flowing water into a new channel, which can potentially expose the underlying bedrock to more water. Meanwhile, the old channel is partially preserved due to the infilling, and can still transmit infiltrating greater quantities water through its fill material than adjoining areas. Thus, it is important that areas of such intense human activity are evaluated periodically to determine impacts on underlying subsurface geology, especially in karst terrains, where infiltrating water can have the greatest impact on the bedrock. This study used near-surface geophysics to map a buried stream channel at a stream restoration site within the Burd Run floodplain near the Shippensburg University campus in south central, PA.

Burd Run flows along the eastern side of the campus. Prior to 1937, its original course was diverted and the surrounding forestland cleared (Woltemade and Wood 2002). In the fall of 2001, Dr. Christopher Woltemade, of the Geography and Earth Science Department at Shippensburg University, led a research project which restored the stream back to its former path near the intersection of Britton and Fogelsanger Road (Woltemade and Wood 2002). The previously diverted stream channel was filled with material from the new channel and the adjacent land was turned into a recreational athletic field. The restoration project, which also included the creation of a riparian buffer along the new stream course, was conducted in an effort to address the prevailing issues of stream bank erosion, nitrate pollution from surrounding farmlands, and elevated stream water temperatures. The subject of this research compared the abilities of three geophysical methods to detect the filled-in channel.

1.2 Scope of the Study

The scope of this study was to use geophysical imaging technology to detect a buried segment of the old Burd Run channel that was filled during the 2001 restoration project. Three geophysical methods including electrical resistivity, electromagnetic induction, and ground penetrating radar were used. To aid this investigation, a detailed topographic survey was performed (with a total station) in order to locate the geophysical readings. Soil cores were also taken to aid geophysical interpretation of the buried channel.

1.3 Research Questions

In this research, two major questions were pursued:

- Is the buried stream channel detectable using shallow electrical geophysical techniques?
- How does the use of multiple geophysical methods help in resolving the buried channel?

Chapter II

THE STUDY AREA

This chapter describes the study location, its geology, hydrology, climate, and soils. The site is within the Burd Run Watershed, near the Shippensburg University campus. It is bounded by latitudes 44º 03' 30" and 44º 04' 00" N and longitudes 77º 30' 45" and 77º 31' 15" W (USGS 2013). More specific information is presented in the sections below.

2.1 A Brief Description of the Study Site

The study site is located southwest of the corner of Fogelsanger and Britton Roads as shown in Figure 2.1. As shown in 2.1a, the northernmost part of the area is covered by wetlands fed by Hornbaker Spring. As depicted in 2.1b an athletic field now partially overlies a part of the previously diverted stream course which is now buried. The area adjacent to the restored stream is set as a riparian buffer with willow trees and other native vegetation. The entire area including the riparian buffer, wetlands and athletic fields is located within the Burd Run floodplain.

a.)

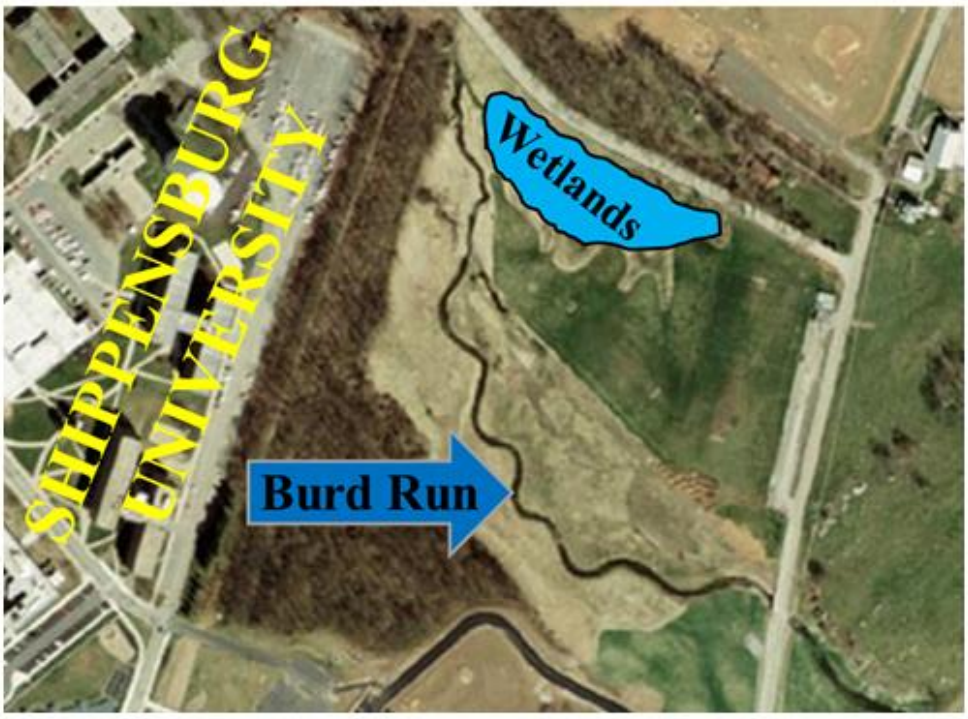

b.)

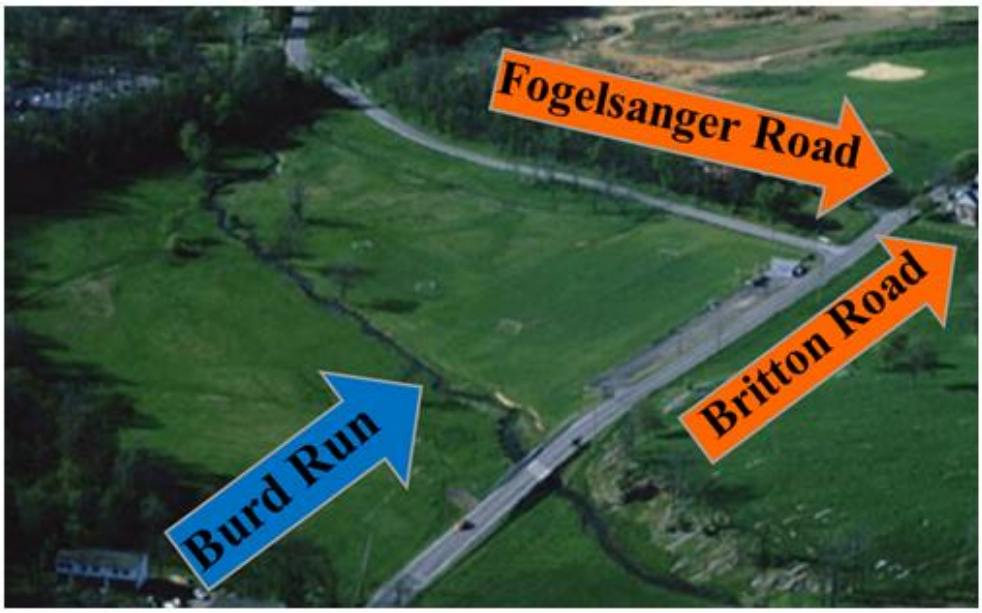

Figure 2.1: Shippensburg Park (a.) following and (b) before the restoration of Burd Run (photos from Woltemade 2007). North is to the top of the photographs.

2.1.1 Climate

The climate of the area is characterized by an average annual precipitation of 1015 mm. Monthly precipitation is nearly evenly distributed, with May and June having the greatest amounts (Figure 2.2). The mean average air temperature is 11.7 ºC, with temperatures varying seasonally. The coldest months are December through February and the warmest months are June through August. Winds in the study area are predominantly southwesterly (Shippensburg 2013).

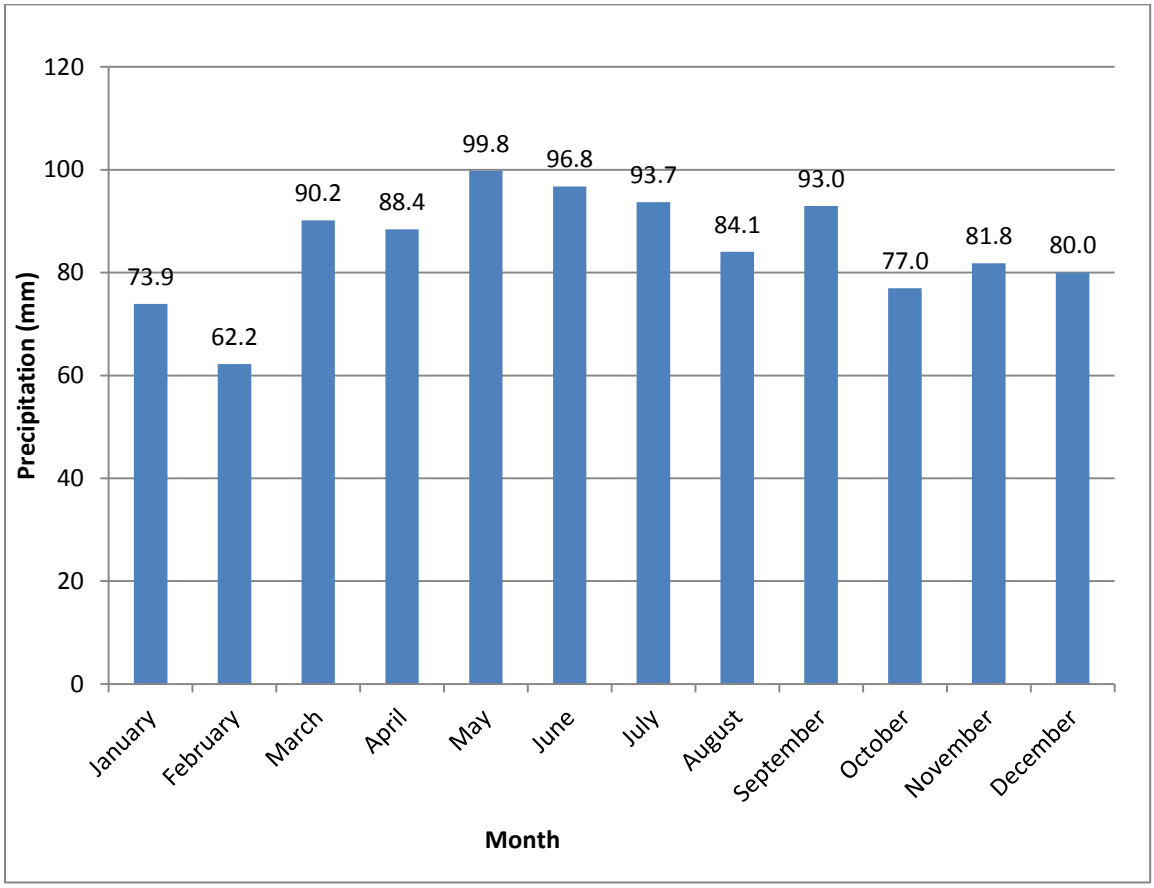

Figure 2.2: Average mean monthly precipitation (in millimeters) for Shippensburg, PA. These data were obtained from Shippensburg University Weather Station (2013).

2.2 Study Site Geology

2.2.1 Physiography and Structural Geology

The study site is located within the Great Valley Section, locally called the Cumberland Valley. According to Sevon (2000), the Cumberland Valley lies within the larger Valley and Ridge Physiographic Province of southern Pennsylvania (Figure 2.3). Cambrian through Ordovician limestone formations are the dominant bedrock of the Cumberland Valley. Many of these formations are only exposed in a few locations due to karstification and soil exposure (Becher and Taylor 1982).

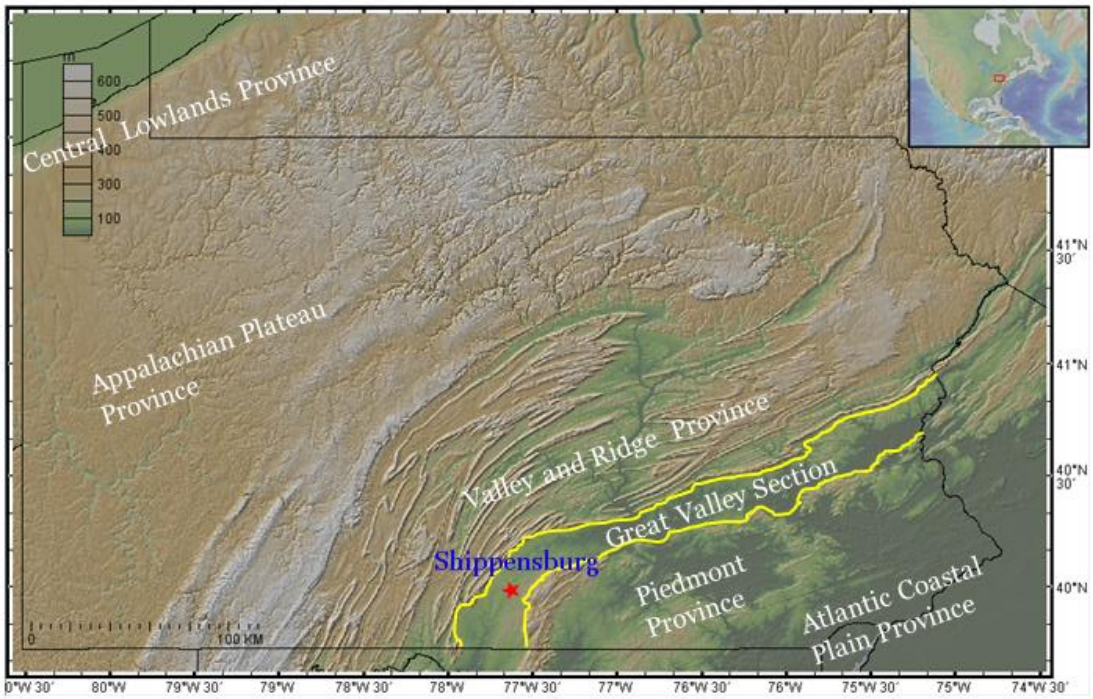

Figure 2.3: Shaded Relief map of PA showing the major physiographic provinces in Pennsylvania as noted by Sevon (2000). Shippensburg (red star) lies within the Valley and Ridge physiographic region of Pennsylvania. The base map is a modified image from http://www.geomapapp.org and Ryan et al. 2009.

The formations of the Cumberland Valley are not homogeneous and contain other lithologies such as interbeds of shale, sandstone, and limestone.

While these sedimentary beds formed in the Cambrian and Ordovician Periods, deformation occurred within Cumberland Valley during the Alleghanian Orogeny. The deformation folded the beds and altered the angle of their dip. Faulting during the Jurassic Period broke up and scattered rock units. These events created the folded and faulted terrain of the Cumberland Valley of the Appalachian Fold and Thrust Belt. In such a terrain, the stratigraphy of Ordovician limestone is often difficult to unravel because units have been highly weathered and are often duplexed in the fault system. (Shultz 1999)

Lolcama et al. (2002) observed that several formations found in the Cumberland Valley also have siliceous layers that are less soluble than surrounding layers and therefore accelerate the karstification of surrounding limestone. The karst in the Cumberland Valley has complicated stratigraphy as extreme faulting, weathering, differential weathering, and modern biologically enhanced processes. These processes can alter the solubility properties of limestone and thus create the lithographic arrangement depicted in the bedrock geology map of the Shippensburg Quadrangle (Figure 2.4). The geological bedrock map shown in Figure 2.4 displays the distribution of the Rockdale Run and Stonehenge Formations of the Ordovician Beekmantown Group. Both of these formations are prone to karst processes.

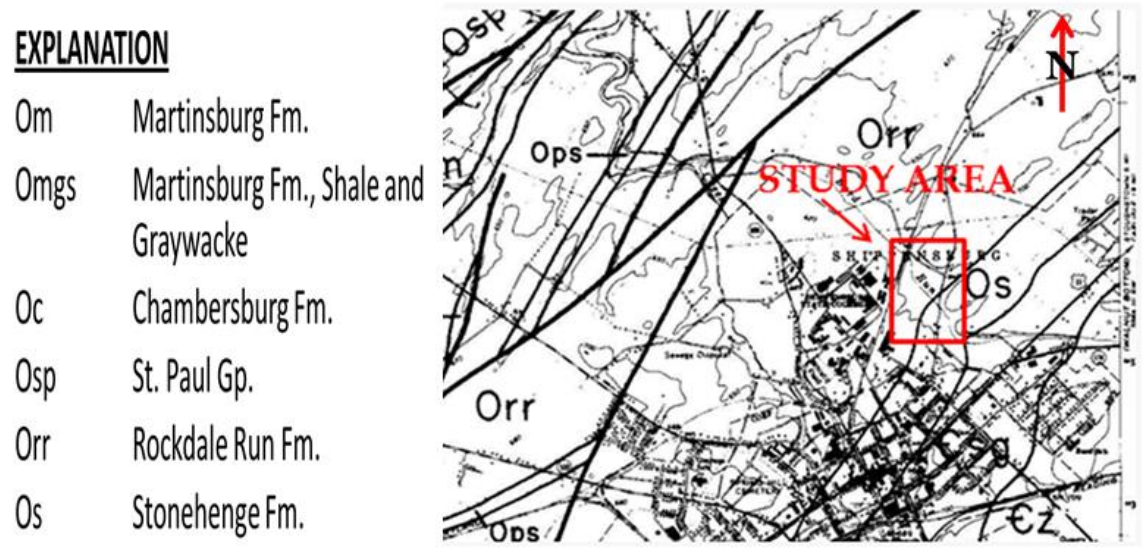

Figure 2.4: A modified portion of the Root (1981) bedrock geology map in the Shippensburg Area in which the red square encompasses the study area. The contact between the Rockdale Run and Stonehenge is likely just south of the study area. Note the faulted contacts delineated by thick black lines.

In the Shippensburg area, the Beekmantown Group consists of four formations which, in ascending order, include: Stoufferstown (not shown on map), Stonehenge, Rockdale Run, and Pinesburg Station Formations (Root 1977). The St. Paul Group is stratigraphically above the Beekmantown Group and includes the Chambersburg Formation (Table 2.1). Both members of the Beekmantown Group mentioned in Table 2.1 are located at the site. These two formations strongest differences are in rock type. While the Stonehenge Formation is generally dominated by limestone, the Rockdale Run Formation consists of limestone, marbloid limestone, and dolostone (Table 2.1). The differences in rock type define the contrasts in the strata. The two formations have similar features of stromatolites and experience pyramidal (pinnacled) weathering.

	Group	Formation	Rock Type	Unique formation features	Layers (top to bottom)
Ordovician	St Paul	Chambersburg	Limestone limestone, dolostone	Platy limestones. Faulting and folding complicate outcrop patterns Chert nodules	
		Pinesburg Station	Dolostone	Severe faulting and folding frequently homogeneous	
	Beekmantown	Rockdale Run	Limestone, marbloid limestone, dolostone	Chert nodules, stromatolites form in laterally linked hemispheroids. Weathers into pyramidal shapes. Limestones are breccias	Dolomite, ooids, stromatolites and cherts Fine-grained and algal limestone (channel filled), fine-grained mechanical limestone,
		Stonehenge	Limestone	Stromatolites in an upright pipelike manner. Weather in pyramidal shapes. chert nodules	conglomerate and dolomite with irregular laminations, algal limestone
Cambrian		Stoufferstown	Limestone	Cobble size tabular limestone siliceous seams	
		Shadygrove	Limestone, marble	Chert nodules and stromatolites Conglomerates, algal mat dolomites, chert nodules. stromatolites are cabbage head and sheet varieties.	
	Conococheague	Zullinger	Limestone, dolostone		
		Elbrook	Limestone, shale, sandstone, siltstone	Dark massive limestone, shaley limestone and limestone	

Table 2.1: Calcareous rocks of the Cumberland Valley (Root 1968, 1977).

2.2.2 Geomorphology and Karst Development

Dissolution of carbonate bedrock often creates an egg carton topography, which is observable north of the study area (where the land is underlain by Stonehenge and Rockdale Run Limestone) as well as to the west of the site (where land is underlain by Rockdale Run Formations). In this region, Stonehenge Limestones have experienced intense folding and faulting to the extent where bedding planes are exposed to dissolution. The continual dissolution along these bedding planes creates a jagged or

pinnacled surface. These pinnacles are not well exposed in stream valleys as they are covered by a mantle of alluvium. The amount of dissolution of these rock units depends primarily upon the weathering resistance of various limestone and dolostone layers. The dissolution rate is lower where low grade, impure calcium carbonate ($CaCO_3$) with dolostone ($CaMg(CO_3)_2$), or other impure limestone is abundant than in areas containing limestone of a higher purity. Therefore, these outcrops of impure limestone are few and fragmented due to the alluvial processes which cover them.

2.1.3 Implications for this Geophysical Investigation

Limestone outcrops were observed within the floodplain at the study site, but not within the limits of the geophysical study area. While the possibility of karst bedrock in the shallow subsurface exists, the depth and abundance has not been verified. Greater significance, in this study, should not be placed on the detection of underlying limestone formations, but rather, the clays which formed from their dissolution. Such clay units are more likely to underlie the buried channel at an observable depth than the parent material from which they formed. If the channel boundaries cut into the residual clay, the difference between the clay and the channel fill material would create clearly identifiable contrasts in the geophysical responses from each method in this study.

2.3 Soils

The USDA conducted surveys using aerial photography of landforms before the restoration project. The soils in the study area consist of Monongahela (MnA) and Melvin Silt (Me) Loams as shown in Figure 2.5.

Monongahela silt loams form in alluvium on old stream terraces and are derived from acidic sandstones and shales (NCSS 2007). Within the study area, these silt loams appear on the limestone floodplain adjacent to Burd Run (i.e. Figure 2.5). The area labeled as Monongahela Silt Loams includes the soil beneath the wetland and most of the area nearest to the corner of Britton Road and Fogelsanger Road.

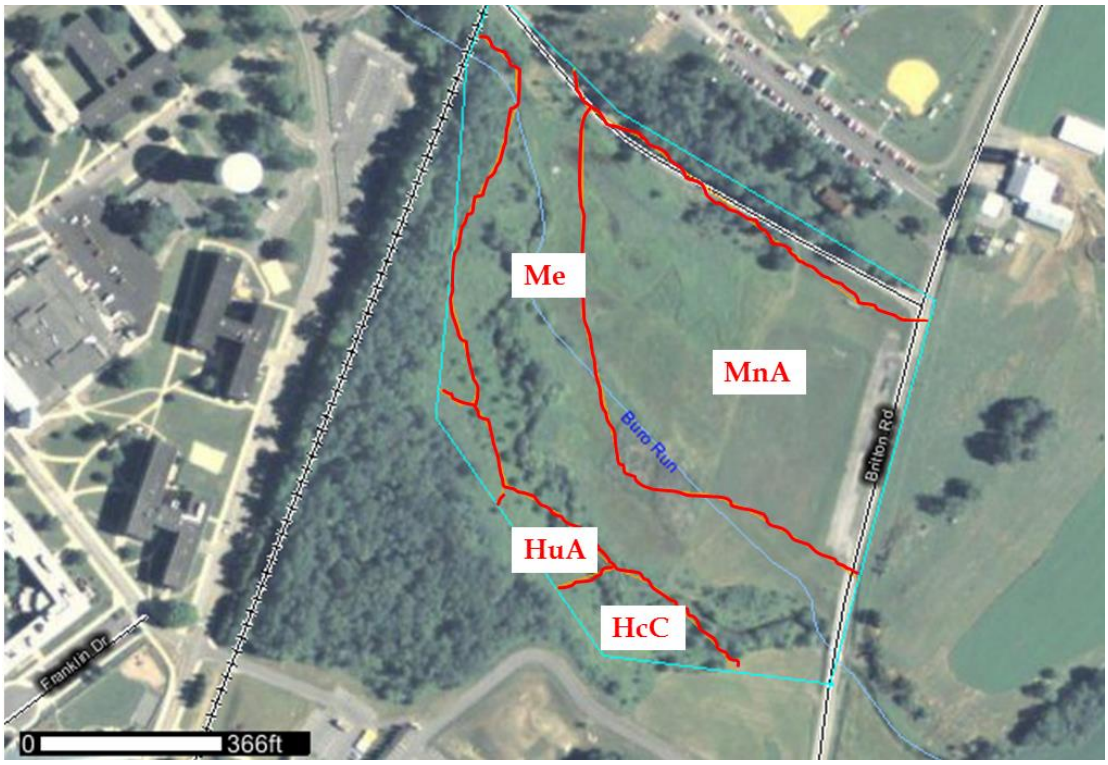

Figure 2.5: The soils of the study site include Melvin Silt Loam (Me), Monongahela Silt Loam (Mna), Huntington Silt loam (HuA), and Hagerstown Silt Loam (HcC) (USDA 2009).

Since the parent material for Monongahela Silt Loam did not originate from the limestone bedrock at the site, they must have come from various source bedrocks upstream. The headwaters of Burd Run extend to South Mountain where quartzites and shales bedrock of the Antietam, Harpers, and Weverton Formations are located (Figure 2.6). Deposits of Monongahela Silt Loam are commonly found on terraces sloping less than 25 percent. These deposits can accumulate to over 40 inches (NCSS 2007).

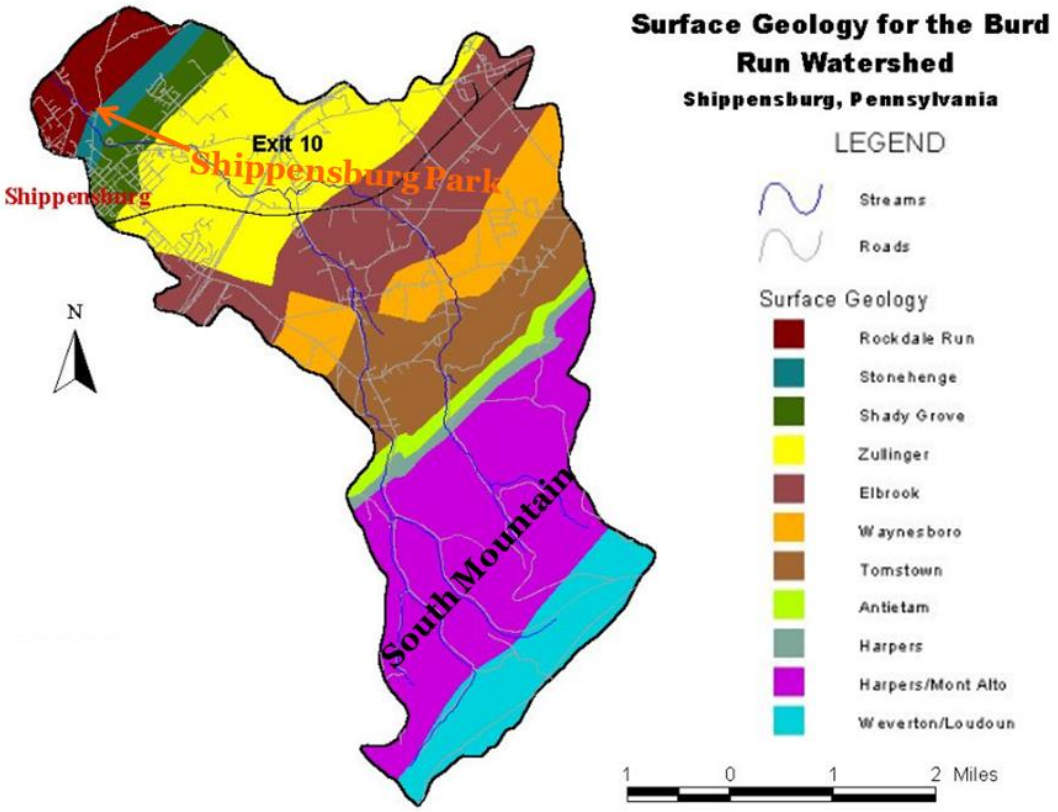

Figure: 2.6: Potential sources of alluvial material at Shippensburg Township Park. (Woltemade 2000).

The area nearest Burd Run is depicted as Melvin Silt Loams. This soil unit usually forms on nearly level to depressed parts of floodplains and in upland depressions. As such, slopes where this silt loam forms are generally below 2 percent. These soils are generally formed in silty alluvium composed of limestone, shale, siltstone, sandstone, and loess. (NCSS 2007) The clay content for the Monongahela Silt Loam is 20.8% and 22.1 % for Melvin Silt Loam (USDA 2009).

Despite their efforts of mapping, the construction of the restoration has relocated some of these soils.

2.4 Hydrology

The entire Burd Run flows from South Mountain northward to Middle Spring Creek, a tributary of the Conodoguinet Creek. While certain sections of Burd Run have an ephemeral flow due to underlying geology, the segment of Burd Run investigated is in part a spring-fed stream. By the time Burd Run reaches Shippensburg campus, the stream collects runoff from 51.8 km^2 of land (Woltemade 2012). Although this reach of the stream is small, flood events can inundate floodplains along banks of Burd Run. The study site is located on one of these floodplains. Buried beneath this floodplain is the channel which is the subject of this study.

The section, or reach, of Burd Run within the study area lies in a wide valley. Within this valley, the stream experienced meandering prior to human interference. Each course of the stream left a mark on the landscape and their associated alluvial deposits were buried over time. The stream restoration project of 2001 buried the most recent last course of the channel in a short period of time. It should therefore be the best-preserved and complete paleochannel within the valley.

Herrmann (1999) provided a few images in his thesis that are useful for this current study, especially with respect to the geometry of the channel prior to its burial during the restoration work in 2001. For instance Figure 2.7 shows the meandering channel. Pools, riffles, point bars, and cut banks were all observed within the channel. Cutbanks were pronounced due to the presence of large trees.

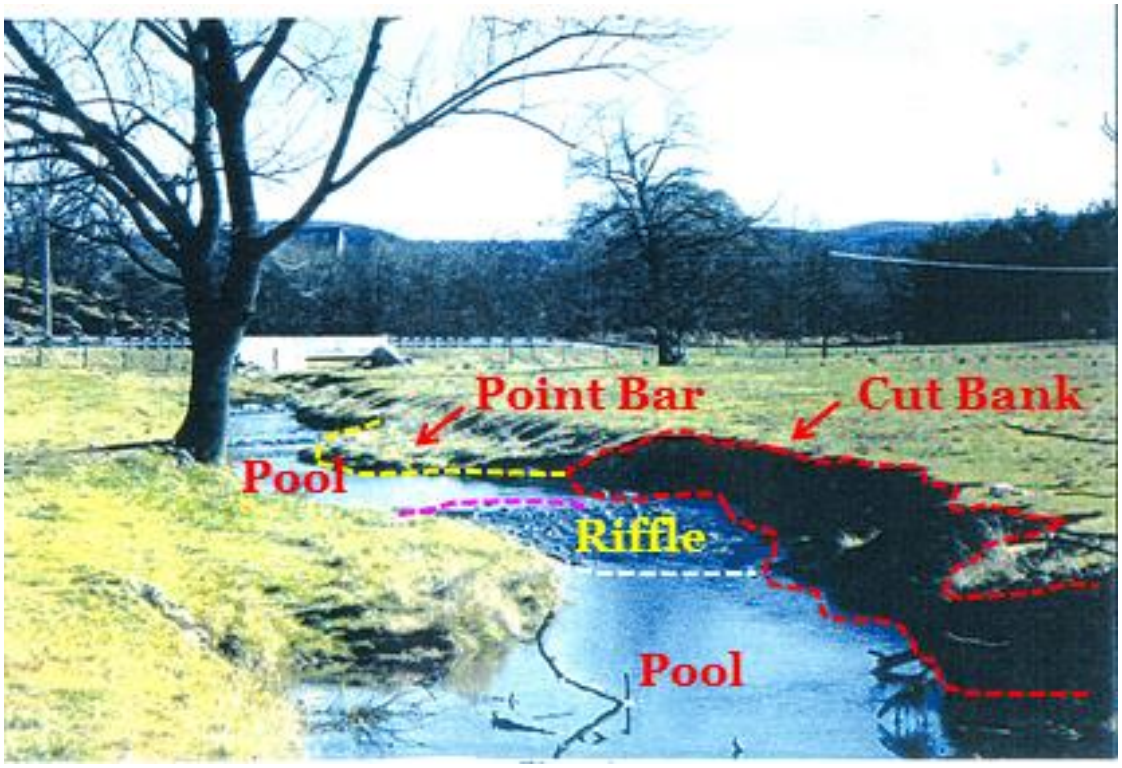

Figure 2.7: Meandering in Burd Run prior to restoration looking southeast (Herrmann 1999).

Herrmann provided four cross-sections of the now buried channel that can help with interpreting geophysical anomalies obtained in this study. All four cross-sections are reproduced and included in Appendix A. However, two of the cross-sections are shown in Figure 2.8 below. Based on these cross-sections, the channel had a width ranging from 4-6 m. The channel dropped roughly 1 m from the top of the bank to the bottom of the channel.

Figure 2.8: Two cross-sections from the Burd Run channel prior to burial.

Herrmann (1999) described the dimensions of a pool in a straight channel as deeper, and narrower, than a riffled section in a similar channel. The variation of bedload associated with pools is generally finer grained material (i.e. clays and silts), than where riffles occur. Figure 2.9 confirms the existence of coarse grains in such a riffle. Variations in grain size within the channel can alter geophysical responses in the results.

Figure 2.9: Coarse-grained cobbles creating riffles in former channel prior to restoration (Herrmann 1999).

Slope failure in stream banks can influence the geometry of the channel. Herrmann (1999) also observed slumping in the cohesive cut banks within the reach. Slumps are visible in Figure 2.10. Slumps in cut banks can form when the stream cuts into soft material underlying harder material creating overhanging cantilevers. Voids can be found beneath an overhanging cantilever or beneath a collapsed cantilever when it lands on an uneven surface. At the study site at Burd Run, the cantilevers are

compositionally harder due to the extensive grass roots on floodplains which reinforced the bank deposits.

Failed cantilevers can be portrayed in cross-sectional profiles of the stream in a variety of ways depending on the position and location of the failed mass, and time elapsed since failure. Generally, a failed slope destroys organized soil horizons on the bank and increases the width of the channel. The failed slope will not be as steep as the original cutbank due to the debris resting at the base of the slope. However, the new slope may not always be smooth due to the blocks of soil which break off of the original slope and would appear as mounds separated by fractures from the new slope.

Figure 2.10: The southern banks of Burd Run experiencing slumping prior to restoration (Woltemade and Wood 2002).

Restoration removed soil from the newly excavated channel, stored this material in between the two channels in a pile (Figure 2.11). This pile was used for the fill material which currently buries the former channel. It was not the intention of the restoration project to preserve the buried channel. As such, construction equipment most likely crossed over the channel during the burial process. The movement would have caused a certain amount of destruction to identifiable channel features in the previous

images. Therefore, it is likely that geophysical anomalies associated with the channel may not be completely consistent with the channel dimensions as shown by the Herrmann cross-sections.

Figure 2.11: The excavation of the current channel (foreground) and the pile of excavated material used to infill the former channel (background) (Woltemade and Wood 2002).

Chapter III

LITERATURE REVIEW

3.1 Review of Geophysical Methods

Various geophysical methods are applied to environmental site investigations. These methods use different principles of physics and mathematics to model geologic strata and subsurface features. Some methods are based on the injection of electrical current into the subsurface in order to observe the flow paths. Other methods use sound waves or propagate electromagnetic waves in the subsurface. All of the methods create anomalies (strong responses above or below the background levels) based on the differing ways that earth materials respond to the propagating signal. Popular geophysical methods used for environmental monitoring include electrical resistivity (transmission of an electrical current), seismic reflection and refraction (transmission of sound), ground penetrating radar (transmission of an electromagnetic signal), electromagnetic induction (transmission an electromagnetic signal), and gravity (measurement of density changes in the subsurface). The specific methods used in this study are discussed in more detail in the following sections.

3.1.1 Electrical Resistivity (ER)

The electrical resistivity (ER) method operates by using transmitter circuitry at the surface to send an electrical current into the ground. The current travels through different earth materials of the underlying subsurface to a receiver. The resistances offered by the materials are recorded by the receiver circuitry at the surface (Figure 3.1). The principle of the ER method is based on Ohm's Law, which gives the relationship

between the electrical current (I), the voltage (V), and the resistance (R) as R=V/I. The application of this relationship is that as the injected electrical current travels through the ground, it encounters both earth materials that are good conductors (allowing easy current flow through them) and bad conductors (more resistive). Based on this conductivity contrast, the ER method is used to identify different features underground. The term resistivity (ρ) is derived from the relationship ρ=K(V/I) and is expressed in Ohm-meters. K represents the geometric factor of the electrode configuration used as it accounts for the manner in which the current and potential electrodes are arranged. While the resistance (R) changes with the area (A) and length (L) of a material, the resistivity (ρ) remains constant for the material. R and ρ are related by the equation, R= ρL/A.

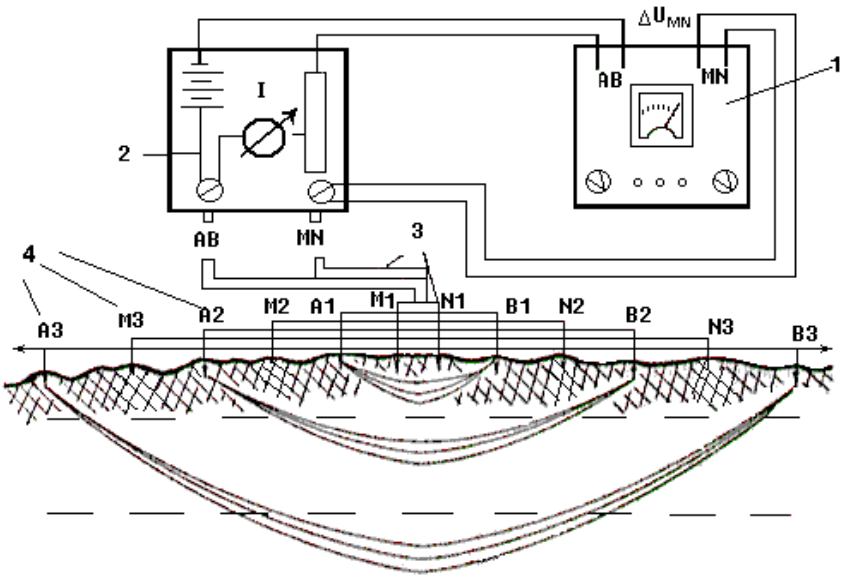

Figure 3.1: Electrical resistivity array showing current propagations in the earth (Tahun 2011).

The ER method is used for a wide range of hydrogeological investigations. There are two main classes of the ER instrument: The galvanic and the capacitively-coupled systems. Galvanic systems are the well-established stake-in-the-ground systems that employ a wide variety of electrode configurations (e.g. Schlumberger, Wenner, dipole-

dipole, etc.), while capacitively-coupled systems use a transmitter-receiver set up only in the dipole-dipole mode so that the entire array is towed on the ground surface, eliminating the need for the time consuming set up of stakes used in other ER methods. A geophysicist must consider site conditions and goals when considering any of these arrays. The most common electrode array types are discussed below.

The Wenner Array has two receiver electrodes placed between two transmitter electrodes and is used for imaging along a profile (transect) at a constant depth (Figure 3.2). A constant spacing (a) between all four electrodes is maintained. As an example, if a spacing equaling 5 m is used, the Wenner Array would give the resistivity image at a constant depth, determined by the 5 m spacing, along the profile. A change in depth of investigation would require a different constant spacing. While the Wenner Array is good at detecting vertical changes in resistivity, it poorly resolves horizontal changes (Gibson and George 2003). Therefore, the Wenner Array is better when detecting stratigraphic features but weak when detecting vertically oriented objects such as dikes.

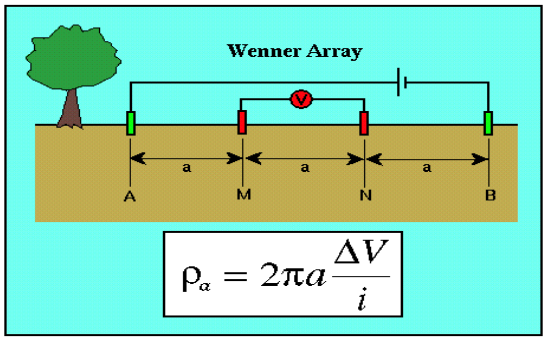

Figure 3.2: The Wenner Array for an electrical resistivity survey (WCU 2012).

Like the Wenner Array, the Schlumberger Array also uses four electrodes, consisting of two receiver electrodes (M and N) between two transmitter electrodes (A and B). The difference is that the electrodes are not evenly spaced (Figure 3.3). The

Schlumberger Array is a depth-sounding method because all four electrodes are moved systematically to increase the depth of investigation at a point. The inner potential electrodes are usually kept at a very small separation, compared to the two outer current electrodes which are expanded continuously to increase the depth of measurements (Figure 3.2 vs. 3.3). At large current electrode spacings, the measured voltage decreases and the signal-to-noise ratio increases; thus, the spacing of the potential electrodes must increase (Gibson and George 2003).

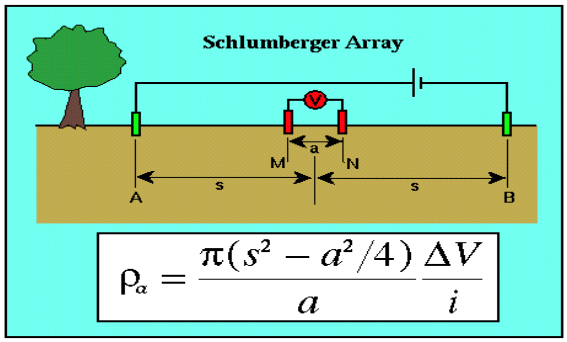

Figure 3.3: The Schlumberger Array for an electrical resistivity survey (WCU 2012).

The major difference between the Schlumberger and the Wenner Arrays is that the Schlumberger Array images a single point at varying depths while the Wenner Array images along a line at a constant depth. Also, data collection using the Schlumberger Array is far more time consuming. However, Nyquist et al. (2007) noted that with the development of computer technology, physical movement of electrodes, as used in the Schlumberger Array, is no longer necessary. Modern equipment has software interfaces that automatically expand the electrodes. The Schlumberger array gives a one dimensional depth sounding which can be useful in finding the water table when drilling a well (Loke 2000).

The Dipole-Dipole (DD) Array (Figure 3.4), also known as the Double Dipole Array, is the array that was used for this study. With the development of computer technology the DD Array has become the method of choice both with the capacitively-coupled and the traditional galvanic resistivity systems even though it is more complicated. In a way, it combines the profiling principle of the Wenner Array and the depth-sounding principle of the Schlumberger Array, and can be used to obtain a 2-D or 3-D section of subsurface geology along a transect. With computer technology, modern resistivity equipment has eliminated the need for the physical rearrangement of the current and the potential electrodes on the field. This is now accomplished by computer software communication between the different pieces of equipment. Thus, surveys of large areas using the DD Array can be accomplished at a small fraction of the time it used to take. The DD array has vertical sensitivity and better identifies vertically-oriented features such as dikes.

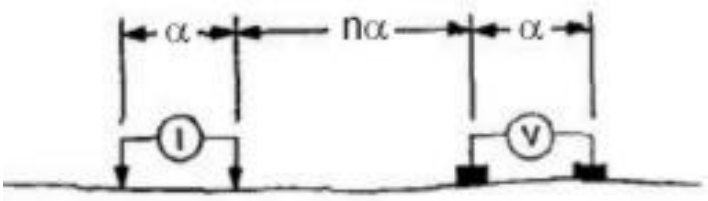

Figure 3.4: The Dipole-Dipole Array (EPA 2011).

The Geometrics Ohm Mapper, a DD Array, was used as the ER method in this study. The Ohm Mapper, which is a relatively new resistivity instrument, is a capacitively-coupled system rather than the traditional galvanic, stake-in-the-ground resistivity systems. Therefore, little refereed research using the OhmMapper is available. A few examples are documented by USGS Reports (Shah et al. 2008).

Although the literature is scant on the OhmMapper tool itself, the DD Array that it employs has been successfully used to map different subsurface geologic features, including those in karst landscapes. For example, the Missouri Department of Transportation used the DD array with a 68 channel Supersting Resistivity unit to search for active sinkholes and air-filled voids underneath an existing state highway and a planned exit ramp. The study placed resistivity profiles 25 feet apart on a grid. The resulting 2D subsurface images mapped zones of limestone (weathered and unfissured), clays, and solution-widened joints/voids but no sinkholes were found (Andersen et al. 2006). The bedrock configuration and the depth to bedrock were mapped on the site**.**

Mahmoudi and Gabr (2009) looked at paleochannels in the Nile River Delta using ER. The paleochannels were portrayed as troughs of low resistivity fill in between pinnacles of high resistivity bed material. Channels can also be represented by higher resistivities than the surrounding deposits depending on the composition of each material. Baines et al. (2002) used a 56-electrode AGI Sting/Swift system to observe high resistivity channel fill composed of sands surrounded by low resistivity muds in British Columbia, Canada.

More locally, Nyquist et al. (2008) used the AGI SuperSting R8/IP Marine (an underwater DD array) to map groundwater discharge in the Burn Run watershed. The profiles depict the natural state of the watershed in three distinct layers of resistivity including coarse alluvial sediments (top layer), residual clay (middle layer), and carbonate rock (lower layer). Nyquist et al. also identified a layer of sandy-clay loam between the residual clay and coarse alluvial sediments (2008).

3.1.2 Electromagnetic Methods (EM)

Electromagnetic methods (EM) work by sending a primary electromagnetic field through a transmitter coil into the ground, which induces a current in the underlying earth materials that it passes through. The current then produces secondary EM fields that are recorded via a receiver coil. The strength of the secondary field is proportional to the conductivity of the earth materials that produce them. The EM method is used to image the subsurface on the basis of conductivity variations in the earth. Two classes of equipment for EM surveys exist: Time-varying and frequency domain systems. The time-varying systems measure magnetic fields by sending pulsed signals over time through the ground that act like smoke rings that expand with depth. Frequency domain systems on the other hand, measure the magnitude and phase of electromagnetic fields relative to subsurface conductivity using a fixed frequency. Time domain electromagnetic (TDEM) systems are reliable for mapping at greater depths, but the process of collecting data is slower and interpretation is more complicated. The process of data collection is faster with frequency domain electromagnetic (FDEM) systems and therefore larger areas can be surveyed.

EM methods have been used successfully to map subsurface features in different geologic settings. For example, Doolittle and Collins (1998) used EM 31 and EM 38 induction meters (from Geonics, Inc.) on a cultivated field with varying depths of clay soils covering limestone bedrock at Pine Grove Mills, PA (Centre County). The EM methods successfully mapped the clay soils of Pine Grove Mills. The soil moisture and bedding planes with dissimilar conductive properties displayed the clay's contrast with the underlying limestone bedrock. This contrast also allowed a clearly visible dip in the

bedrock to be detected. The above study site in Centre County shares some similarities with the proposed study site in Shippensburg. For instance, they are both in the Valley and Ridge region and situated on folded limestone. Generally, the EM method is insensitive to subsurface layers or features having similar electrical properties, and the EM is most effective in areas where the effects of one property dominate over other properties (Doolittle and Collins 1998).

Two important factors that help in the detection of buried stream channels with EM are soil variations and water saturation. Prior to being buried, an active stream channel has the ability to transport minerals of varying origin and composition into a landscape. When the course of one of these channels is diverted and becomes buried, the foreign minerals remain. Generally, larger grain size clasts deposit in channels than in floodplains due to the velocity required to keep each suspended. In the case of Burd Run, the mechanically weathered sands, gravels, and cobbles (composed of the shales of the Harpers Formation, and quartzites of the Weverton and Antietam Formations) would be present in the silt loams while residual clays (chemically weathered from the limestones of the Rockdale Run and Stonehenge formations) would be more dominant beneath them. The variation in mineral size and composition would create a contrast in electrical conductivity. The difference in grain size also creates more pore space in the filled-in channel allowing it to hold and transport more water than surrounding soils. The saturation of soils with water tends overpower variations in soil conductivity. If only certain areas are saturated (such as a buried channel), they will appear as anomalies when compared to the surrounding soil.

Danielsen et al. (2003) used three methods of transient EM (TEM) including high moment TEM, conventional 40X40 TEM, and pulled array TEM to locate buried water resources in the Skjød Valley of Denmark. The investigation identified a previously unknown buried valley stream system as a linear pattern of elevated resistivity (above 100 Ωm) compared to the surrounding clay (2-7 Ωm).

Andre et al. (2010) used the EMP400 to study hydrogeophysical variations of soil layers at a vineyard in south France. Variations in conductivity were most likely linked to soil variations in the vineyard and not to differences in soil moisture. In a homogeneous soil, water content would be the sole factor in creating anomalies in conductivity.

A valley carved by alluvial processes will have a variety of well sorted deposits of differing conductivity. A buried channel could have higher or lower conductivity than surrounding soils depending on soil composition alone and be completely masked in saturated conditions. Dry conditions would be best for observing a buried channel. However, the conductivity may remain elevated beyond the extents of the channel as the borders of a channel are rarely naturally impermeable. The EMP400 is a cheaper and less cumbersome EM instrument than others and is capable of collecting the same type of data over smaller areas such as the buried channel at the Burd Run study site.

Ahmed and Carpenter (2003) used the EM 31 to map filled dolines associated with soil pipes connecting hydraulically active bedrock fractures to the surface at Perry Farm Park in Illinois. They found high conductivity near sinkholes due to elevated soil moisture from a recent thunderstorm, and therefore theorized that the groundwater was flowing towards the doline.

3.1.3 Ground Penetrating Radar (GPR)

GPR transmits relatively higher frequency electromagnetic signals than other EM applications. These signals are emitted from a surface antenna (transmitter) into the ground. The transmitted signals get absorbed or reflect off of subsurface objects that have dielectric properties (i.e. a change from more positive to negative materials, such as sand to clay, limestone to shale, or wet to dry materials) and return to a receiver. GPR signals propagate at given frequencies (f) through the subsurface at a certain wavelength (L) at a given velocity (v) and are related by the equation, v=Lf. Information from the travel time (t) and the velocity of the transmitted/reflected signals is used to model underlying subsurface features. Depth (d) can be determined through the equation:

$$d=0.5(v^2t^2+x^2)^{1/2} \qquad \text{(Eq. \#1)}$$

where x is the transmitter- receiver offset and t is the time variable. Antenna frequencies for GPR range from 10 MHz to 1500 MHz, and this difference controls the depth of investigation. An antenna with a higher frequency (MHz) shows greater clarity at shallow depths but loses resolution quickly as the depth increases. Antennae with lower frequencies are for deeper investigations though they have lower vertical resolution.

GPR has limitations on highly conductive materials such as wet, clayey soils which tend to dominate karst landscapes and ferromagnetic materials. While the silt loams at Shippensburg Park contain clay, other studies have proved successful in similar soils.

Clement and Ward (2008) used GPR with a 100MHz antenna to study soil moisture variations across a prototype berm with a 1.0 m thick layer of silt loam. The study detected temporal changes within the silt loam layers from four visits at different points in the year.

GPR is also very reliable at mapping buried stream channels. Burrell et al. (2008) conducted a study in the southern High Plains of Texas in which point bars with trough scours were detected in a buried stream channel using 100MHz and 200MHz antennae. Stevens and Robinson (2007) detected both clay facies and distributary channel facies in lacustrine deltas of northern New York featuring cut and fill structures within a lacustrine delta using a 100MHz antenna.

Chapter IV

METHODOLOGY

4.1 Preliminary Site Assessment

4.1.1 Locating the Buried Stream Channel

Before using geophysics to detect and map the Burd Run buried stream channel, it was necessary to first determine its approximate course through a preliminary site assessment. Fortunately, a short, ephemeral, and exposed segment of the former channel still exists to offer a visual clue about its location and direction (Figure 4.1). It must be noted that the surface water which appears in places, where the channel is not currently soil-filled, flows towards the present day stream.

Figure 4.1: The edge of the fill material where the former channel is exposed.

While the course of the exposed stream is visible near the edge of the study area, the course of the buried portion of the former channel was determined by comparing historical images of the former course to those of the present landscape. The exposed channel is visible with modern geospatial technology (aerial photography provided by Google Earth). Google Earth offers imagery of the site from several observations since 1994. Shown side by side, in Figure 4.2, are the Google Earth aerial imagery of the study site in 1994, prior to the stream restoration work, and a Google Earth image of the site in 2008, after the restoration project. Both the old and the current stream channels are visible. Google Earth has the ability to overlay the two pictures so an image could be drawn on one and be in the same location on the other. This method creates an image which depicts the course of the buried channel as fairly linear from the point it is exposed to the point upstream where it deviates from the current channel.

Figure 4.2: The old and present-day courses of Burd Run (GoogleEarth 2012).

Marking paint was used to trace the edges of the buried channel segment in the field from the exposed part into the surveyed area as shown in Figure 4.3. Five 30 m long

transects were measured and laid out (east-west), and aligned perpendicular to the filled stream channel direction. These transects were placed 10 m apart from each other. Topographic surveys and appropriate geophysical investigations were performed along these transects (Figure 4.3).

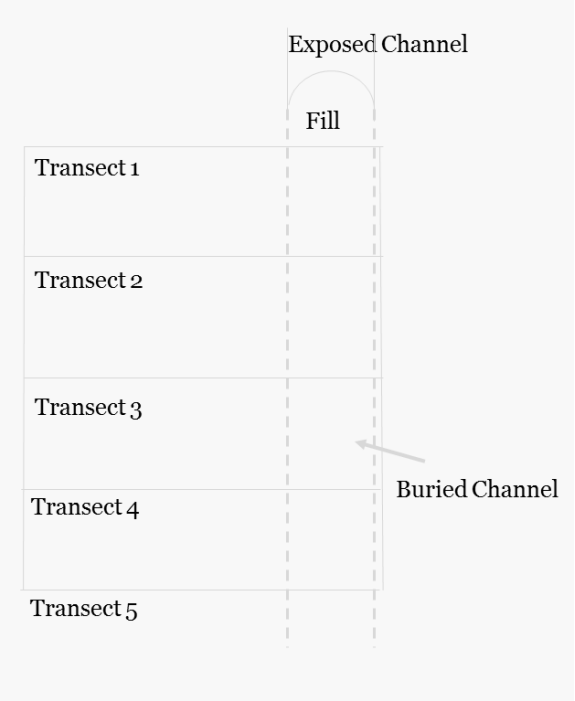

Figure 4.3: Sketch of survey transects relative to the buried channel.

4.1.2 Topographic Survey

A Topcon GTS 223 Total Station was used to collect elevation points every 1 m along each of the five transects. A Geoexplorer 3000 series GeoXM Trimble GPS Receiver was used to georeference one fixed location, in this case a manhole cover. The manhole cover was used as a starting point (base site) to geospatially define the distance separating all necessary information including the ends of each transect, elevation points, and the outline of the exposed channel. The trimble data were downloaded to ArcGIS, and the topographic data from the total station were transferred to a Microsoft Excel file

where the data points were corrected to a UTM 18^0 N NAD 1983 Conus Cors96 coordinate system. Figure 4.4 shows that the data points were plotted correctly with respect to one another in linear transects, thus providing for an accurate representation of topography along all five transects.

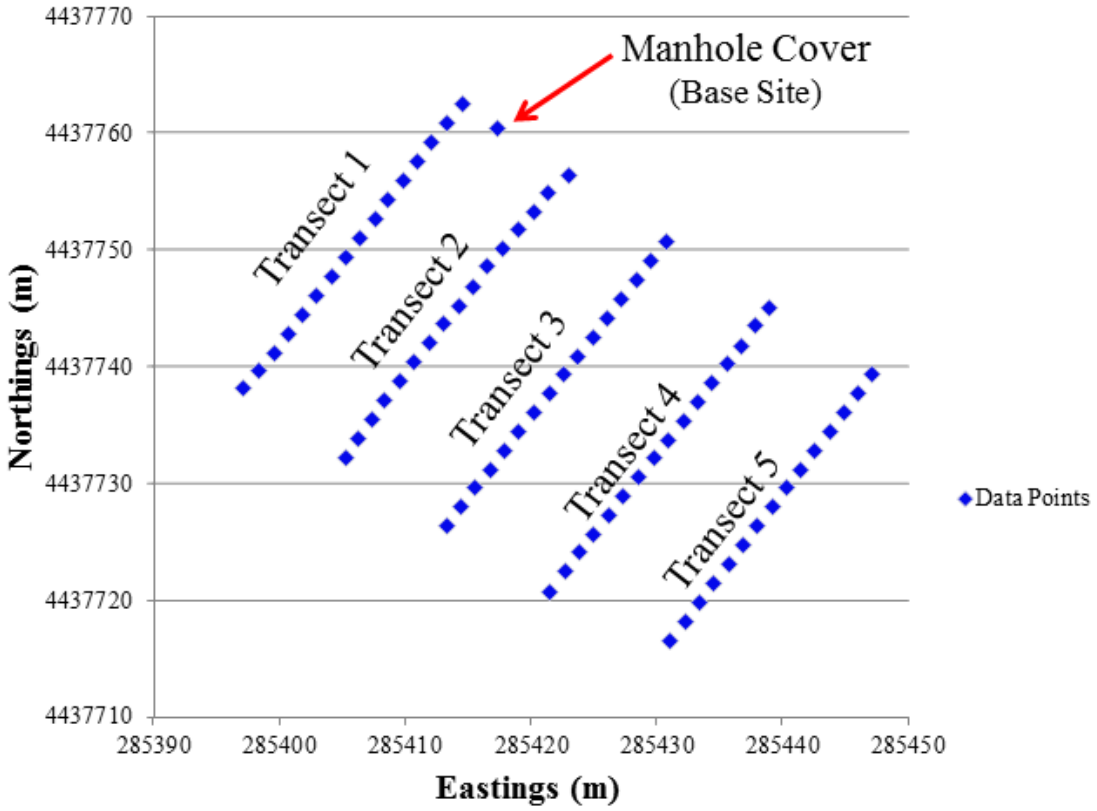

Figure 4.4: Topographic transects shown in the UTM 18^0N NAD1983 Conus Cors96 coordinate system.

As stated in Chapter 2, topography varies very little across the study site. The greatest variation in topography observed is man-made, created by the infilling of the old stream channel that has formed a mound above it. Looking from north-south, elevation increases slightly from transect 1 towards transect 5. There is also a slight increase from east to west, which is depicted in Figure 4.5. The increase in elevation around 5 m to 9 m

is associated with one edge of the fill material. A drop off between 13 m and 20 m of transects 1, 2, and 3 could possibly be associated with the channel. However, a lack of a drop off on the other side of transects 4 and 5 suggests the fill extends beyond the channel. Overall, point-to-point elevation changes over the surveyed areas are less than one meter. Elevation increases minimally as one goes upstream (Figure 4.6).

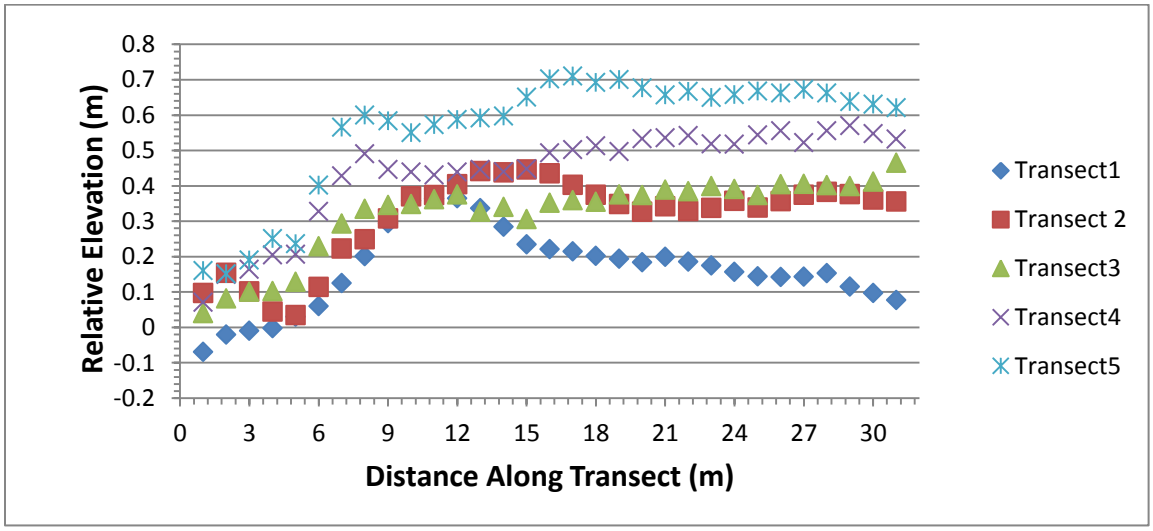

Figure 4.5: Variations in elevation along transect 1-5 as collected by a Topcon GTS 223 total station (oriented northeast to southwest).

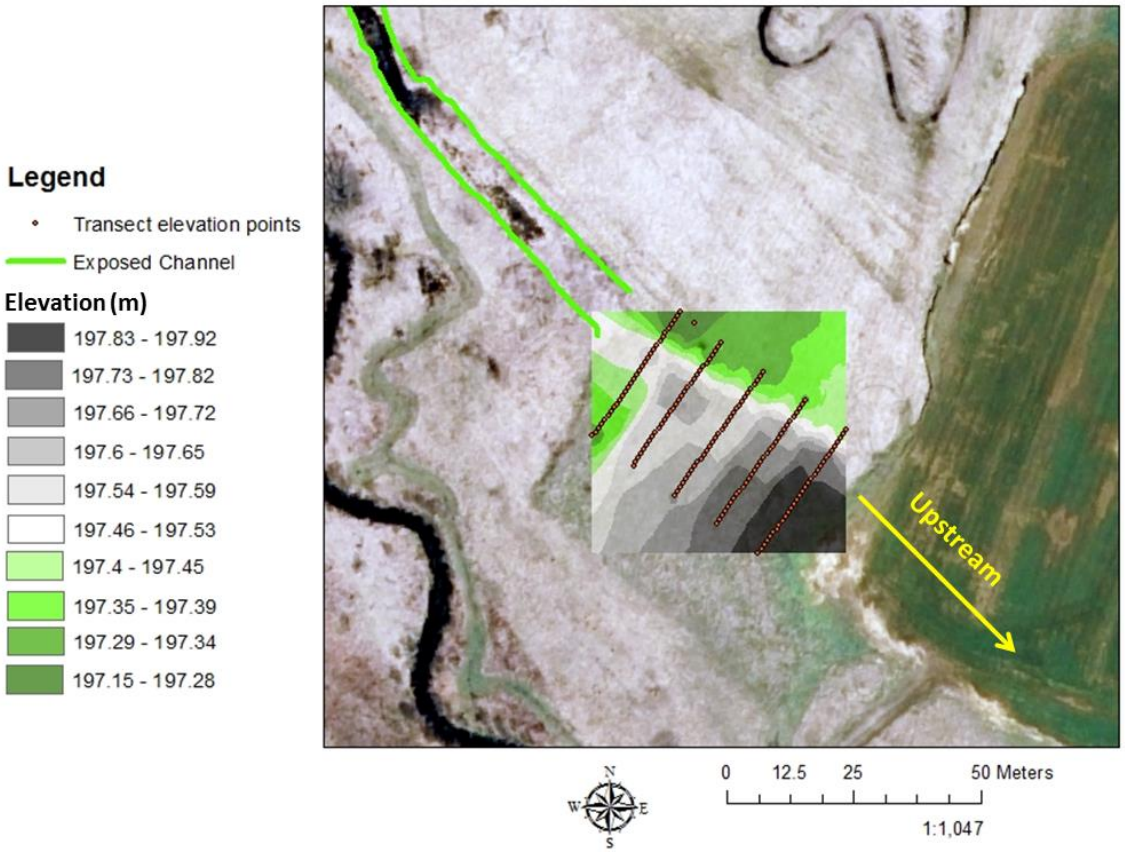

Figure 4.6: Contour map (produced in ArcGIS10) of the Burd Run study site based on measured elevation points along occupied transect.

4.1.3 Soil Sample Collection

Geophysical imaging can reveal the buried channel through anomalies caused by different rocks and soils in the fill material. However, these can only be interpreted as such after collecting and analyzing soils samples on the site. Soil samples were taken using a 1.5 m bucket auger in order to examine the soil composition over and adjacent to the buried stream channel. Figure 4.7 shows the relative position of the auger holes (labeled A-F) to the buried channel and the survey transects. Soil samples were taken between both transects 1 and 2, and between transects 4 and 5. These points were

distributed near the boundaries of the study area at points where the soils along the geophysical investigation transects would not be disturbed.

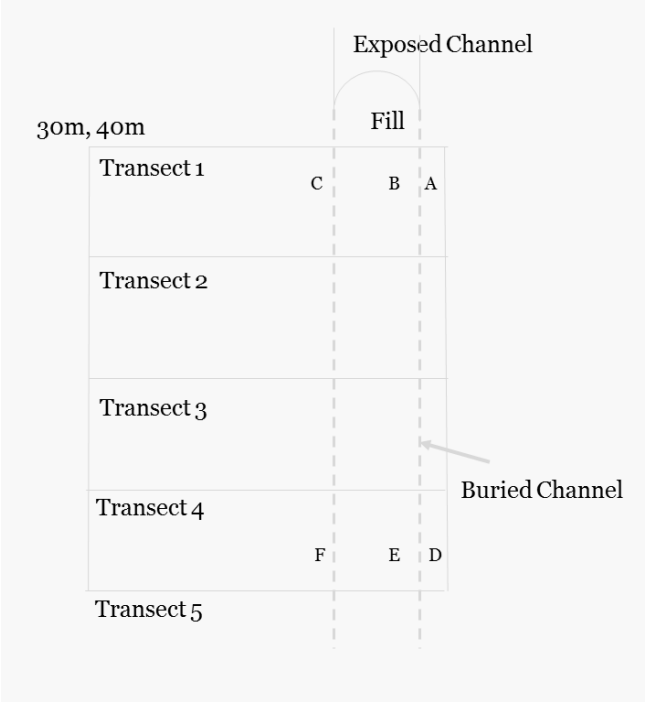

Figure 4.7: Soil sample locations represented by letters A-F.

Photographic profiles of the soil samples were created by placing the collected soils in linear order of their removal and photographed. Soils in these profiles were analyzed in the field using hands to feel for a sandy texture, and rolling the sample into a ball and squeezing the sample through the thumb and index finger creating a ribbon to test the cohesion and plasticity properties. Soil color and moisture were also noted.

The auger holes at A, C, D, and F were augered outside of the channel boundaries. The top horizon of site C contained orange-brown silt clay with no sand, and some coarse rounded quartzite gravel. However, the sand content increased and the gravel became impenetrable between 35 cm and 43 cm (Figure 4.8). Soil composition

beneath 43 cm cannot be determined due to this impenetrable coarse gravel. The rounded gravel is evidence of alluvial deposition, and is expected at depth in a modern floodplain.

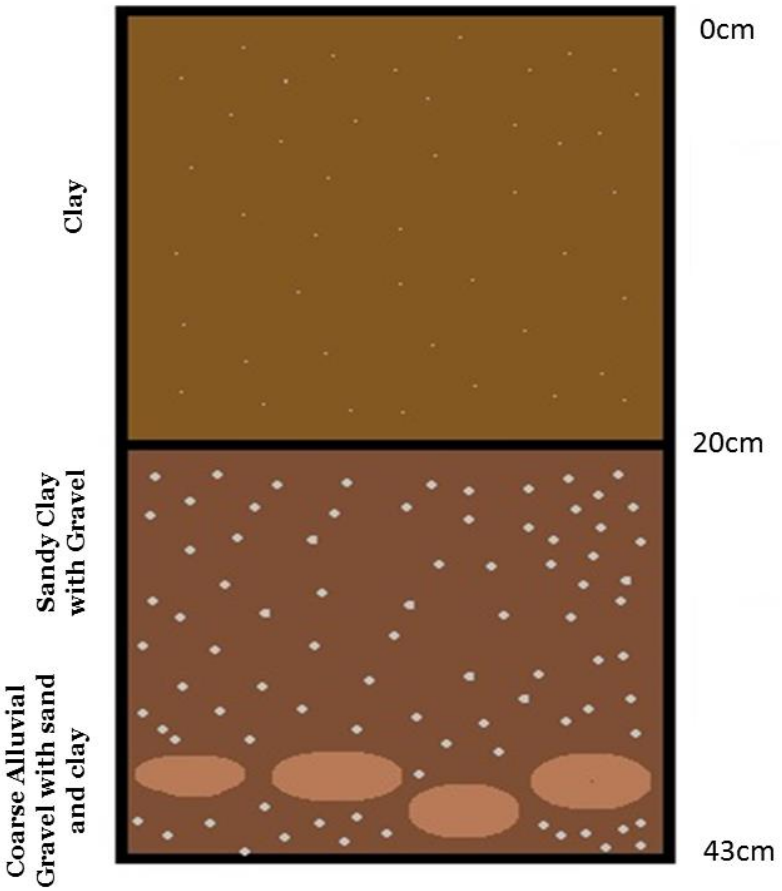

Figure 4.8: Soil sample at C.

The auger holes at B, and E were taken directly over the filled-in channel. This soil was very easy to auger. Site B contained orange-brown clay with no identifiable sand; a few small quartzite cobbles were at observed at 0-35 cm and are depicted in Figure 4.9. From 35-65 cm, the soil changes to a blackish-brown color and becomes a sandy clay loam. Water was observed at about 65 cm. The soil beneath 80 cm changes to

light gray, and can be classified as coarse alluvial gravel and sand. The auger could not penetrate below 98 cm because of cobbles.

The relatively greater depth penetrated by the auger confirms that this hole was made within the confines of the old channel. As mention in Chapter 2, fill soils removed from the current channel were stored together on site during the excavation. The movement broke up and mixed the soil allowing for the relative ease of auger penetration. However, the variability of fill material was probably not evenly mixed. This means pockets of both fine and coarse material may retain their original composition. Below the fill material, it is possible that no auger penetrated the coarser bedload of the buried channel. For Location B, the change in soil color at 35 cm demonstrates that the fill is not homogeneous, and fluctuations in groundwater level may have altered some of these soils even in the brief amount of time since the restoration project.

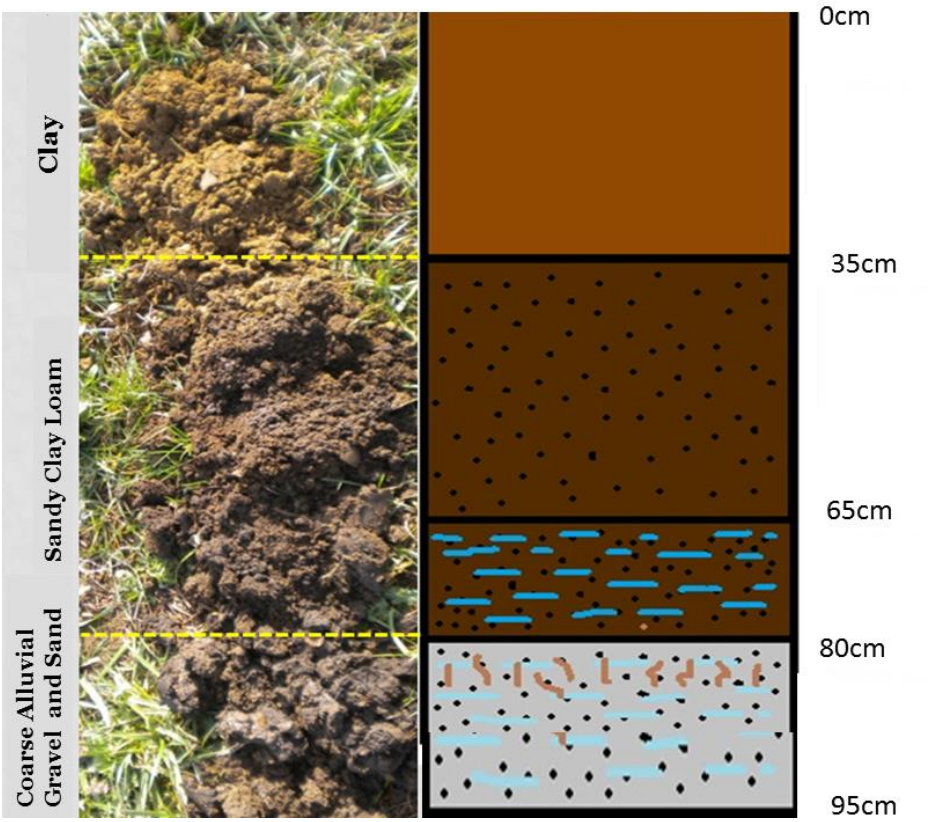

Figure 4.9: Soil sample compared to a picture of the soil sample at location B.

Interpolations of the soil composition at sites B and C can give a rough idea of what should be detected from a geophysical investigation in Figure 4.10. The natural floodplain is represented by site C, while the channel is represented by site B. To summarize the soil sampling, there are at least two layers of fill material consisting of sandy clay. Layers of coarse alluvial gravel prevent an auger from penetrating below the sandy clay loam in areas outside the buried channel. The ability to penetrate deeper into the channel would be due to the fact the channel was already cut into the coarse alluvial gravel. Additionally, the fill material overlying the buried channel became less compacted as it was broken up during the excavation from the current channel. Mixing with other excavated soils occurred as it was being stored and relocated. The horizon that

defines the channel is sandy clay loam which penetrates the water table. Auger holes were terminated due to an abundance of cobbles below the water table. The similarity in top layer of penetrable soil in both the filled-in channel and the undisturbed floodplain suggests a fill soil was used to flatten the landscape or silts and clays were alluvially deposited on the floodplain after the channel was filled since there was little development of soil horizons.

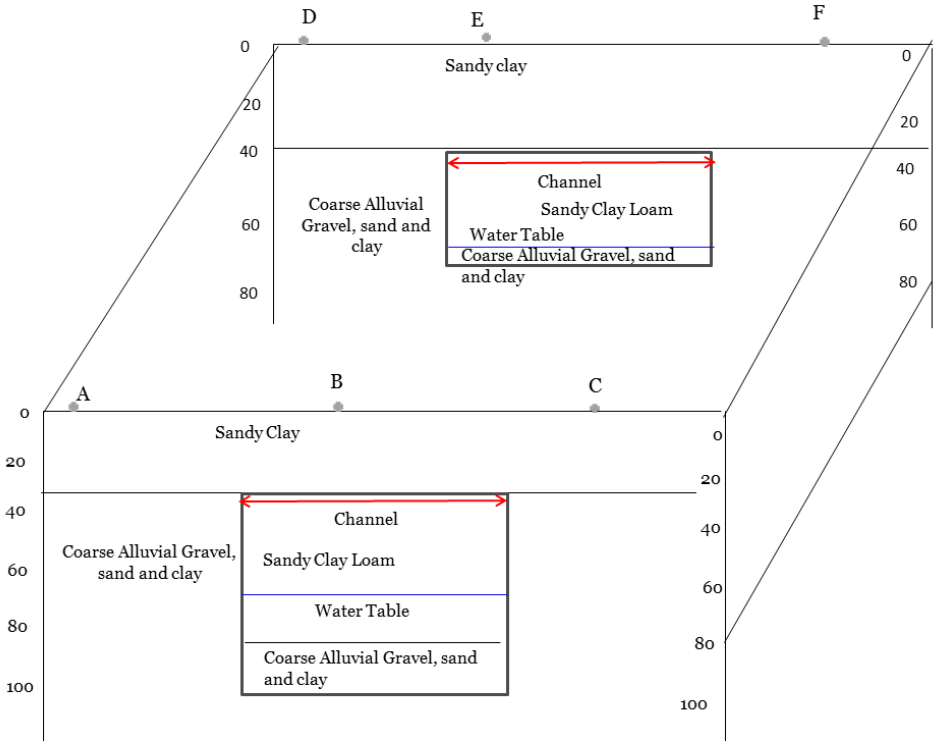

Figure 4.10: Model of subsurface composition (depth in cm).

4.2 Data Collection

As stated earlier in Chapter One, the thrust of this research was to detect and map the buried segment of Burd Run using near-surface geophysical technology. This section provides a detailed description of the specific equipment of the three geophysical techniques and methodology used for data collection.

4.2.1 Electrical Resistivity (ER)

The OhmMapper from Geometrics, Inc. was used along the same transects as the topographic survey. The OhmMapper is made up of a main console, one transmitter, and four receivers that can be connected via cable connectors. The primary components of the OhmMapper are set up in the same manner as Figure 4.11. As described in Chapter 3, the OhmMapper uses a capacitively coupled dipole-dipole array. One dipole in the system consists of the receiver with a dipole cable on each end, while the other uses the transmitter set up in the same fashion. The depth of investigation (DOI) increases with increased dipole length and rope length. For this study, four receivers were connected in series with a dipole length of 5 m. The 5 m cable size is the shortest length available with the OhmMapper. As such, it allows for the shortest dipole length and sets the investigation at comparatively shallower depths. A shallow investigation also allows for better resolution since an increased dipole length increases the vertical spacing between each reading. The receiver collects data from the signal emitted from the transmitter frequency of 16 kHz. A non-conductive rope connects the transmitter to the receiver to prevent electrical current from travelling directly to the receiver, allowing the current to

travel through the ground. The study used a non-conductive rope attached at a length of 1 m to further decrease the DOI.

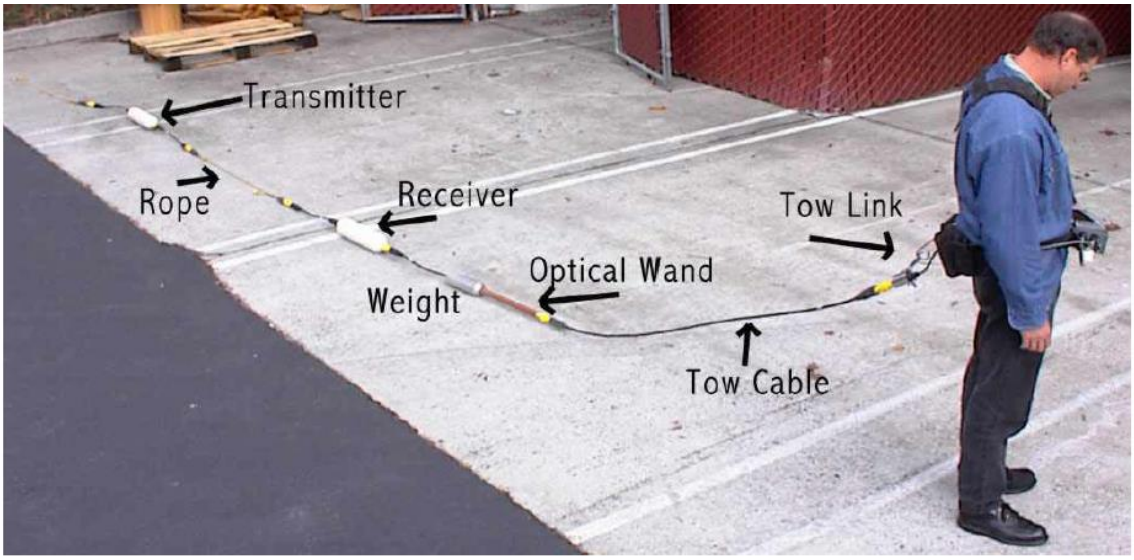

Figure 4.11: The setup of OhmMapper system with one receiver (Geometrics, Inc. 2001).

Four receivers were used in order to collect data at four depths and interpolate the area between the measured depths. The console, receivers, and transmitter were turned on and the OhmMapper data collection was completed. The survey was performed in mapped survey mode to allow for multiple transects to be mapped. Data from the OhmMapper are collected continuously, sending two signals every second. The OhmMapper determines horizontal distance by manually marking points every 10 m. The OhmMapper was towed unidirectionally along the five transects traversed in the topographic survey, but continued until the transmitter passed over the entire channel. These parameters allowed the OhmMapper to create a vertical profile along each transect. The field data were transferred to the computer and processed using the MagMap2000 and Res2Dinverse software.

4.2.2 Ground Penetration Radar (GPR)

The Ramac X3M Ground Penetrating Radar (GPR) from Mala Geosciences, Inc. was used in this investigation because, similar to the OhmMapper, it collects continuous data along each transect. The entire GPR system is composed of 4 shielded antennae (100 MHz, 250 MHz, 500 MHz, and 800 MHz), an X3M Control unit, a MALA rough terrain cart, a sled with a measuring wheel, a RJ45 cable, a laptop computer with Ground Vision software, and towing rods with a waist buckle and shoulder mount. While these four antennae cannot be used simultaneously, they can be switched out to alter depth of investigation and resolution. For this study, two antennae were used: The 100 MHz and the 250 MHz. The 100 MHz and the 250 MHz antennae were chosen to penetrate soils with high clay content. Lower frequency antennae have the ability to penetrate deeper although with less resolution than its higher frequency counterpart.

Due to its larger size, the 100 MHz antenna was dragged on a sled, with all the other accessories assembled as shown in Figure 4.12. The control unit was turned on and allowed to warm up during a trial run. Proper settings were adjusted using the Ground Vision software. Signals are released by a trigger connected to the measuring wheel and can be adjusted to go off at certain distances. The trigger interval for the 100 MHz antenna was 5 cm. The time window for this investigation was 397 while the 444 samples were taken. The sampling frequency (MHz/unit time) for the 100 MHz antenna was set at roughly eleven times its antenna frequency at 1117.24 MHz/ns. Data from the GPR survey were transferred to a computer and processed with RadExplorer software.

Figure 4.12: The 100 MHz GPR antenna being towed on a sled.

The 250 MHz antenna was pushed on a cart (Figure 4.13), and the proper settings were readjusted to a 250 MHz frequency using the Ground Vision software. The trigger interval was set to 2.5 cm, and the sampling frequency for the 250 MHz antenna was set at roughly ten times its antenna frequency at 2694.08 MHz/ns. The time zero was 51495 ns. The GPR survey was performed for 50 m along the same topographic and ER transects as described earlier. The data collected from each antenna provided a vertical profile of the buried stream channel.

Figure 4.13: The 250 MHz antenna being pushed on a cart.

4.2.3 Electromagnetic Induction (EM)

A wide variety of EM methods are available for geophysical investigations. However, the EMP 400 from GSSI, Inc. (Figure 4.14) was chosen for this study because it is a high resolution, frequency domain, instrument with a short intercoil spacing (1.219 m). This means that it is both easier to use and more efficient for high-resolution, shallow surveys, such as desired for this study. Its high-resolution in the depth range of 0-2 m makes it particularly suitable to the detection of soil conductivities in a shallowly buried stream channel like the one in this study. For the same reason, the EMP 400 has also been used successfully for several archaeological investigations (e.g. Novo et al. 2012).

Figure 4.14: The EMP400 used at the study site.

The EMP400 can collect data at three frequencies between 1 and 20 kHz. This equipment has multiple frequencies in order to collect data at different depths. The lowest frequencies are able to penetrate deeper into the shallow subsurface. The maximum Depth of Investigation (DOI) for this device is around 2 m depending on the earth material being studied. For this investigation a single frequency was enough. The frequency was set to 8 kHz in order to collect data at a depth of approximately 1 m, the depth where the sandy-clay layer that represents the channel (as determined in the soil survey) can be found. Electrical conductivity values measured with the EMP400 are calibrated in reference to an arbitrary point in the field where the instrument is calibrated prior to data collection. This point becomes the zero value from which each successive point deviation is measured in mS/m.

Many variables including field conditions (soil moisture), orientation, dipole moment, and mode are important in data collection. In this study, data were collected on two separate dates to evaluate the effect of soil moisture. The first dataset was collected shortly after a rainstorm event after the grounds had become saturated. The second was collected during a period of dry soil conditions. The results were intended to portray the difference between saturated and unsaturated field conditions in order to determine which conditions best isolate the buried channel.

The EMP400 was held parallel to the transect known as in-line orientation. This orientation provided better assurance that each data point was collected along its given transect. When the antennae coils are placed parallel to the ground, the primary field propagates perpendicular to the surface, or vertically. This alignment, referred to as the vertical dipole moment, penetrates at greater depths than if placed perpendicular to the ground (a horizontal dipole moment).

Conductivity measurements were made at discrete points along 21 transects, each 20 m long. The first EM transect was performed along transect 1 of the ER and GPR survey and the last EM transect (21) was performed along the last profile transect (5). All other EM transects spaced every 2 m between the first and last transects. Along each transect, measurements were made at 2 m intervals. High resolution sampling allowed for a detailed conductivity picture from where the buried channel could be identified on the basis of anomalies. The collected EM data were recorded into a field notebook and returned for processing and analysis in ArcGIS10 and Surfer10 software.

Chapter V
ANALYSIS AND RESULTS

5.1 Introduction

As discussed in previous chapters, the three geophysical methods used in this study include Electrical Resistivity (ER) Survey, Electromagnetic Survey (EM), and Ground Penetrating Radar (GPR). This chapter presents detailed results of the analyses and interpretation for each geophysical method.

5.2 Electromagnetic Survey

As discussed in Chapter 4, the EM survey was conducted for 21 transects each 20 m in length. Data from two periods (wet and dry) were used to create separate maps of the differences between saturated field and unsaturated field conditions in order to determine which conditions best isolate the buried channel. Below, the results acquired from each period are discussed.

Figure 5.1a shows the EM result for the day following a storm. The results of tests in the EM survey were spaced 2 m apart. These points were entered into ArcGIS10 and Surfer10 software for interpolation. A qualitative comparison of interpolation methods, available in Surfer10 (Appendix B), determined that the Modified Shepard Interpolation method was the most accurate method to create Figure 5a. As seen on the legend, conductivity varied from 5 to greater than 25 mS/m over the surveyed area. The range of electrical conductivity values represents the variation of subsurface soil composition. Generally, the contrast in conductivity is insignificant across most of the field. The one exception lies in the northwest corner, where conductivity values that range between 17

and 27 mS/m. These elevated values correspond to the location of an exposed manhole cover. The presence of the manhole cover created higher conductivity values in its vicinity that masque the minute differences in conductivity between the channel fill and natural floodplain soils. Despite the near-uniform conductivity pattern, slightly elevated conductivity values (areas in yellow) around the middle portion of the figure are noticeable. This is roughly where the buried channel lies. However, the conductivity contrast is not sharp enough to fully delineate the channel. This low contrast demonstrates how saturation of the ground overpowers differences in soil conductivities and confirms the findings of other studies (e.g. Grandjean et al. 2011) that conclude dry conditions are necessary to observe strong differentiations in soil types with the EMP400.

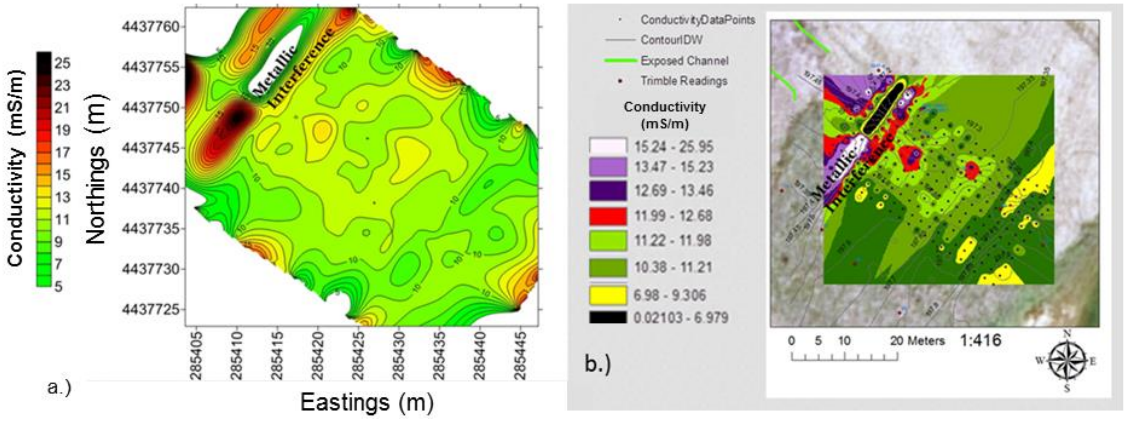

Figure 5.1: Conductivity anomalies under saturated soil conditions, created with; a.) Surfer 10, and b.) ArcGIS 10 software.

Figure 5.1b used the same data as 5.1a, but ArcGIS10 was used to further the comparison of interpolation methods. Since ArcGIS is not equipped with the Modified Shepard interpolation method, the map presented in Figure 5.1b was derived with the Inverse Distance Weighted (IDW) Interpolation method. IDW distributes the interpolated data so that the interpolated surface is influenced more by near values than more distant

values. One drawback to IDW is that this method interpolates well beyond the limits of the study area to create a rectangular grid. Inputting the results into a second interpolation method verifies that the anomalies are products within the data and not simply created by methods of the interpolation. Results of this interpolation method generally agree with those of the Modified Shepard Method applied in Surfer 10 software. The interference caused by the manhole cover is present in the northwest, while a field of minor changes in conductivity lies within the southeast section of the primary study area. Two anomalous conductivity areas (11-14 mS/m; bright red spots around the middle) stand out mainly because of the color representing them. These anomalous areas were caused by water puddles.

Figure 5.2 presents results of a survey conducted after a week without rain. Unlike the first exercise, readings were no longer taken close to the manhole cover to avoid data distortion. The difference in EM response, interpolated with the Shepard Method, in Figure 5.2a is clear. While conductivity on this day ranged from 4 to 16 mS/m, a linear anomaly of elevated conductivity (greater than 11mS/m) is depicted running northwest-southeast. Conductivity values within this anomalous path were generally interpreted to represent the soil composition within the buried stream channel at a single depth (e.g. Danielson et al. 2003).

Outside of the strong anomalous zone of the buried channel, conductivity variations are indicated by the predominantly green and blue shades (northeast side image). These variations are associated with compositional differentiations in the poorly-graded gravel and sand, mixed with clays outside of the channel. The few areas of elevated conductivities observed beyond the borders of the channel, similar to those of

lower conductivities within the channel, are expected because of the human activity associated with in-filling the channel. Such disturbance may have changed water seepage and soil saturation patterns to create the inhomogeneities detected by the EM method.

Results in Figure 5.2b depict similar anomalies including a similar linear pattern of high conductivity (greater than 11 mS/m). This anomaly is observed when the IDW was used in ArcGIS 10 to produce the conductivity contours.

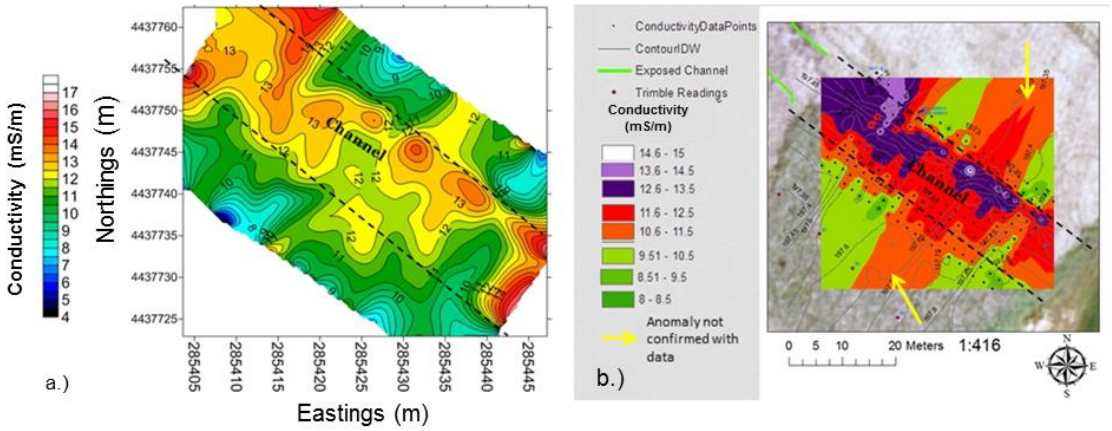

Figure 5.2: Conductivity anomalies under less saturated soil conditions, created with; a.) Shepard interpolation in Surfer 10, and b.) IDW interpolation in ArcGIS 10 software. The black dotted lines estimate the width of the anomaly in comparison to the exposed channel.

The results are similar even though two different software (Surfer vs. ArcGIS) and two different interpolation methods (IDW vs. Shepard) are used. This is an indication of the integrity of the conductivity data collected in the field.

5.3 Electrical Resistivity Survey

The ER survey was conducted along 5 transects which varied in length, and were angled perpendicular to the buried channel. Transect 1 was the closest to the exposed streambed and data collection was spaced 10 m along each successive transect from this

point. The raw data was downloaded from the OhmMapper, and ran through an interface program (MagMap2000) in order to be readable by a processing program. The processing program (Res2DInverse) inverted the data creating the apparent resistivity and final models. The final models were obtained by comparing the calculated data with the observed (raw data) and represents the true distribution of subsurface resistivity underneath each transect.

All figures in this section show the 2-dimensional resistivity sections obtained on their given transect. The top image (a) shows the raw data, the middle (b) shows the calculated apparent resistivities, and the final model is shown in (c). The clean images of each transect are presented in Appendix C (Section 1). Below, the interpreted results acquired on each individual transect are presented and discussed.

As marked up on Figure 5.3 (on the next page), four anomalous areas are identified and interpreted to represent different soil types. Coarse alluvial gravels are found on both sides of transect 1. The resistivities associated with these gravels are generally greater than 250 Ωm. Such gravels were transported by Burd Run as it carved out the valley and were also identified by Nyquist et al. (2008). The center of the transect has two anomalies with comparatively lower resistivities (112-207 Ωm). These anomalies represent the sandy clay loams discussed in Chapter 3, and by Nyquist et al. (2008). Another area of moderate resistivity (180-281 Ωm) lies slightly to the southwest, reaches a depth of 2 m, and is associated with the buried channel.

In the literature, resistivity anomalies interpreted to represent buried channels differ from location to location depending on the composition of the stream's bedload and its surroundings. Baines et al. (2002), for example, identified a buried stream

channel on the basis of a high resistivity anomaly. In other instances, such as Mahmoudi and Gabr (2009), a low resistivity anomaly is interpreted to be consistent with the detection of a buried channel.

When the dimensions of the resistivity anomaly associated with the buried channel is compared to Herrmann's (1999) measurements, the 6 m anomaly width lies in the range (4-6 m) measured prior to burial. Herrmann (1999) measured the depth of the channel (from top of the bank to channel bottom) as roughly 1 m, while the depth to the bottom of the anomaly is around 2 m. Therefore, roughly 1 m of fill rises above the banks of the channel. Above the anomalous zone, interpreted to be the channel, the resistivity range (181-281 Ωm) represents a mixture of two soil masses. These soils would have been mixed during the restoration to create the mound over the channel.

Anomalies beneath most of the transect, including beneath the channel, have considerably lower resistivities (less than 100 Ωm) common to clay; which is most likely residual in nature, having decomposed from the limestone beneath and agrees with the findings of Nyquist et al. (2008).

While the operator of the OhmMapper started at one end of each GPR transect, measurements started at an indiscreet point behind him. Measurements had to be compared to GPR results to verify and geo-locate each anomaly along the five transects.

The resistivity distributions, and or anomalies observed on transects 2-5 are very similar to those already described for transect 1, with only minor variations. This is understandable because of the area surveyed; not much heterogeneity can be expected. To avoid repetition, the resistivity models for transects 2-5 are simply shown (Figures 5.4-5.7) and not discussed.

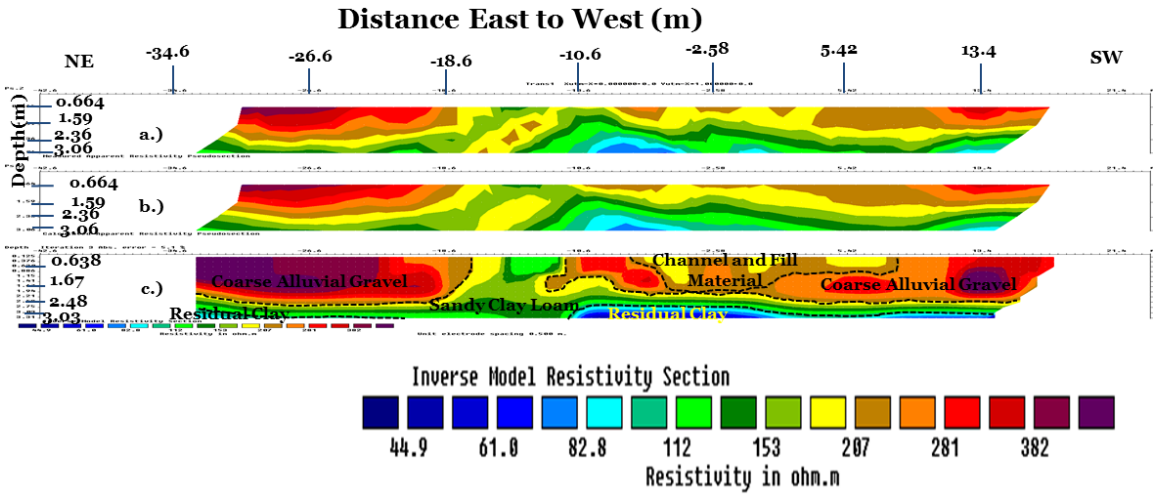

Figure 5.3: a.) Raw apparent resistivity data, b.) calculated apparent resistivity, and c.) interpreted inverse model resistivity results for transect 1.

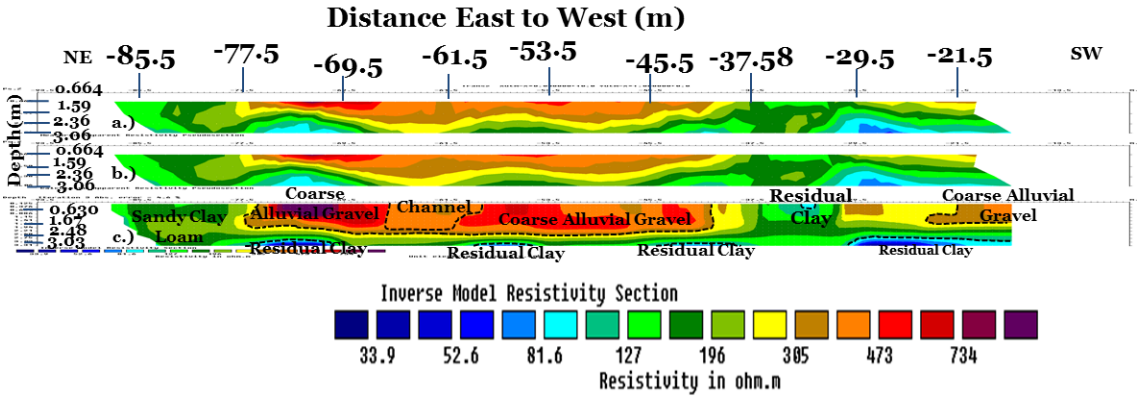

Figure 5.4: a.) Raw apparent resistivity data, b.) calculated apparent resistivity, and c.) interpreted inverse model resistivity results for transect 2.

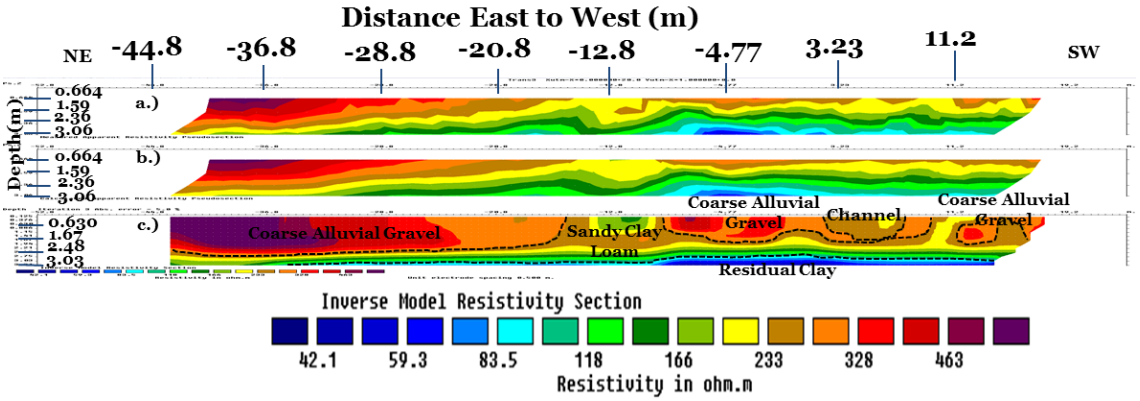

Figure 5.5: a.) Raw apparent resistivity data, b.) calculated apparent resistivity, and c.) interpreted inverse model resistivity results for transect 3.

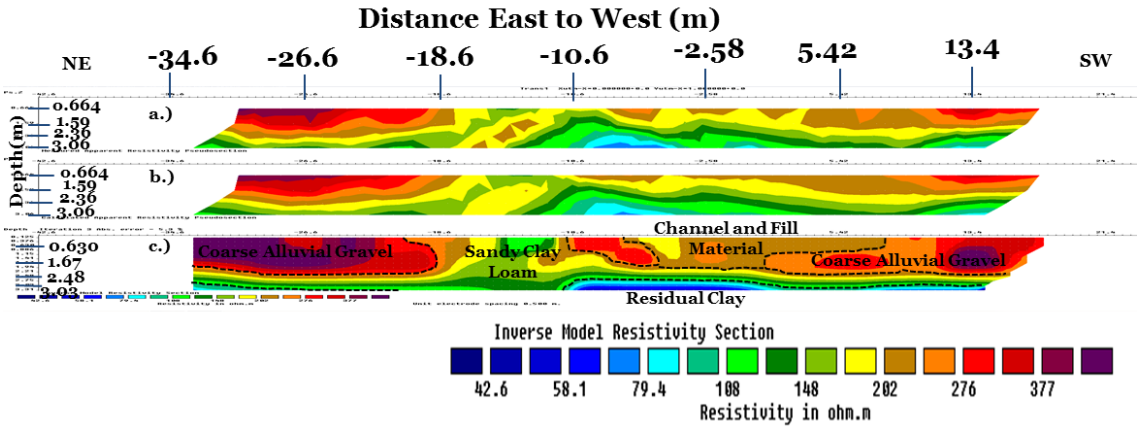

Figure 5.6: a.) Raw apparent resistivity data, b.) calculated apparent resistivity, and c.) interpreted inverse model resistivity results for transect 4.

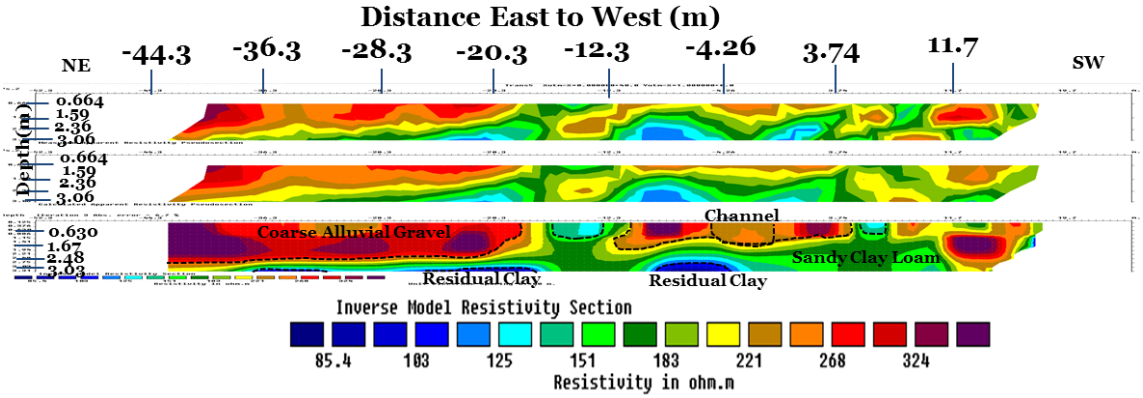

Figure 5.7: a.) Raw apparent resistivity data, b.) calculated apparent resistivity, and c.) interpreted inverse model resistivity results for transect 5.

Electrical resistivity profiles in this study agree with the upper two resistivity layers identified by Nyquist et al. (2008) in greater resolution. Sandy clay loam ranges in resistivity from 105-221 Ωm in the study area. Pure residual clay ranges below 100 Ωm. The greater resolution allows for the detection of an anomaly: The anthropogenically filled channel. Resistivity in the filled channel varies from 180 Ωm to 473 Ωm and occurs throughout all five transects. The variation suggests that the fill within the channel varies greatly in composition. Results from all transects define coarse alluvial gravels near the east and west sides as varying in resistivity from 221- 1000 Ωm.

5.4 Ground Penetrating Radar

Ground Penetrating Radar (GPR) survey was conducted on the same transects as the ER survey. However, the GPR lines were slightly shorter (50 m) than those ran for the ER because of the ER's tow array. Two antennae with 100 MHz and 250 MHz frequencies were used for the GPR survey. The data were processed and analyzed with Radexplorer software using the following filters in the order recommended by RadExplorer: DC removal, time zero adjustment, trace edit, background removal, and topographic correction. DC removal, trace edit, and background removal all remove interference that is more pronounced than the data and thus presents a clearer image. Time zero adjustment adjusts the time axis (Y-axis) so that zero equals ground level. Since GPR perceives ground as flat, data must be adjusted by means of topographic correction. Consequently, the topographic data collected with the total station were used to correct the GPR data for surface elevation changes using the topography filter in RadExplorer. The interpreted results acquired on each individual transect are presented and discussed below. The produced radargram for each frequency is included in Appendix C (Section 2).

Figure 5.8a shows the GPR radargram obtained on transect 1 using the 100 MHZ antenna. A radargram is a collection of traces that represent travel times of the electromagnetic pulses which are emitted from the transmitting antenna. Unlike the EMP400 which reports data in numerical values (mS/m), the higher frequency GPR reports data as dielectric responses. The features of interest on the radargram are the brightly colored (white) as opposed to the dark (background) because they represent high reflectivities. When a GPR signal of known velocity hits a subsurface target it is reflected

back to the receiver. The two-way travel time of the signal is used with its velocity to determine the depth of the target. Hence, the radargram can be used to identify zones of strong reflectivities (anomalies) along a transect (horizontal scale) and their depth of burial (vertical scale).

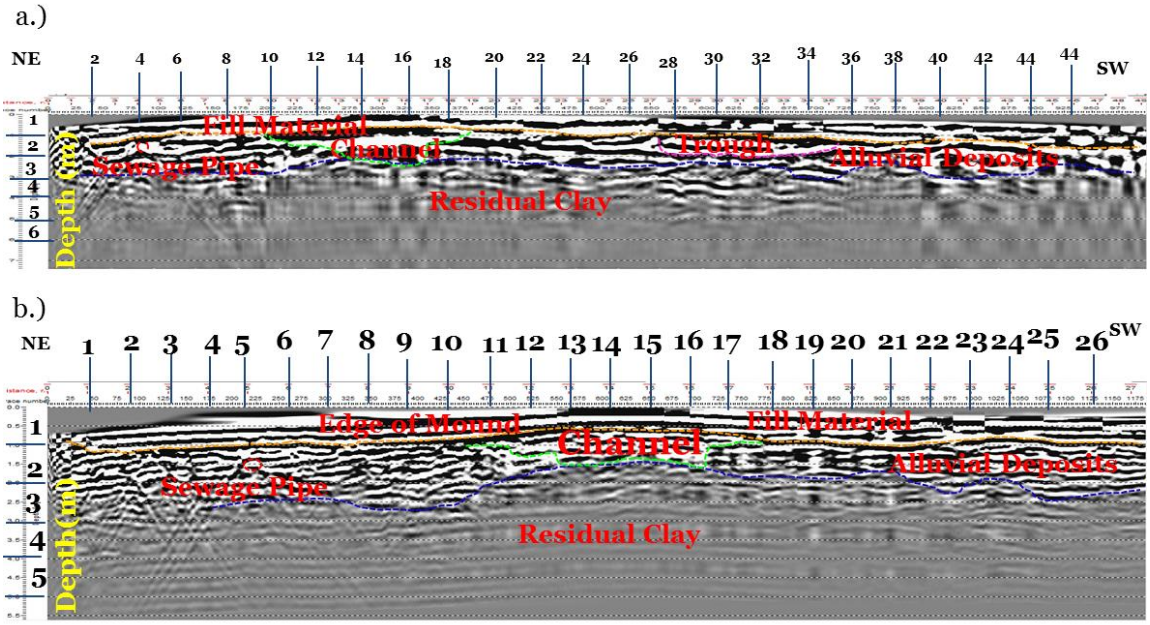

Figure 5.8: Interpreted GPR radargrams using a.) the 100 MHz and b.) 250 MHz antennae along transect 1.

The most noticeable feature in the radargram (Figure 5.8a) is the lack of response occurring below 3 m across the whole transect. Certain materials, such as clay, create interference in the data by absorbing or attenuating the radar signal. This is noticed from the sudden absence of reflectivities on the radargram. The inability to interpret data beneath the channel may be due to saturated clay, similar to the interference caused by the clay facies which were detected in Stevens and Robinson (2007). The depth of the clay can be determined by noting the depth where reflectivities disappear suddenly on the radargram. In this case, clay depths vary across the transect dipping at points and rising to pinnacles at others.

Another noticeable feature is the strong reflectivity zone observed around the depth of 1.5 m and located 4 m from the beginning of the transect. This is aligned with the sewage pipe which runs parallel to the channel. Comparatively, this sewage pipe was too small to be detected by the ER survey.

Note that the near-continuous bright line at the top of the section represents the ground surface (i.e. reflected signals off the ground surface). The patterned, bright, white lines mimic soil layering along the transect. A pattern of lines stretch from the 4-48 m marks and reach depths of 1 m. These lines are fairly thick, continuous, and represent fill material deposited during the restoration project. The thick responses are due to the relatively short period of time the soils they represent have had to be compacted and develop soil horizons. The continuity means these soils haven't recently been disrupted. Below these soils, the reflective lines are thinner and less continuous than the overlying responses. This group of reflections represents natural alluvial deposits of the floodplain.

The alluvial deposits are disrupted by concave pattern of strong reflectivity between the 11 and 17 m marks from the beginning of the profile. This feature is roughly 6 m wide and lies approximately 2- 2.5 m below the surface, and it is interpreted to be the location of the buried stream channel. The shape of the anomalous zone is also consistent with GPR images of channels found in Stevens and Robinson (2007). This shape is also fairly consistent with the geometry of the exposed part of the channel and the channel cross-sections mapped by Herrmann (1999) prior to the restoration work (Appendix A). Furthermore, the 6 m channel width of the anomaly is within the range stated in Chapter 2, and the depth of the channel (from top of the bank to the bottom of the channel) is

approximately 1 m. Within the concave pattern of the channel, reflections are comparatively wider and more continuous than the reflections of surrounding soils.

The radargram for the 250 MHz antenna are shown in Figure 5.8b. This radargram is very similar to the 100 MHz results, with the exception that the 250 MHz antenna produces results with the higher resolution in the near subsurface. Due to this higher resolution, a smaller horizontal length of each transect was analyzed. Therefore, only the first 27 m were analyzed as this was expected to be location of the buried channel.

Similar to Figure 5.8a, in Figure 5.8b a concave pattern of strong reflectivity appears between the 11 and 17 m marks reaching a depth of 2 m. This reflective pattern corresponds to the location of the buried stream channel, but higher resolution shows a shape (a flat bottom and steep sides) more consistent with Herrmann's (1999) cross-sections 12, 13, and 19E in Appendix A. Figure 5.9 compares Herrmann's cross-section 19-E with the 250 MHz radargram from transect 1. Transects 2-5 are presented in Appendix D as the method of comparison and results are fairly similar.

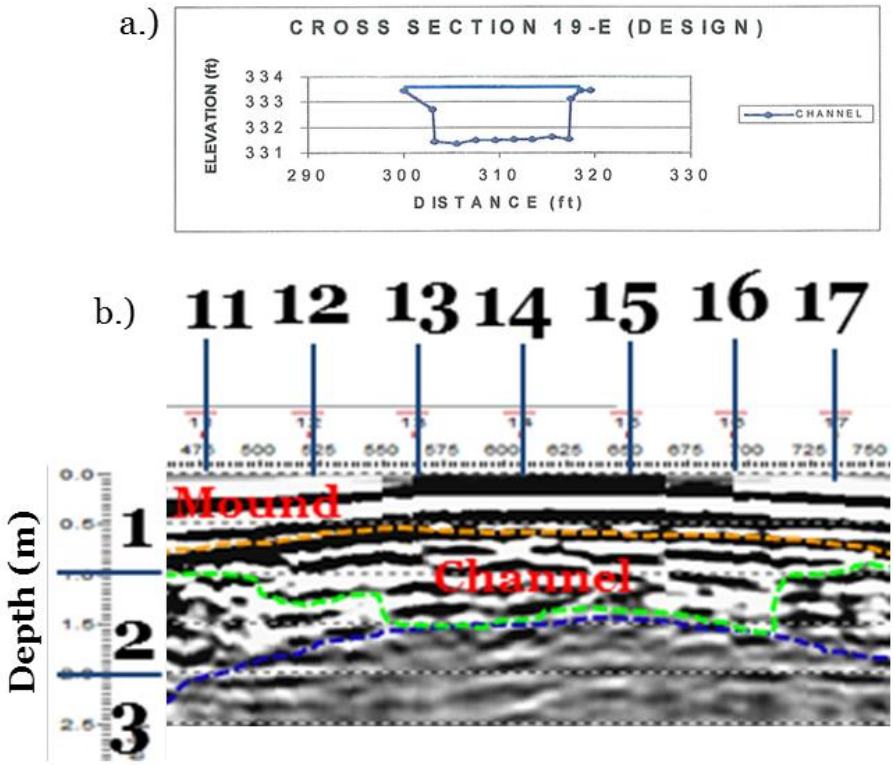

Figure 5.9: A comparison in shape between a.) Cross-section 19-E (Herrmann 1999) and b.) the channel anomaly detected in the 250 MHz radargram from transect 1.

Well stratified fill material dominates the top 1 m of the transect as depicted in the near-horizontal pattern of reflectivities. These organized layers can define an unconformity with overlying alluvial deposits in a floodplain (e.g. Rother et al., 2007). However, a majority of the shallow soil at Burd Run was anthropogenically deposited. Below the top layer, the presence of quartzite cobbles in the underlying alluvial deposits is responsible for the observed uneven pattern of strong reflectivities. A visual comparison of 5.8a and 5.8b reveals the better resolution of the 250 MHz (5.8b). Whereas Figure 5.8a detects only major groups in the subsurface (e.g. changes in soil classifications from sand to clay), Figure 5.8b detects variations within the material (e.g. depositional patterns). The reflective patterns above the banks of the channel are rather flat, which would reinforce the concept of rather homogeneous fill that hasn't been

terribly disrupted nor had sufficient time to develop well the established horizons visible in Figure 4.9. Similar to 5.8a, the sewer pipe also shows up in 5.8b.

The results on transects 2-5 are very similar to those obtained on transect 1 with both the 100 MHz and 250 MHz antennae. Note however, the slight shifts in the position of the anomalies defining the buried channel. This is possible because even though the stream channel is fairly linear, it also lies along a diagonal, thus causing the transects to intersect it at slightly different locations. Otherwise, the anomalies that define the channel look pretty similar. Figures 5.9a&b, 5.10a&b, 5.11a&b, and 5.12a&b, respectively, show the radargrams obtained with the 100MHz and the 250 MHz on transects 2-5. Cleaner (unmarked) radargrams are also show in Appendix C.

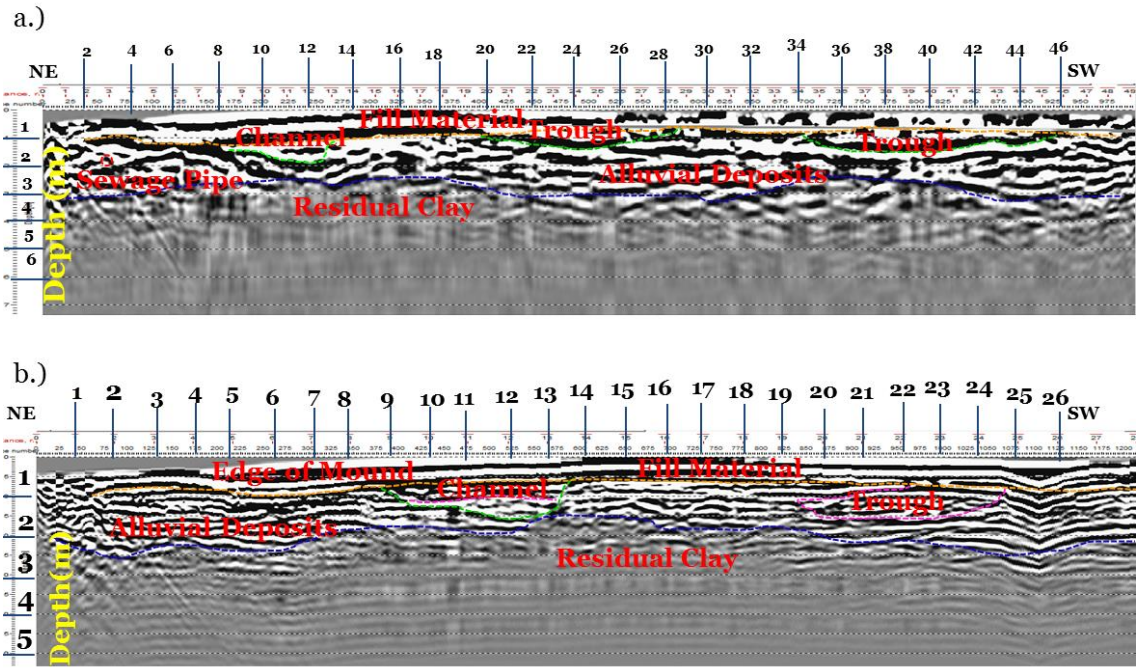

Figure 5.10: Interpreted GPR radargrams using a.) the 100 MHz and b.) 250 MHz antennae along transect 2.

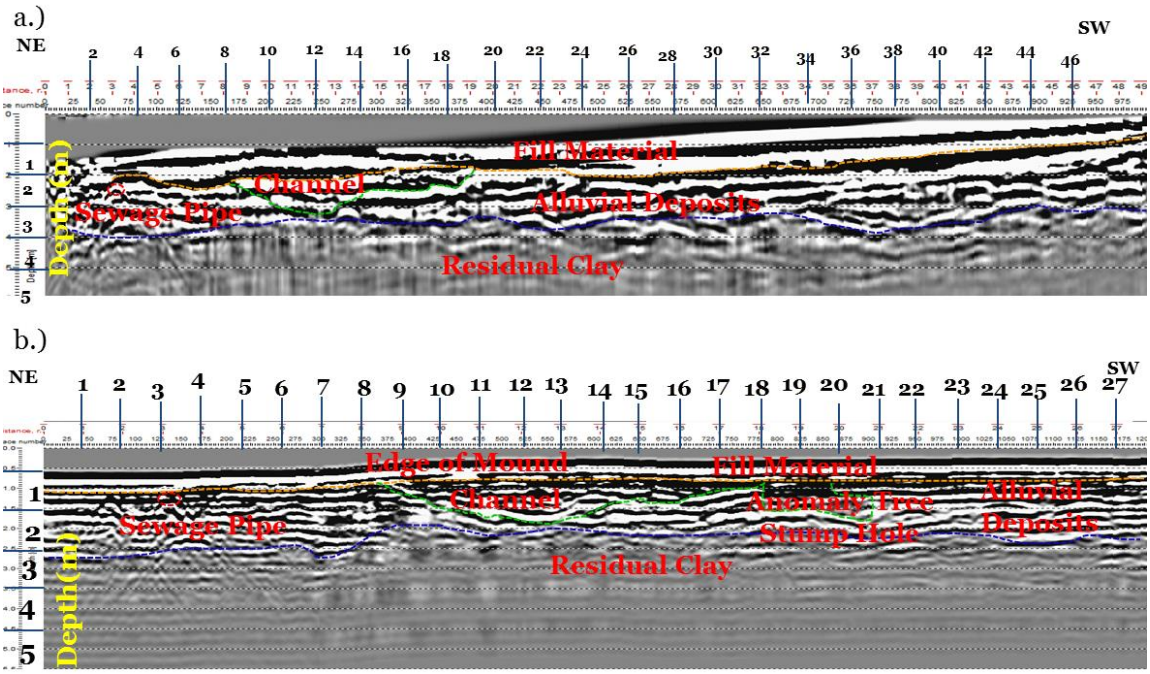

Figure 5.11: Interpreted GPR radargrams using a.) the 100 MHz and b.) 250 MHz antennae along transect 3.

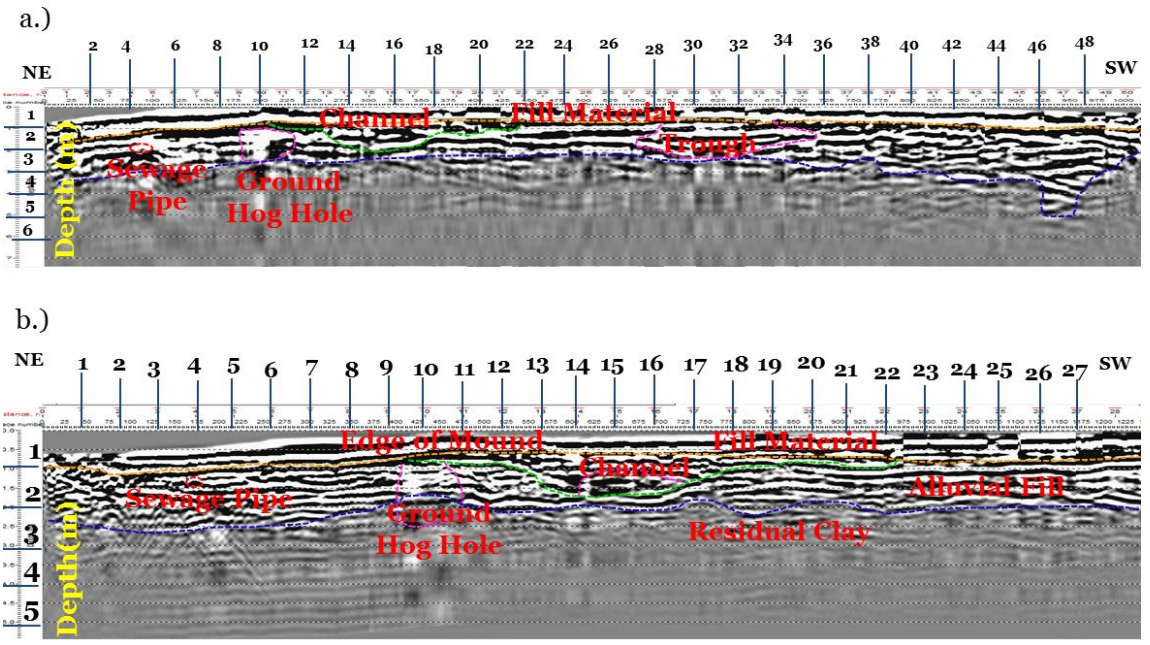

Figure 5.12: Interpreted GPR radargrams using a.) the 100 MHz and b.) 250 MHz antennae along transect 4.

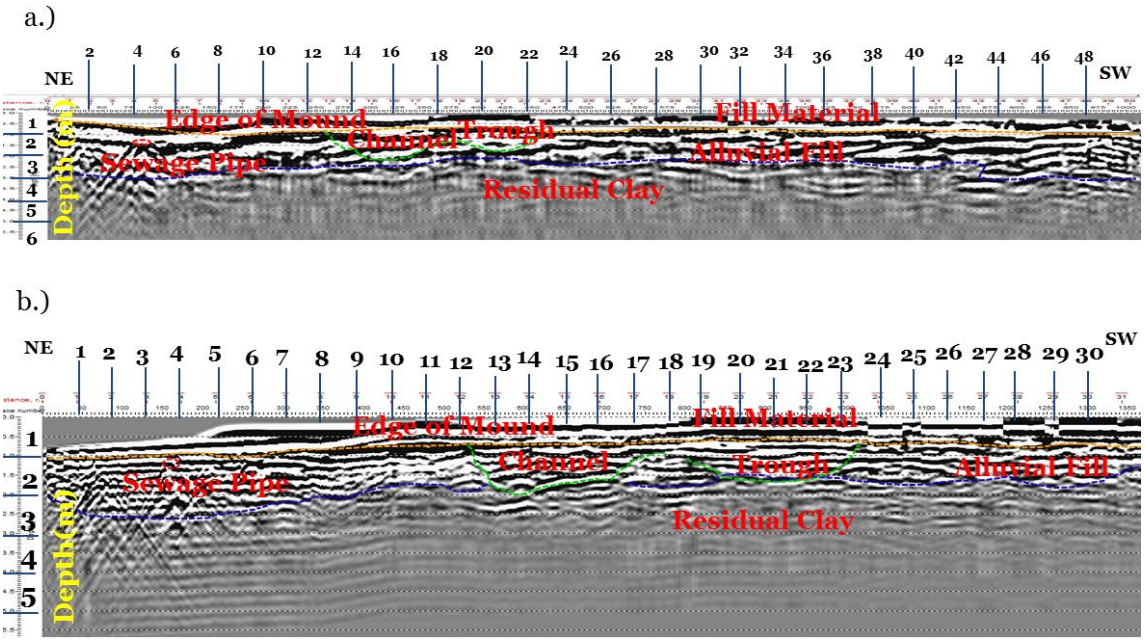

Figure 5.13: Interpreted GPR radargrams using a.) the 100 MHz and b.) 250 MHz antennae along transect 5.

5.5 Integrated Results

For purposes of comparison, anomalies produced or obtained from all three geophysical methods are integrated to assess the performance of each method against the others. Although this was done for all transects (1-5), only results for transect 1 are discussed fully here. This is because the linearity of the buried channel investigated and the relatively small size of the study section makes the results very similar. Images depicting the results of transects 2-5 are included in Appendix E.

Figure 5.14 presents the interpreted results for ER and for the 250 MHz antenna of the GPR in a side by side comparison. However, an overlay of these methods can display exactly where the dimensions of anomalies are aligned. As such, Figure 5.15 compares the interpreted results of all three methods in two comparative overlays for transect 1. In 5.15a, the conductivity anomaly map obtained with the EMP400 is shown. The interpretation is already given in section 5.1.2. The little black dots are conductivity

reading points which were interpolated using the Modified Shepard method. The black solid lines enclose the linear anomalous zone that is interpreted to be the buried channel.

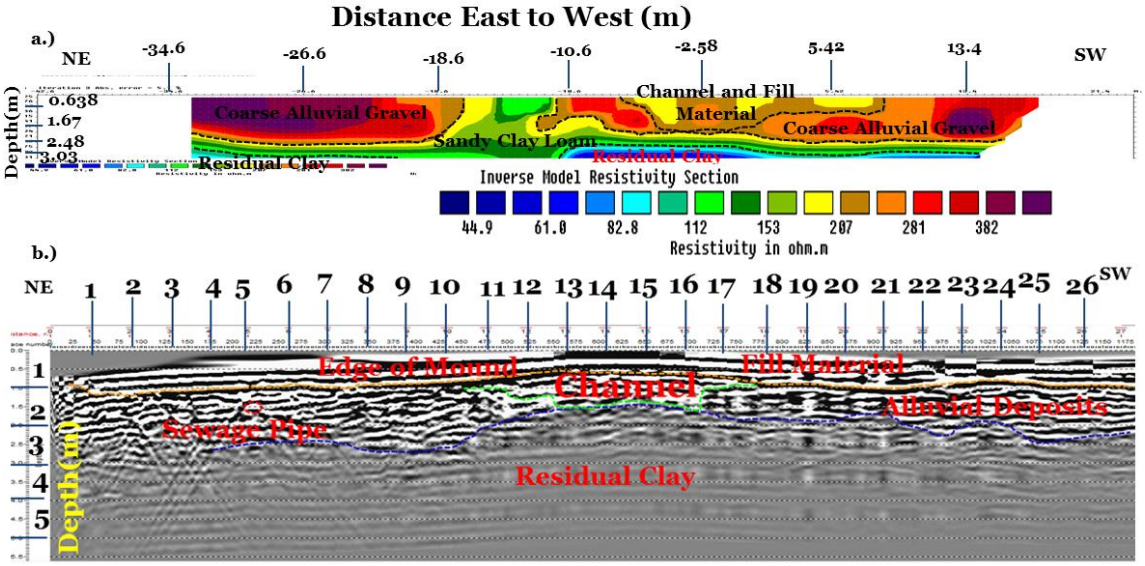

Figure 5.14: A comparison of interpreted results of a.) the final resistivity model and b.) 250MHz GPR antenna for transect 1.

Figure 5.15b shows the interpreted results of resistivity overlaid on a GPR radargram. It should be noted that this comparison is limited because the spatial extent of data for each method is slightly different. However, the broad zones of anomalies correspond and that is the essence for this combination. For example, the resistivity anomaly (orange to yellow area on ER section) corresponds to the concave anomaly dictated with GPR. These were both interpreted and confirmed to be the location of the buried channel.

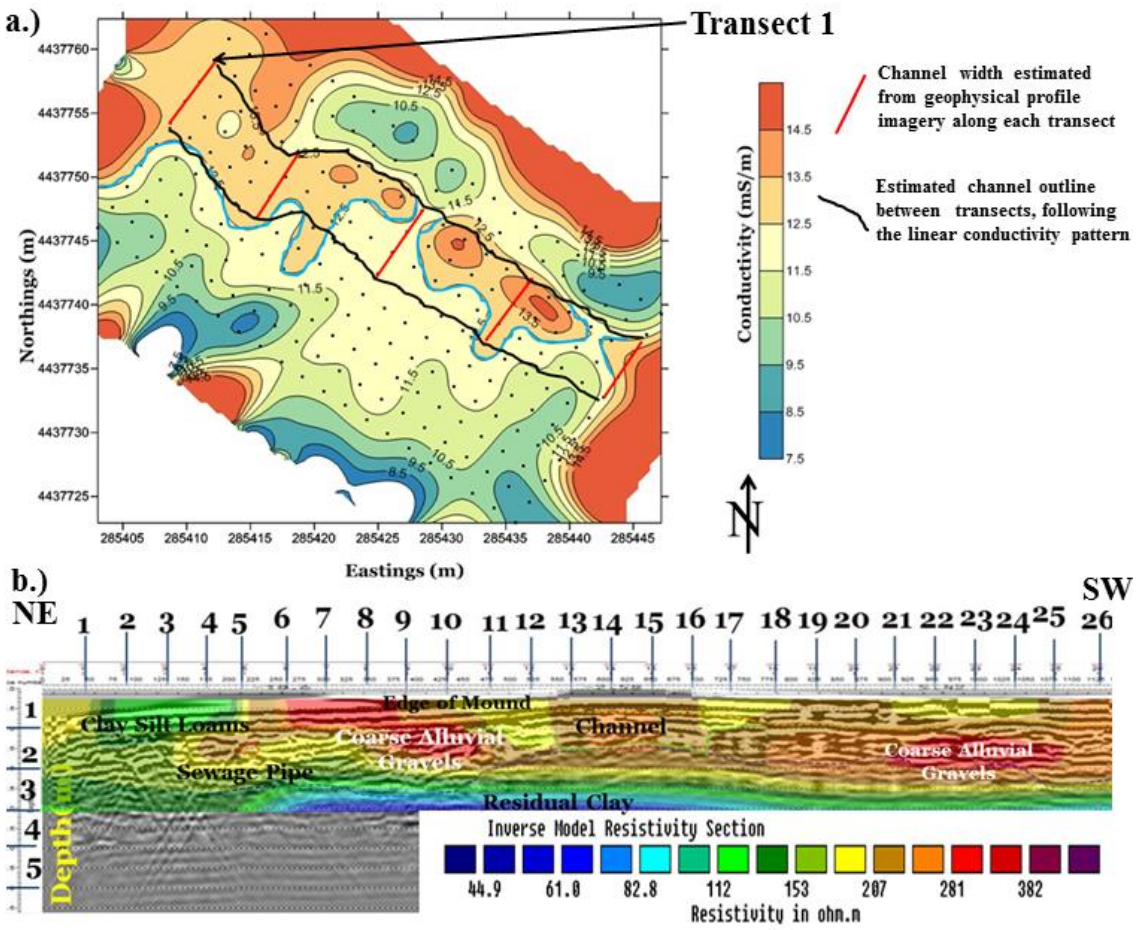

Figure 5.15: A comparison of the results from a.) EM, and b.) ER and GPR (250 MHz antenna) for transect 1

Other anomalous areas for both methods, such as the sewage pipe and the manhole covers are also consistent. A curious occurrence places the sewage pipe reflections in close proximity to a low resistivity anomaly in this transect. The reflection appears at a slightly greater depth than the low resistivities. In transects 4 and 5 (presented in Appendix D), the area of low resistivity is directly above the sewage pipe.

Unlike the ER and GPR, that show interpolations along a line, the EM interpolation is over an area which makes it impossible to overlay all three methods. Note the red lines in between the bold black lines on the EM section. The red lines represent

the channel widths interpreted from the ER and GPR surveys. The black lines interpolate the channel width between each transect's estimated channel width. The EM method also successfully detected the buried channel.

When compared to the surrounding natural landscape, the EM results portray the channel as a high conductivity anomaly. Comparatively, ER results display the channel feature as possessing low resistivity. These results verify the inverse relationship of conductivity and resistivity. Therefore, it is safe to conclude that all methods were successful in detecting the buried channel. See Appendix D for results on transects 2-5.

Chapter VI

Summary and Conclusions

Research was carried out at a stream restoration site near Shippensburg University in south-central Pennsylvania in the Burd Run floodplain. The major goals were to successfully detect the a stream channel that was filled in during a stream restoration project using three near surface geophysical methods and to compare each method's strengths in resolving this subsurface feature. The geophysical survey was performed using EM, ER, and GPR. This chapter summarizes the capabilities of each method, and then compares the results of all three methods for each transect. From these comparisons conclusions are drawn and future research suggested.

6.1 Electromagnetic (EM) Survey

Electromagnetic methods (EM) work by sending a primary electromagnetic field through a transmitter coil into the ground, which induces a current in the underlying earth materials that it passes through. The current then produces secondary EM fields that are recorded via a receiver coil. For this survey, the EMP400 from GSSI, Inc. was used at a single frequency, in a stationary manner, to cover 21 transects across the buried channel; each was 20 m in length. This survey was conducted the day after a storm event, and a week after a storm event as to determine the effects of soil moisture.

Results from the day after the storm depict a rather homogeneous field since saturated conditions caused ground conductivities that varied very little, making it impossible to dictate the buried channel. The most notable anomaly occurred due to the interference caused by the proximity of an exposed manhole cover. Results from the survey conducted during a dry period showed conductivity differences (anomalies) that led to the detection of the buried channel.

6.2 Electrical Resistivity (ER) Survey

The ER method operates by sending electrical currents into the ground via a transmitter. These currents travel through various subsurface materials and eventually are detected by receivers on the surface. For this survey, the OhmMapper from Geometrics was used over five transects that were oriented perpendicular to the channel.

The ER method was beneficial in identifying subsurface materials at depth. Identification of the subsurface materials is crucial in understanding how surface features formed. Results from the ER survey produced five profiles of the buried channel, in which the channel was represented by an anomaly of relatively low resistivity. These results not only produced the anomalies associated with the buried channel, but other aspects of the surrounding a floodplain on a karst landscape. Soils within 2.5 m of the surface are mostly alluvial, and include anomalies representing coarse alluvial gravels and sandy clay loams. Soils below this point were generally associated with residual clay. As noted in Chapter 2, these clays formed through the dissolution of the underlying

limestone of the Rockdale Run Formation. However, the bedrock was not detected in this study.

Although the OhmMapper is a capacitively-coupled device with limited depth capabilities (3-10 m), this drawback was not problematic in such a shallow investigation. Features which were detected at the limits of the DOI included the top layer of fill and alluvial material (when close to the surface) and residual clay (at greater depths). Determining the lateral location of anomalies along the transect is challenging as the location of transmitter and receiver at the start and termination of each transect weren't geospatially marked. Results of other methods helped define these for the ER survey. The length of the array and the distance between receivers could possibly create design challenges for surveys in a limited space. This study site and the target turned out to be of sufficient size. Therefore, the ER survey was able to overcome these obstacles and produce successful results.

6.3 Ground Penetrating Radar (GPR) Survey

GPR transmits short-pulsed electromagnetic waves from a surface antenna into the ground. These transmitted signals get reflected off subsurface objects and return to a receiver. A Ramac X3M Ground Penetrating Radar (GPR) from Mala Geosciences, Inc. was run along five transects (each 50 m long) that were point perpendicular to the channel. Two antennae (100 MHz and 250 MHz) were used.

All ten transects successfully detected a concave upward reflective pattern which denotes the channel. The 100 MHz antenna was able to detect the entire channel, but at a lesser resolution. While portions of the channel's bottom were clouded by the clay

content of the soil, results detected by the 250 MHz antenna were successful in high resolution depictions of the multiple layers within the buried channel.

Two minor limitations created noticeable interference in the results. Parabolic attenuations were created by an adjacent sewage main, but did not disrupt the detection of the channel. Clay within the soil, (especially residual clay) also limited the depth of penetration, and created minor interference in the buried channel. Nevertheless, the channel was detected and that was the goal of this study.

6.4 Conclusion

Shallow electrical geophysical methods were successful in detecting the buried channel, within a floodplain, at Shippensburg Township Park. The use of multiple geophysical methods allowed for a strong comparison of anomalies representing the buried channel; in which, each method elaborated on the knowledge of features gained by the others. Evidence of each method's success is presented below.

EM results portrayed a 6 m wide linear anomaly of elevated conductivity within the study area. This linear anomaly is aligned with the exposed channel. The linear anomaly was detected due to a difference in soil composition between the buried channel and surrounding areas.

ER results excel at portraying differences in composition between the channel and surrounding areas at depth. Results portray features which suggest that the buried channel was carved into an alluvial floodplain on a karst landscape.

GPR is a reliable method for portraying the dimensions of the channel due to its high resolution. Banks of the channel are buried beneath 0.5-1.0 m of fill material from the restoration project. Remnants of the channel are 4-6 m wide.

The three methods portray similar dimensions within the channel when compared to those measured by Herrmann (2009). Furthermore, the combination of the results of each method creates a more accurate depiction of the buried channel. In this respect, the results from one geophysical method can also help validate the results from another (e.g. the detection of an inverse relationship between EM and ER).

With this in mind, the methods used in this study are most powerful when their results are combined in a comparison. Through the use of ER, EM, and GPR, this study suggests that a majority of the buried channel within the study area remains intact and thus detectable with geophysical methods.

6.5 Suggested Future Research

Further geophysical investigations at the study site may be needed to better understand the bedrock configuration. The current study did not seem to locate the bedrock because the focus was on the shallow subsurface around the depth of the buried stream channel. This would determine if dolines exist beneath the areas which lack residual clay.

As the exposed old channel retains water, a hydrogeological study would determine if the buried channel still retains water.

It would be interesting to compare the traditional stake in ground ER method with the results of the capacitively coupled ER system used in this study in order to see which method better resolves the channel.

Another interesting study would be to vary the velocity of the GPR systematically in order to determine which velocity setting best resolves the channel.

For the EM profiler, it would be of interest to use the continuous survey mode as opposed to the discreet mode of data collection used in this study. Another study should also consider using both the horizontal and vertical dipole modes. This study only used the vertical dipole mode.

References

Amhed S, Carpenter, PJ. 2003. Geophysical response of filled sinkholes, soil pipes and associated bedrock fractures in thinly mantled karst, east-central Illinois. *Environmental Geology*. 44:705-716

Andersen NL, Apel DB, Ismail A. 2006 Assessment of Karst Activity at Construction Sites Using the Electrical Resistivity Method (Greene and Jefferson Counties, Missouri)

Andre F, Saussez S, Van Durmen R, Van Leeuwen C, Moghadas D, Delvaux B, Vereecken H, Lambot S. 2010. AGU Fall Meeting. San Francisco, USA

Baines D, Froese DG, Bauman P, Nimeck G. 2002. Electrical resistivity ground imaging (ERGI): a new tool for mapping the lithology and geometry of channel-belts and valley fills. *Sedimentology*. 49:441-449

Becher AE, Taylor LE. 1982. Groundwater resources in the Cumberland and contiguous valleys of Franklin County, Pennsylvania, Pennsylvania Geological Survey, 4th ser., Water Resource Report 53: 67

Burrell J, Gurrula, H Mickus, K. 2008. Frequency Domain electromagnetic and ground penetrating radar investigation of ephemeral streams: case study near the Southern High Plains, Texas. *Environmental Geology* 55(6):1169-1179

Clement WP, Ward AL. 2008. GPR surveys across a prototype surface barrier to determine temporal and spatial variations in soil moisture content. The Handbook to Agricultural Geophysics. CRC Press, Boca Raton, FL, United States. 305-315

Danielsen JE, Auken E, Jørgensen F,Søndergaard V, Sørenson KI. 2003. The application of the transient electromagnetic method in hydrogeophysical studies. *Journal of Applied Geophysics*. 53:181-198

Doolittle JA, Collins ME. 1998. A comparison of EM induction and GPR Methods in areas of karst. *Geoderma*. 85:83- 102.

Geometrics, Inc. 2001. OhmMapper TR1 operation manual. San Jose, CA

Gibson PJ, George DM. 2003. Environmental Applications of Geophysical Surveying Techniques. Boriotti S, Dennis D. New York, NY. Nova Science Publishers, Inc. 137,140. 4.

GoogleEarth. 2012. GoogleEarth imagery for Shippensburg, PA. Date accessed 8/01/2012

GrandJean G and the DIGISOIL Team. 2011. Scientific Synthesis of the DIGISOIL project. Report N^0 FP7-DIGISOIL-D5.1:54

Herrmann, J. 1999. A stream restoration study on a small ungauged stream in south central Pennsylvania. Master's Thesis. Shippensburg University, Shippensburg, PA.

Loke, MH. 2000. Electrical imaging surveys for environmental and engineering studies. Date accessed: 01/18/2013. http://www.ceri.memphis.edu/people/bodin/envgeo/Magstuff/PDFs/Loke_2Dnotes.pdf

Lolcama JL, Cohen HA, Tonkin MJ. 2002. Deepe Karst conduits, flooding, and sinkholes: lessons for the aggregates industry. *Engineering Geology*. 65. 151-157

Mahmoudi AE, & Gabr A. 2009 Geophysical surveys to investigate the relation between Quaternary Nile channels and the Messinian Nile Canyon at East Nile Delta, Egypt. *Arabian Journal of Geosciences*. 2(1):53-67

Marine Geoscience Data System. 2013. Global Multi-Resolution Topography Data Grid Version 2.4. Columbia University. Date Accessed: 7/29/2013. http://www.geomapapp.org/

National Cooperative Soil Survey. Date Accessed: 7/27/2011 U.S.A. https://soilseries.sc.egov.usda.gov/OSD_Docs/M/MONONGAHELA.html https://soilseries.sc.egov.usda.gov/OSD_Docs/M/MELVIN.html

Novo A, Vincent ML, and Levy TE.2012. Geophysical surveys at Khirbat Faynan, an ancient mound site in southern Jordan. *International Journal of Geophysics*. 2012(432823): 1-8

Nyquist J, Peake JS, Roth MJS. 2007. Comparison of an optimized resistivity array with dipole-dipole soundings in karst terrain. *Geophysics*. 72 (4): 139-144.

Nyquist JE, Freyer PA, and Toran L. 2008. Stream bottom resistivity tomography to map ground water discharge. *Groundwater*. 46(4):561-569

Root SI. 1968. Geology and mineral resources southeastern Franklin County, Pennsylvania. Pennsylvania Geological Survey. Fourth Series. Harrisburg

Root SI. 1977. Geology and Mineral Resources of the Harrisburg West area, Cumberland and York Counties, Pennsylvania. Pennsylvania Geological Survey. Fourth Series. Harrisburg

Root SI. 1981. Map 513: Shippensburg Quadrangle, Pennsylvania. Pennsylvania Geological Survey. Fourth Series. Harrisburg

Rother H, Jol HM, and Schulmeister J. 2007. Stratigraphy and tectonic implications of the Pleistocene valley fill in the Hope Valley, Cantebury, South Island, New Zealand. Geological Society of America. Special Paper 432: Stratigraphic Analysis using GPR. P. 155-167

Ryan, W.B.F., S.M. Carbotte, J.O. Coplan, S. O'Hara, A. Melkonian, R. Arko, R.A. Weissel, V. Ferrini, A. Goodwillie, F. Nitsche, J. Bonczkowski, and R. Zemsky (2009), Global Multi-Resolution Topography synthesis, Geochem. Geophys. Geosyst., 10, Q03014, doi:10.1029/2008GC002332.

Sevon WD. 2000. Map 13, Physiographic Provinces of Pennsylvania. Pennsylvania Geological Survey. DCNR 4th Series

Shultz CH. 1999. The Geology of Pennsylvania. Pennsylvania Geological Survey. Special Publication 1: 256-263

Shah SD, Smith BD, Clark AK, Kress WH.2008. A Multi-Tool Geophysical and Hydrogeological Investigation of a Karst Aquifer System, Cibolo Canyon Development Area, Bexar County, Texas. USGS Scientific Investigations Report 2008-5023

Shippensburg University.2013. Climatology. Date accessed: 2/18/2013. http://webspace.ship.edu/weather/

Stevens CW, Robinson SD. 2007.The internal structure of relict lacustrine deltas, northern New York. Geological Society of America. Special Paper 432: Stratigraphic Analysis using GPR. p. 93-103

Tahun A. 2011. Methods and Materials. Date Accessed: 4/5/2011. http://www.ans-nt.co.cc/2011/01/materials-and-methods.html

USDA. 2009. Web Soil Survey. Date accessed 12:43PM 5/9/2011. http://websoilsurvey.nrcs.usda.gov/app/WebSoilSurvey.aspx

US Environmental Protection Agency. 2011. Resistivity Methods. Last Updated: 11/7/2011. Date accessed: 7/14/2012 http://www.epa.gov/esd/cmb/GeophysicsWebsite/pages/reference/methods/Surface_Geophysical_Methods/Electrical_Methods/Resistivity_Methods.htm

USGS.2013. Shippensburg Quadrangle, Pennsylvania, 7.5 minute series

West Carolina University. 2012. Resistivity. Date Accessed: 8/5/2012 http://www.wcu.edu/9614.asp

Woltemade CJ. 2000. Soils Series for the Burd Run Watershed. Burd Run. Shippensburg University. Date accessed: 01/18/2013 http://www.ship.edu/uploadedImages/Ship/Geo-ESS/BurdRun/soils.jpg

Woltemade CJ, Wood A. 2002 Comprehensive Riparian Restoration Along Burd Run. *Land and Water*. 46(2):27-3

Woltemade CJ.2007. Earth Science 110 Introduction to Geology slides. Shippensburg University. Date Accessed: 4/5/2011. http://webspace.ship.edu/cjwolt/geology/slides/str-sum.htm

Woltemade CJ. 2012. Burd Run watershed: Watershed Description. Shippensburg University. Date accessed: 09/11/2012. http://www.ship.edu/Geo-ESS/BurdRun/Project_Overview/

APPENDIX A

Appendix A: Channel cross-sections of the buried channel prior to restoration (Herrmann 1999)

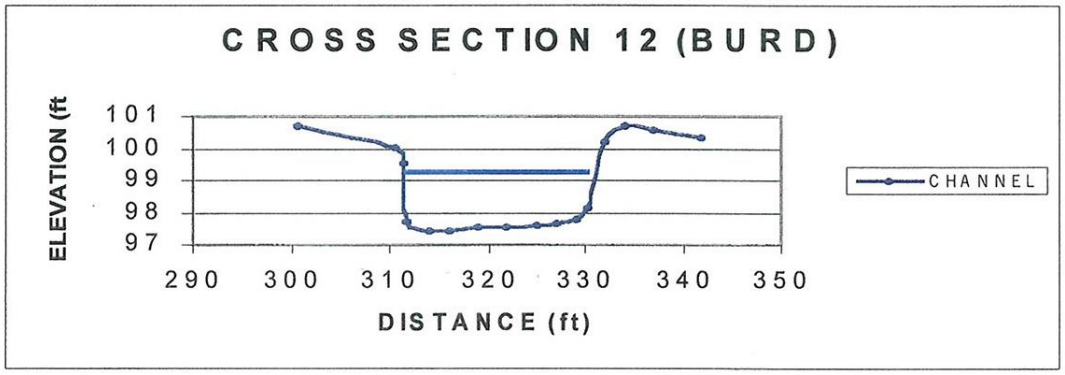

Figure A1: Cross-section 12-Burd Run (Herrmann 1999)

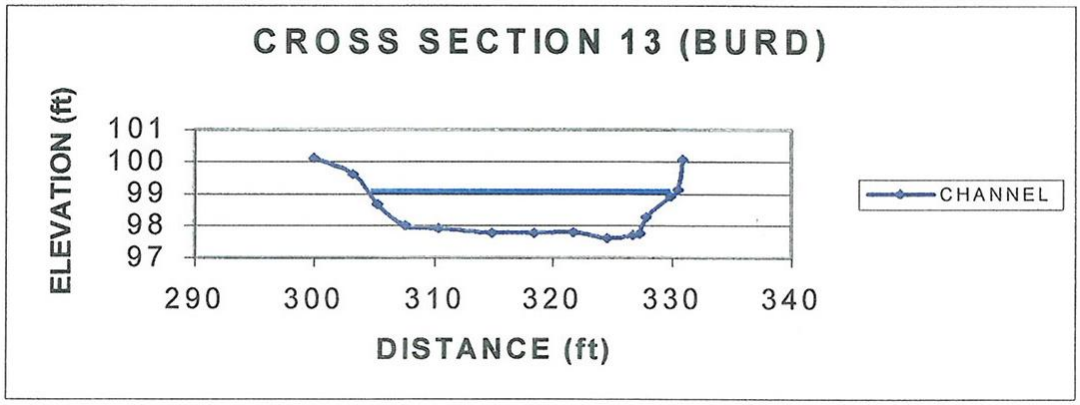

A2: Cross-section 13-Burd Run (Herrmann 1999)

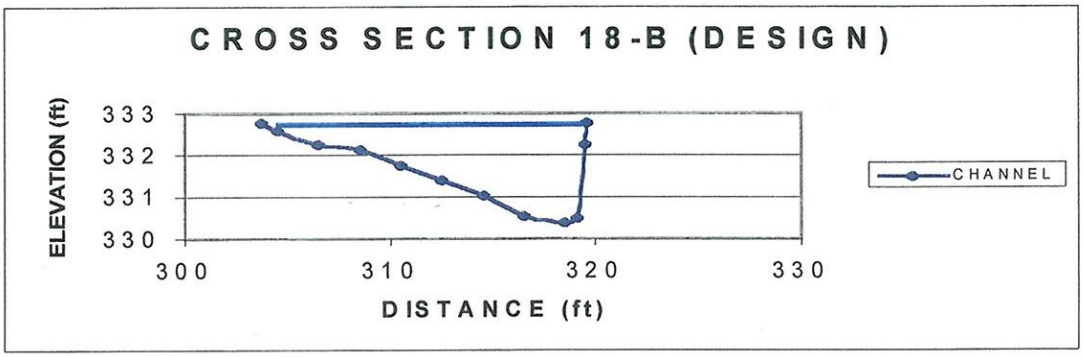

A3: Cross-section 18B-Burd Run (Herrmann 1999)

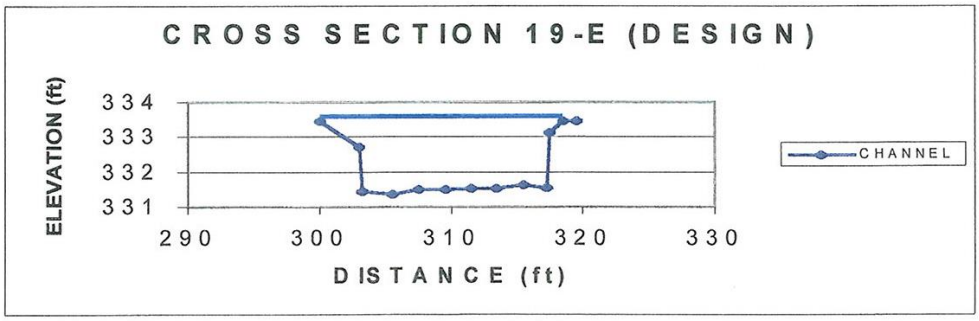

A4: Cross-section 19E-Burd Run (Herrmann 1999)

APPENDIX B

Appendix B: Interpolation methods used with EM data

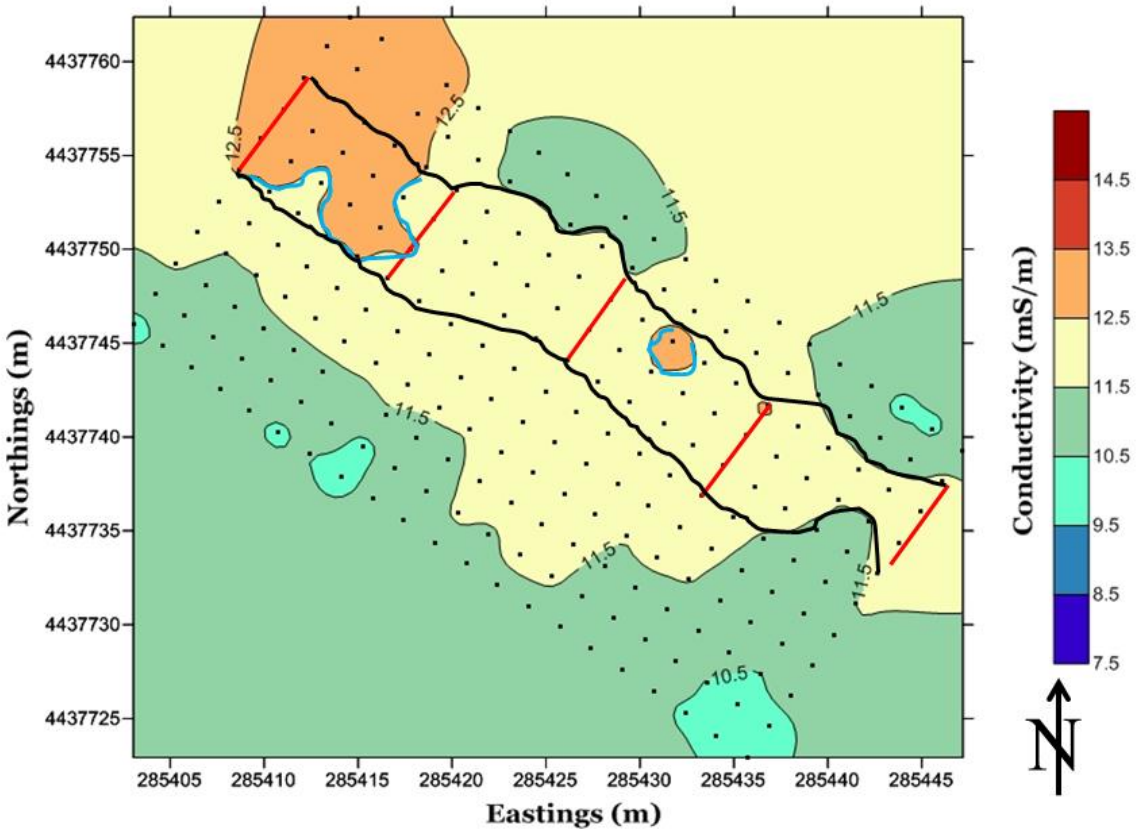

B1: Inverse distance weighted (IDW)

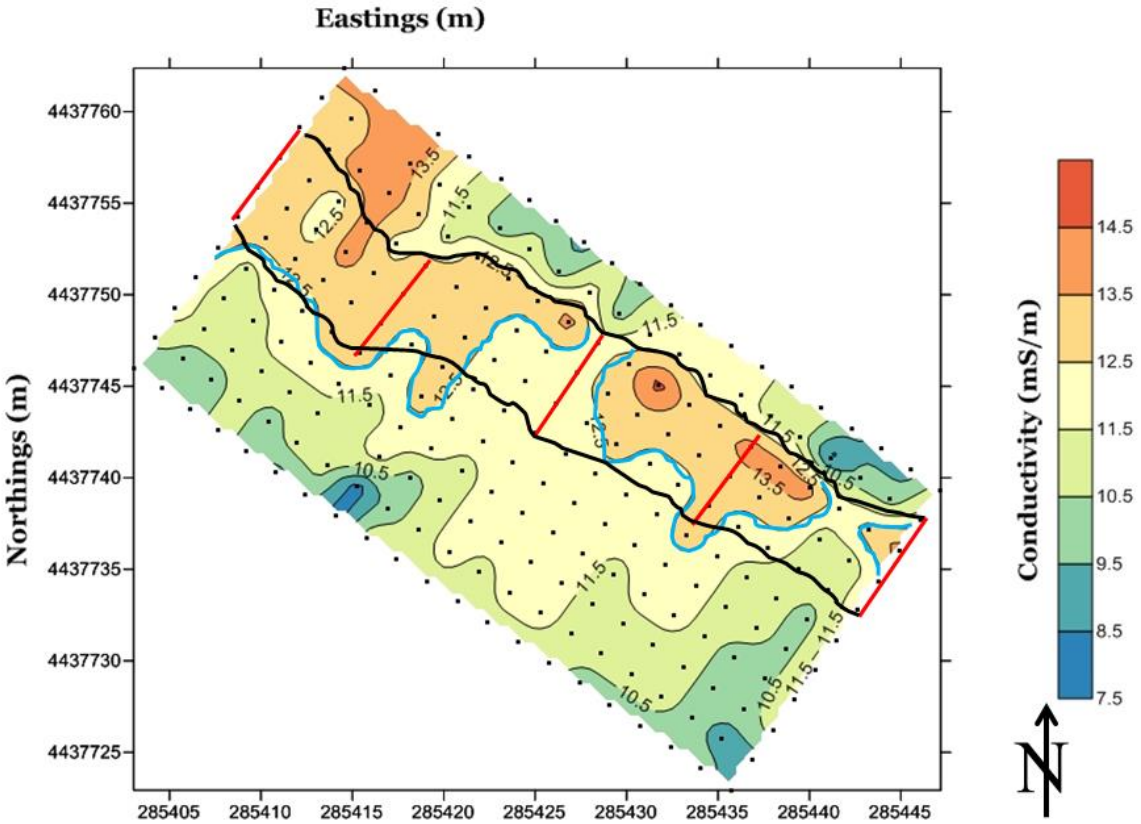

B2: Natural Neighbor

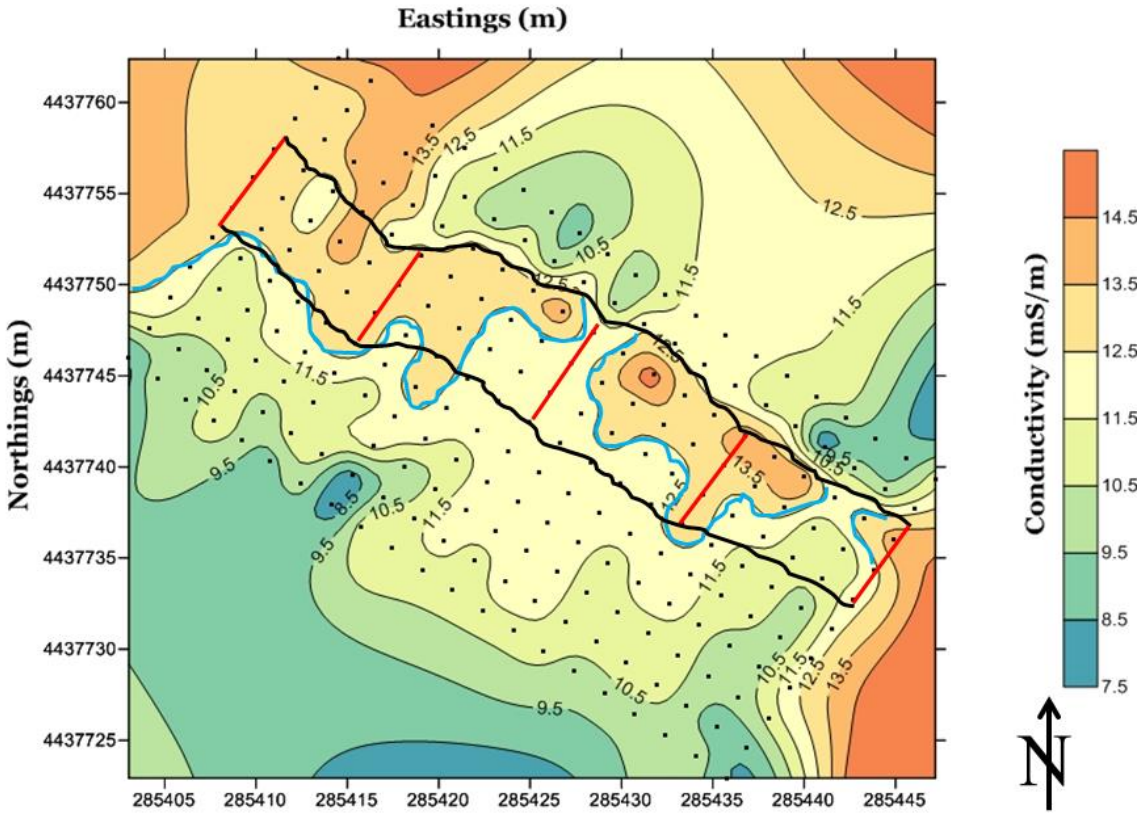

B3 Minimum Curvature

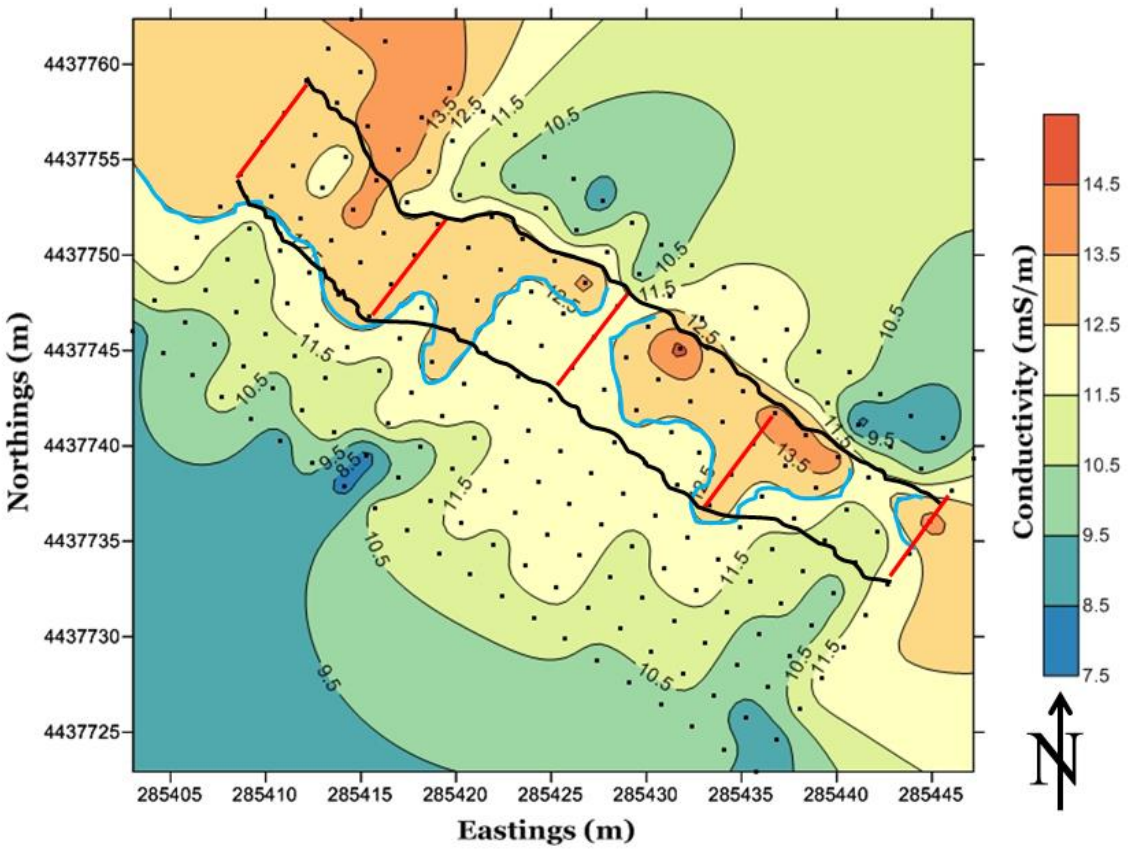
Northings (m)
4437760
4437755
4437750
4437745
4437740
4437735
4437730
4437725
285405
285410
285415
285420
285425
285430
285435
285440
285445
Eastings (m)
Conductivity (mS/m)
14.5
13.5
12.5
11.5
10.5
9.5
8.5
7.5
N

B4: Kriging

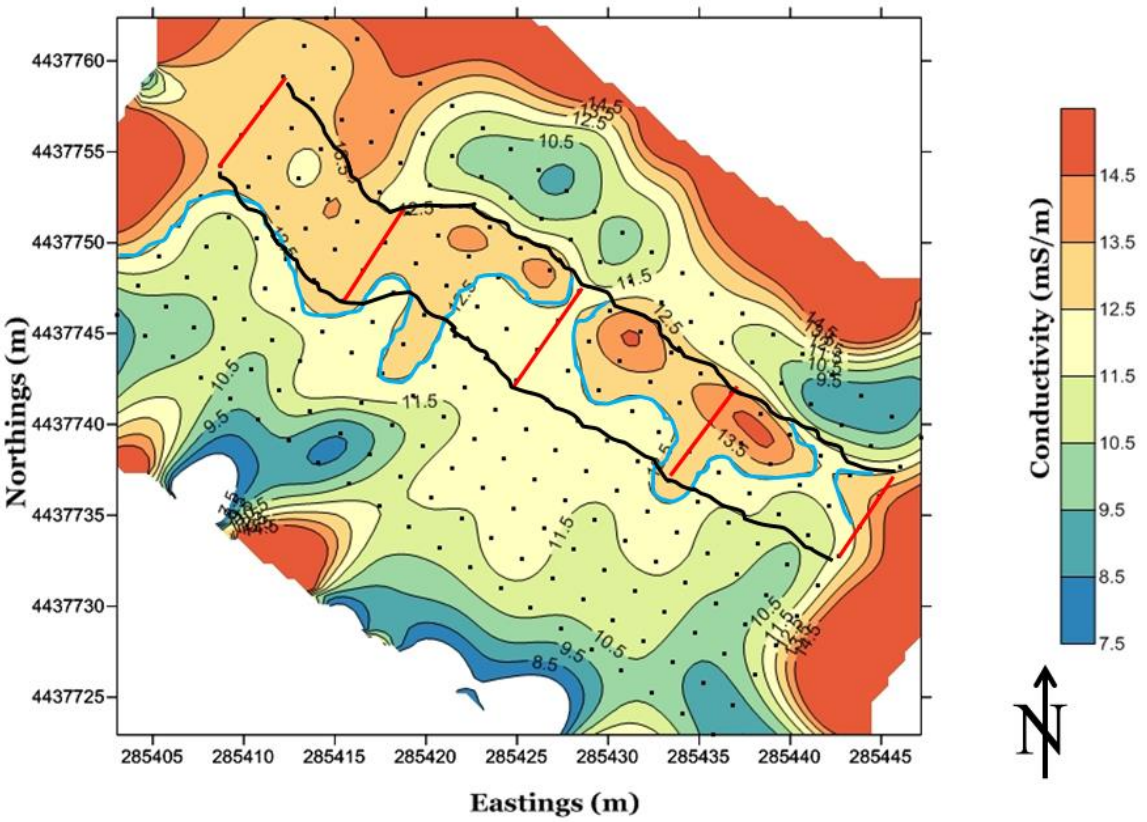

B5: Modified Shepard (Chosen interpolation method)

APPENDIX C

Appendix C: Clean ER & GPR Models

(Models presented in Chapter 5 were drawn on these profiles to facilitate interpretation)

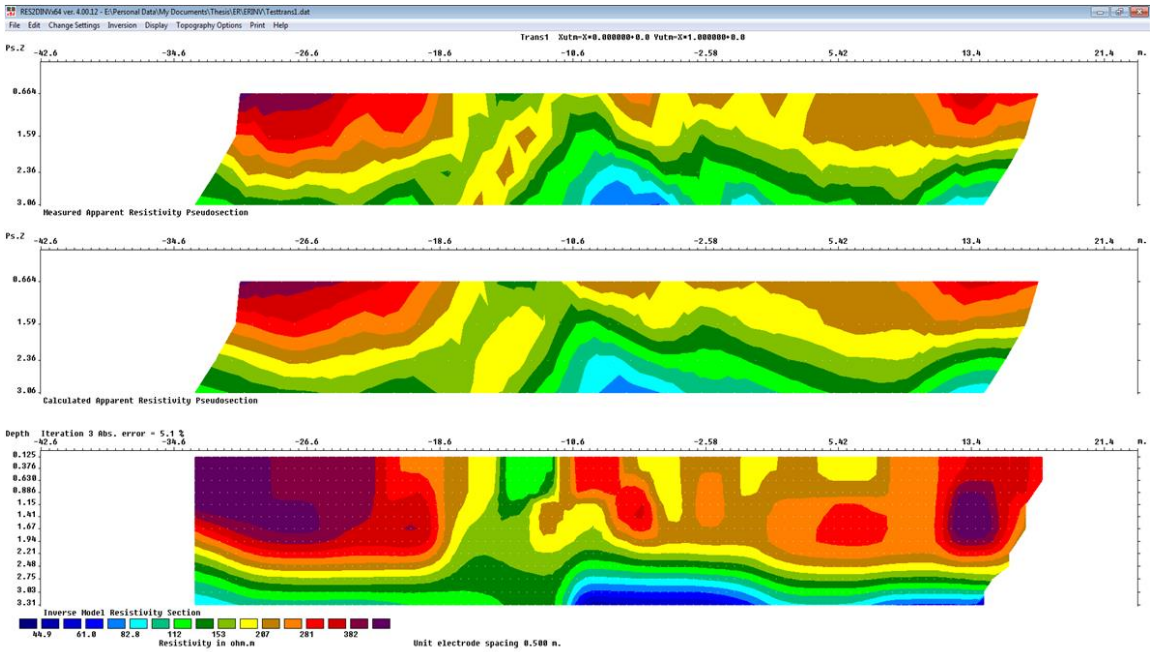

C1: ER Results on Transect 1

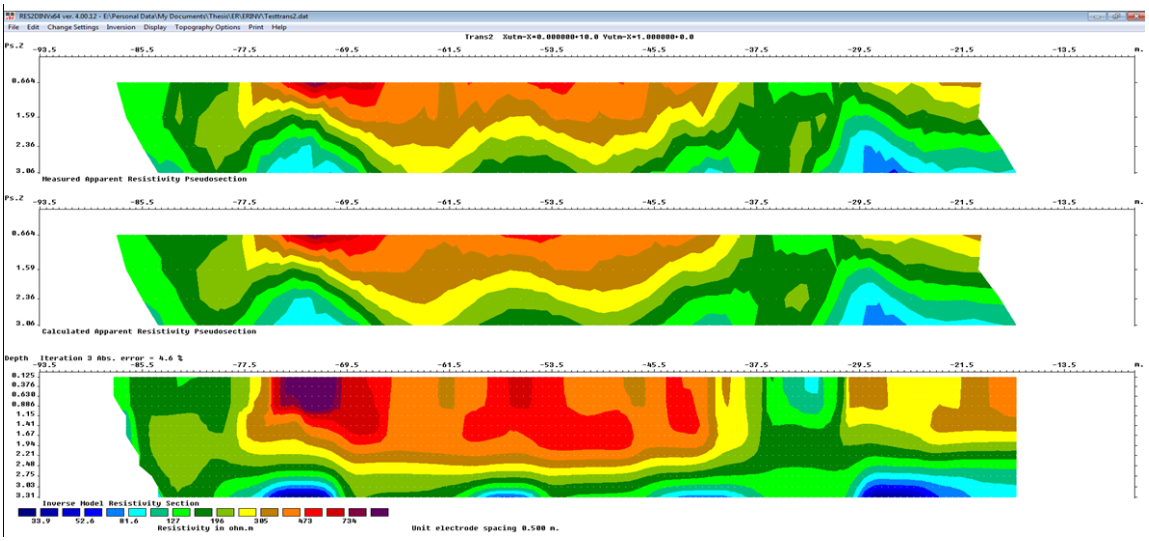

C2: ER Results on Transect 2

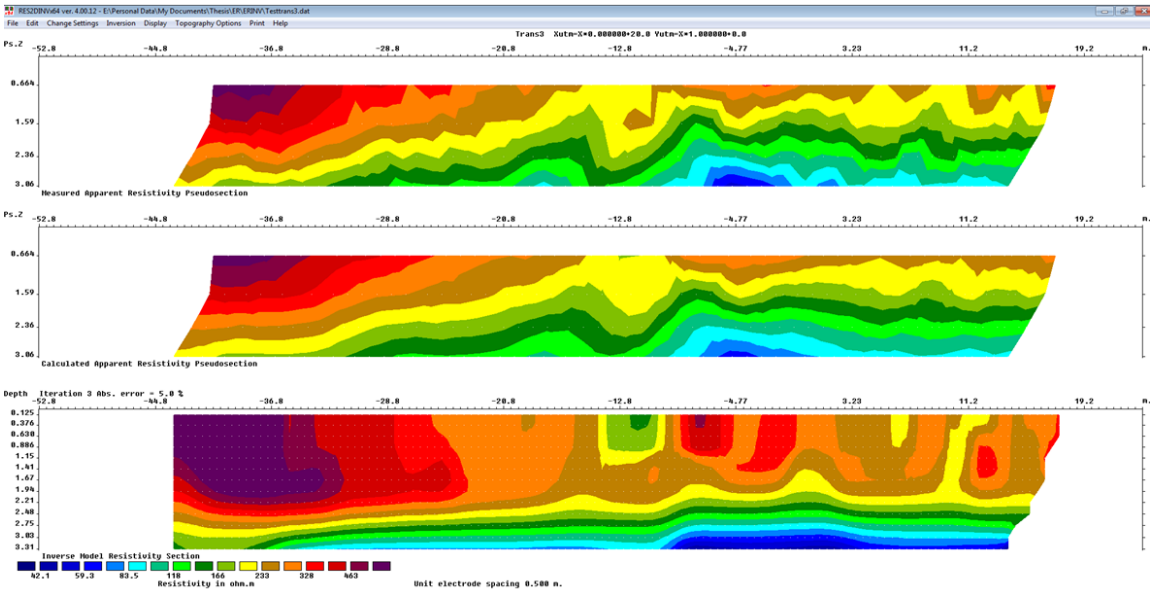

C3: ER Results on Transect 3

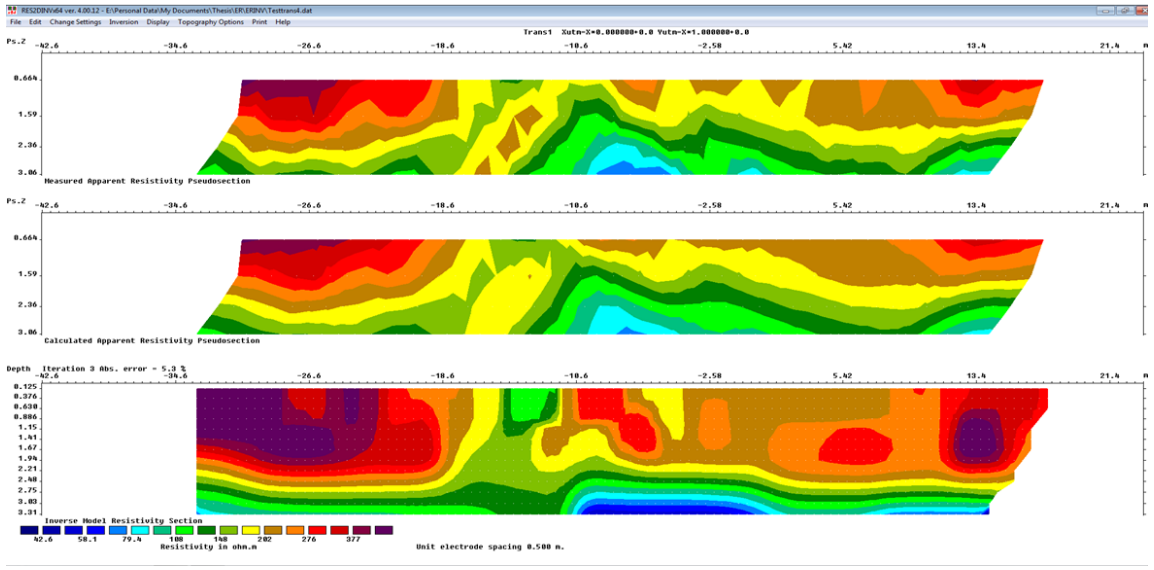

C4: ER Results on Transect 4

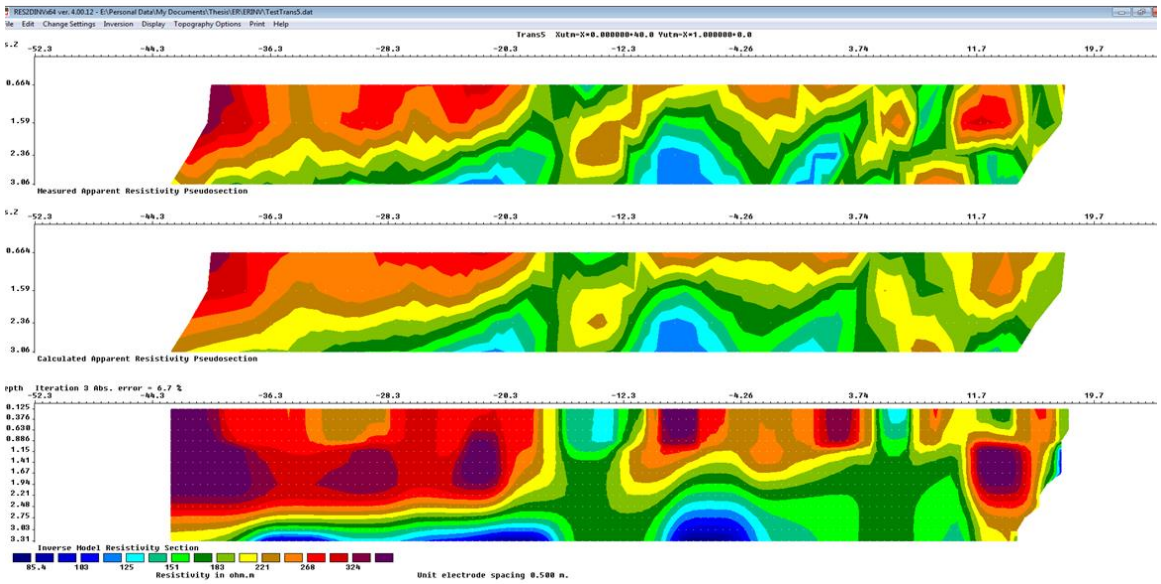

C5: ER Results on Transect 5

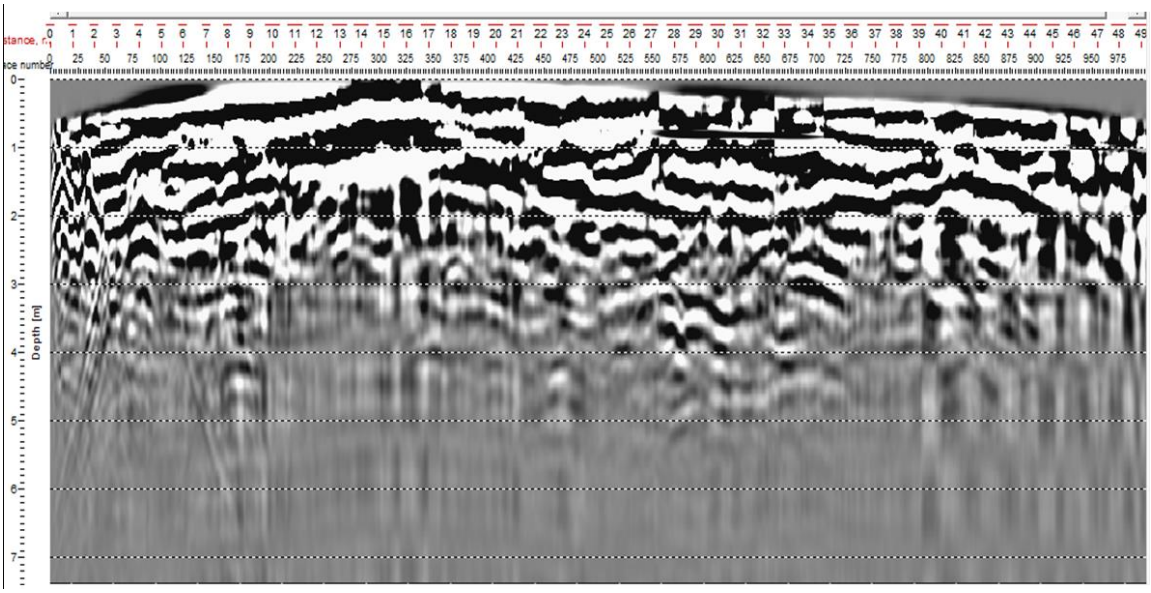

C6: GPR radargram using a 100MHZ antenna along transect 1.

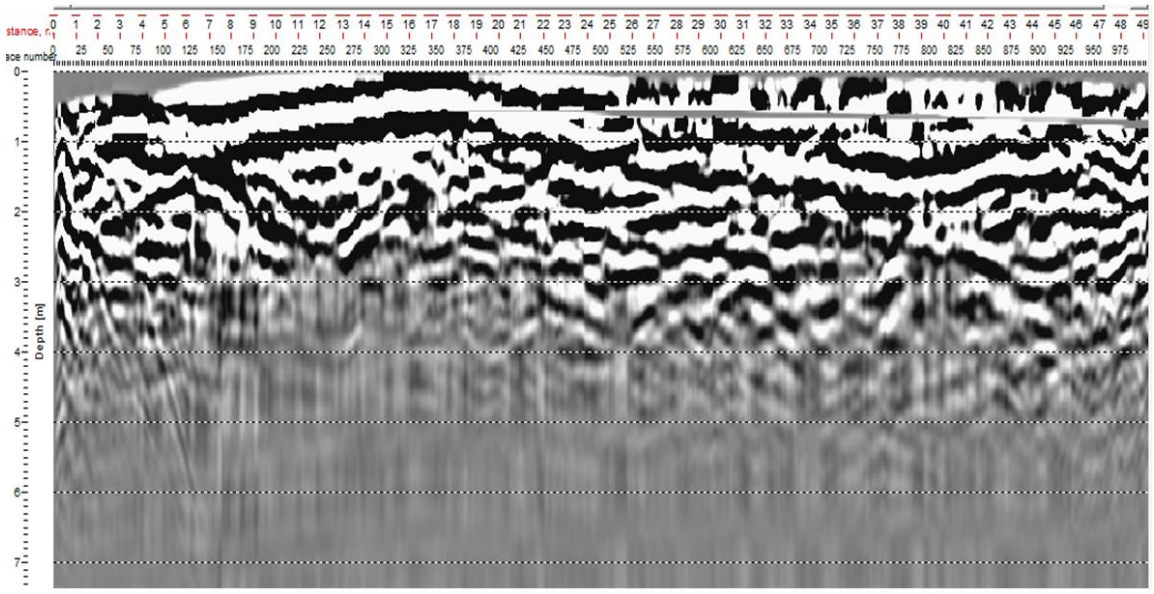

C7: GPR radargram using a 100MHZ antenna along transect 2.

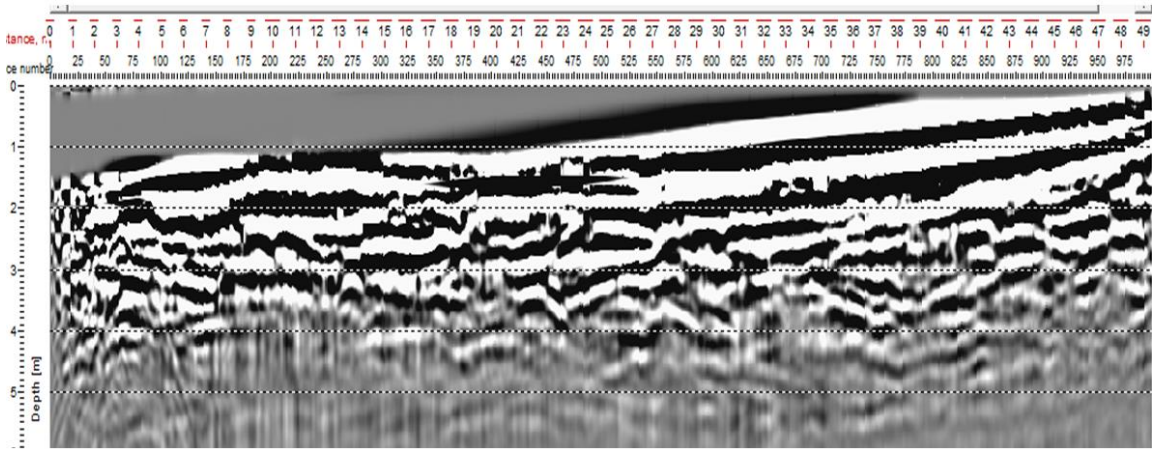

C8: GPR radargram using a 100MHZ antenna along transect 3.

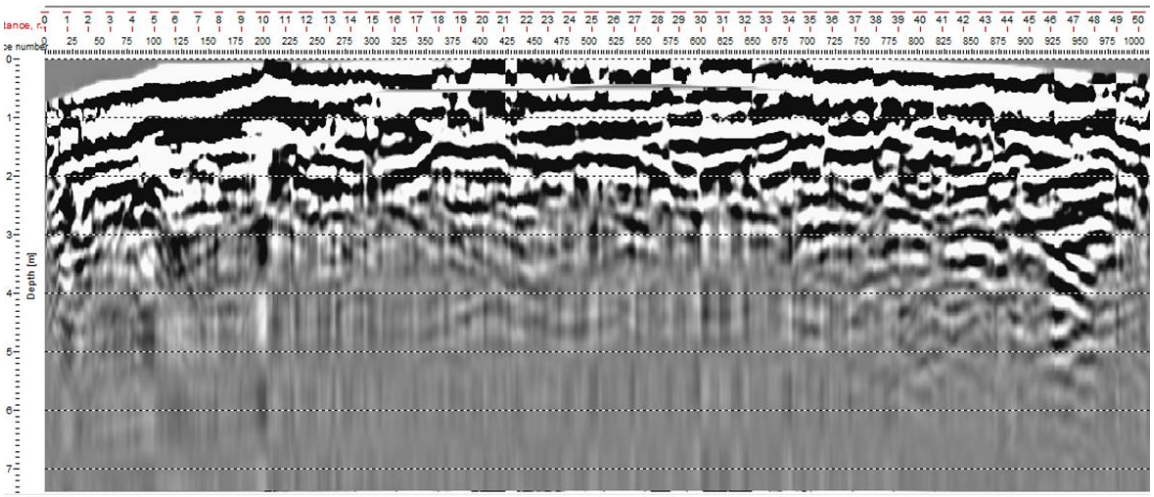

C9: GPR radargram using a 100MHZ antenna along transect 4.

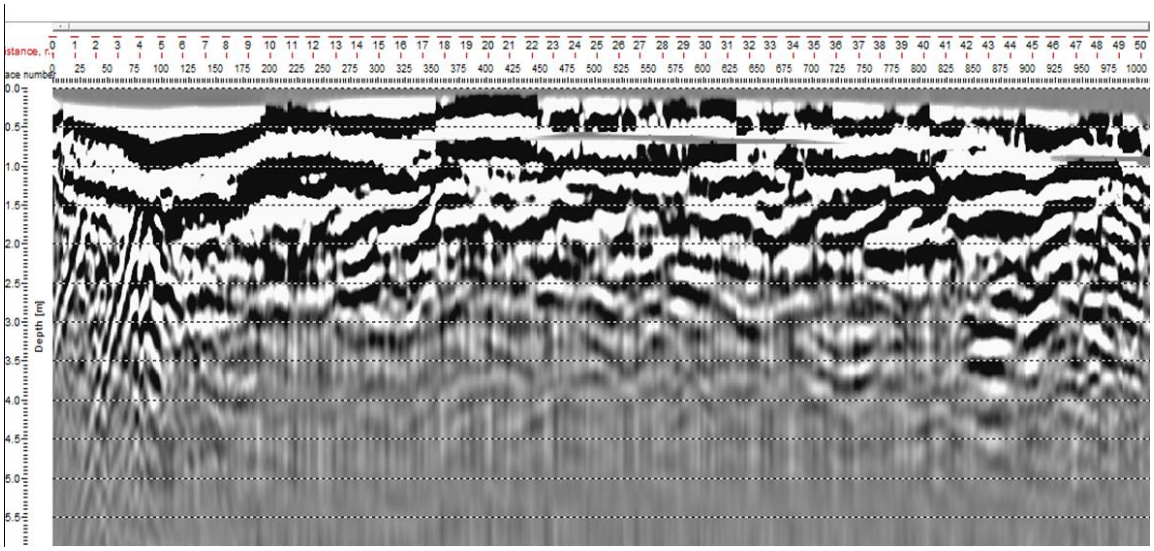

C10: GPR radargram using a 100MHZ antenna along transect 5.

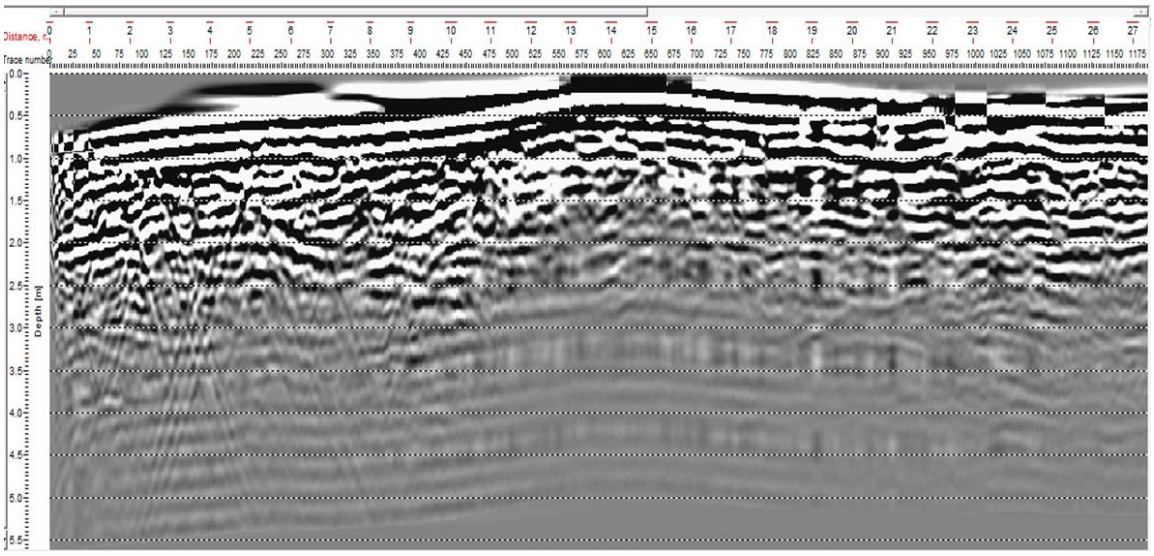

C11: GPR radargram using a 250MHZ antenna along transect 1.

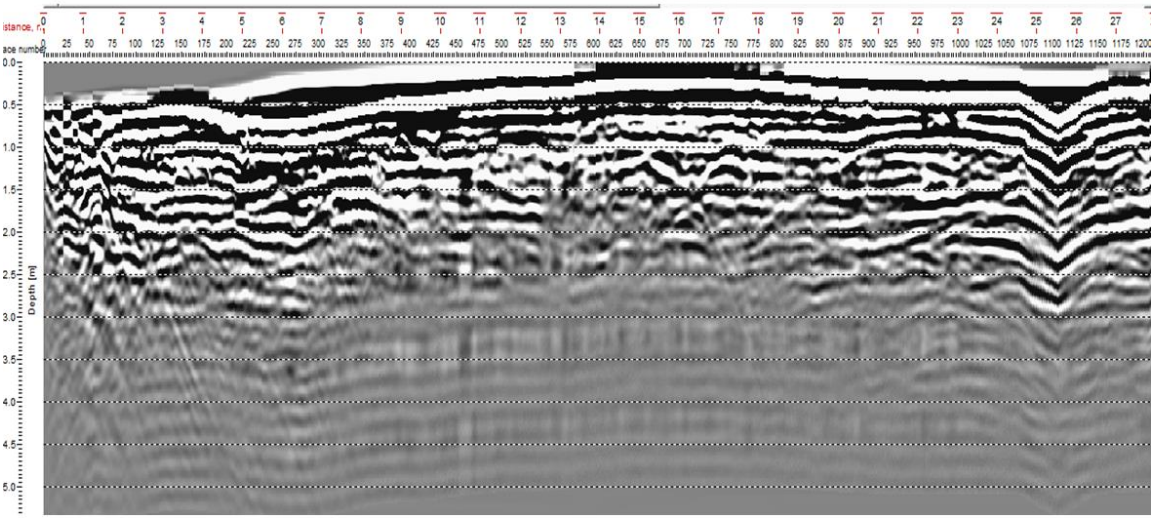

C12: GPR radargram using a 100MHZ antenna along transect 2.

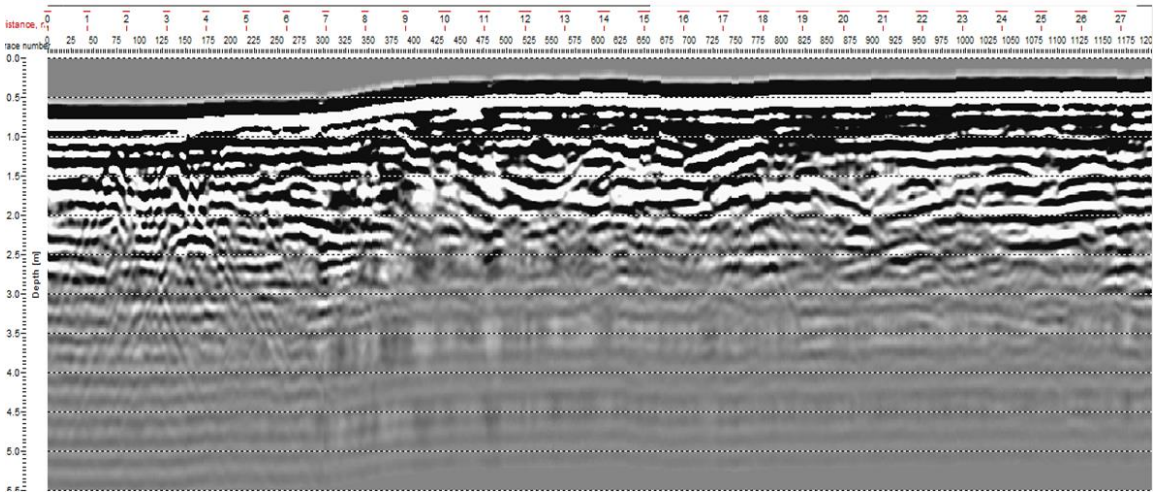

C13: GPR radargram using a 100MHZ antenna along transect 3.

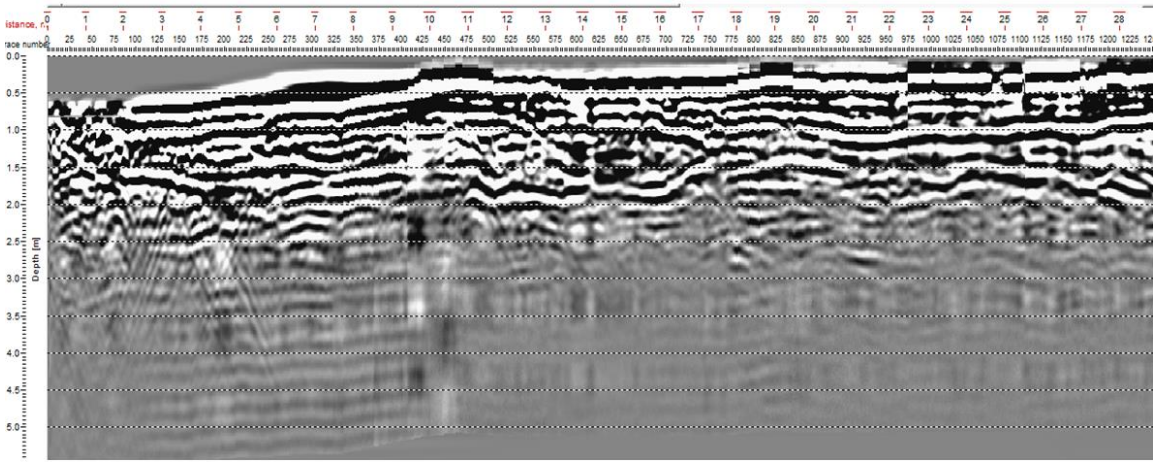

C14: GPR radargram using a 100MHZ antenna along transect 4.

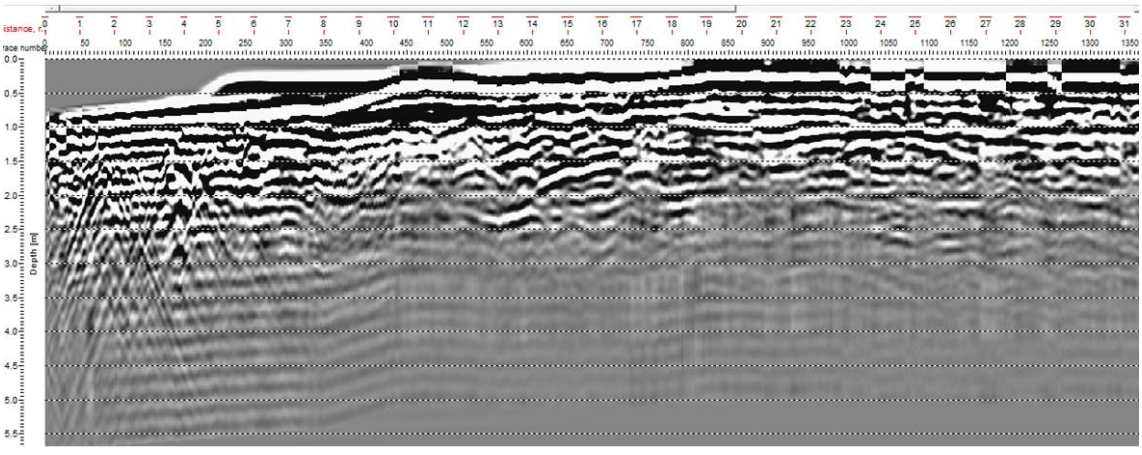

C15: GPR radargram using a 100MHZ antenna along transect 5.

APPENDIX D

Appendix D: Channel Comparison

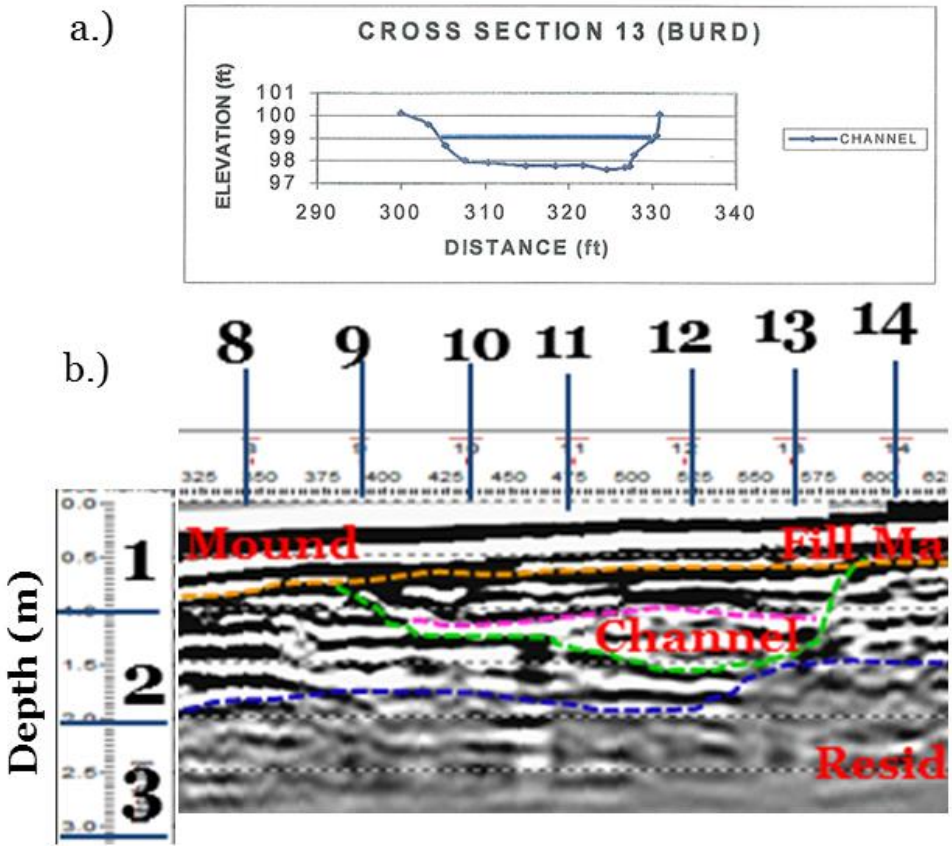

D1: A comparison in shape between a.) cross-section 13 (Herrmann 1999) and the channel anomaly in the 250 MHz radargram in transect 2.

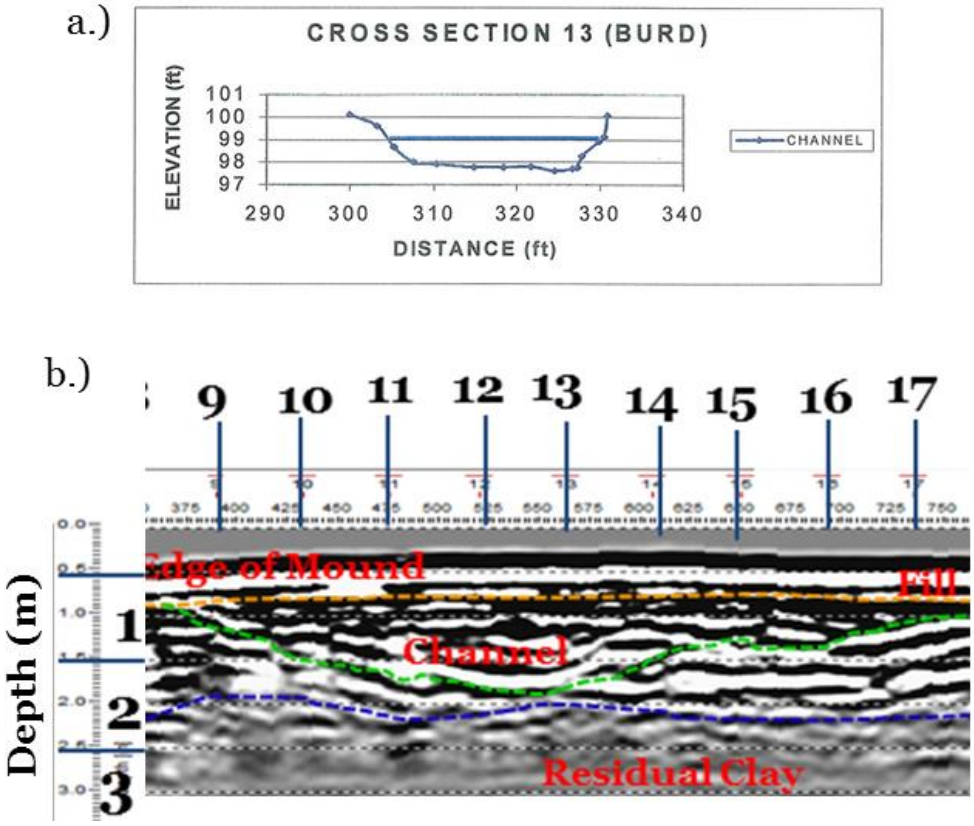

D2: A comparison in shape between a.) cross-section 13 (Herrmann 1999) and the channel anomaly in the 250 MHz radargram in transect 3.

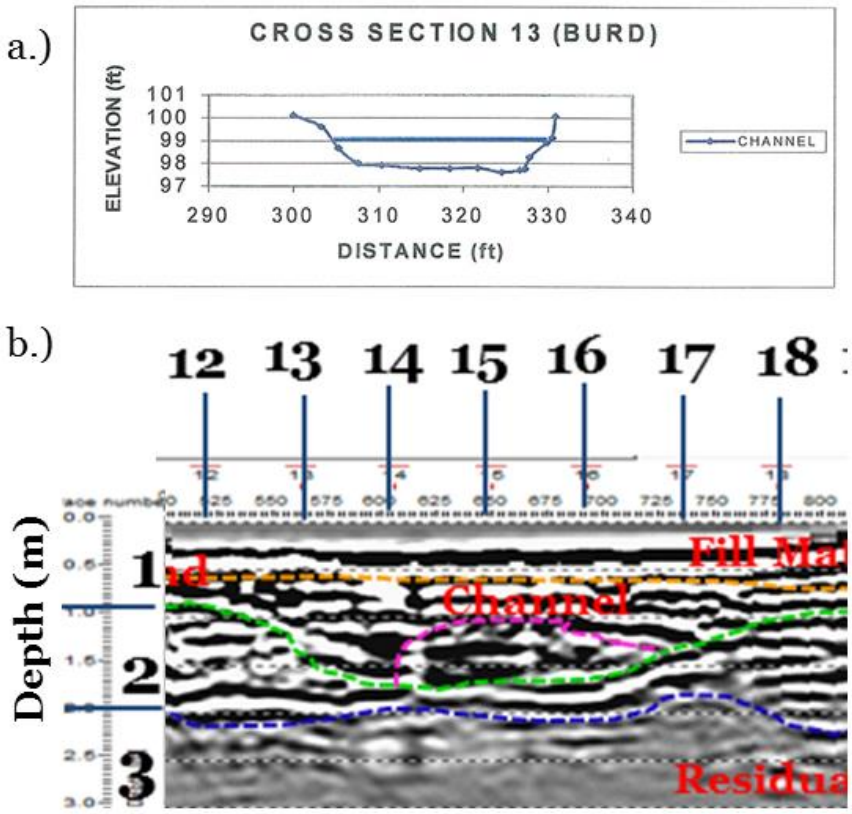

D3: A comparison in shape between a.) cross-section 13 (Herrmann 1999) and the channel anomaly in the 250 MHz radargram in transect 4.

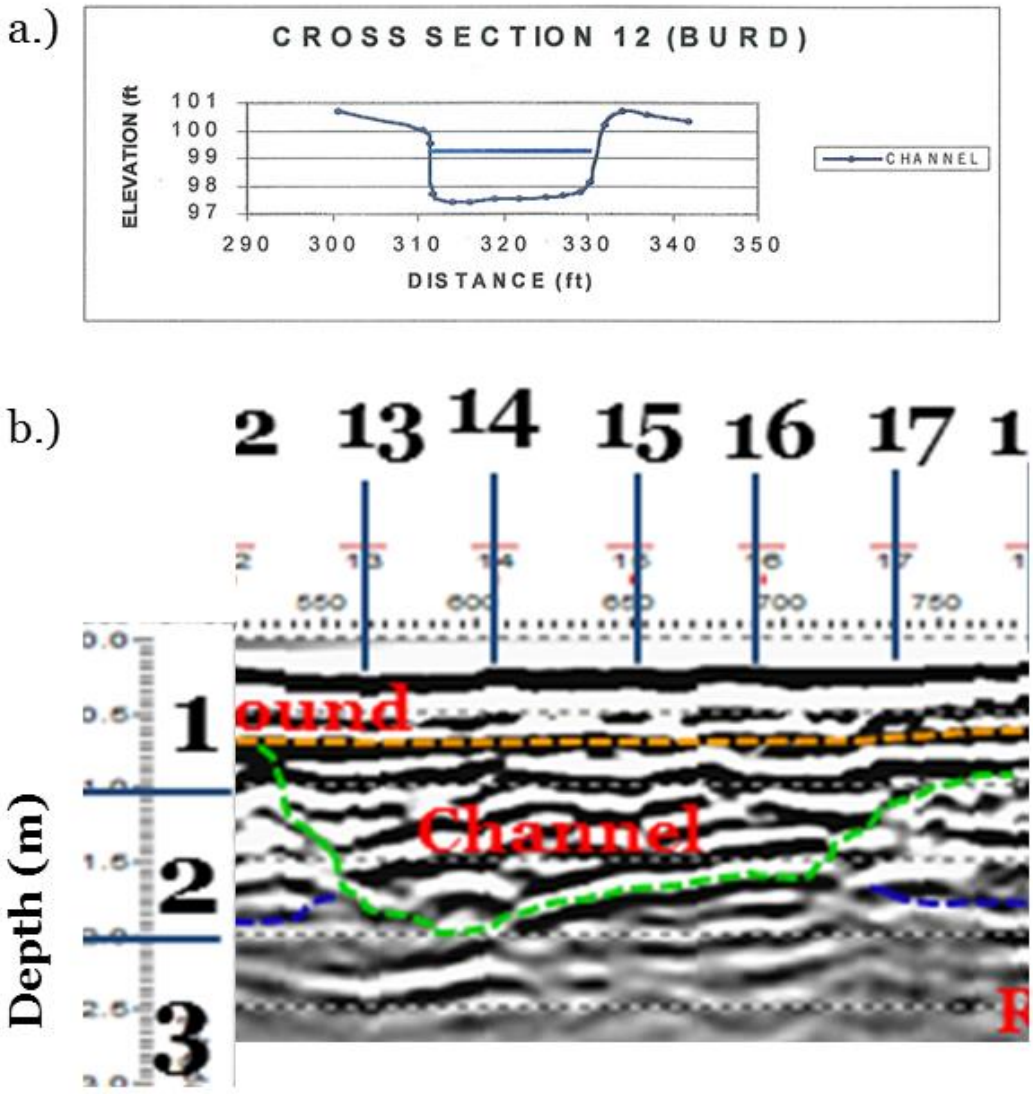

D4: A comparison in shape between a.) cross-section 12 (Herrmann 1999) and the channel anomaly in the 250 MHz radargram in transect 5.

APPENDIX E

Appendix E: Integrated Results

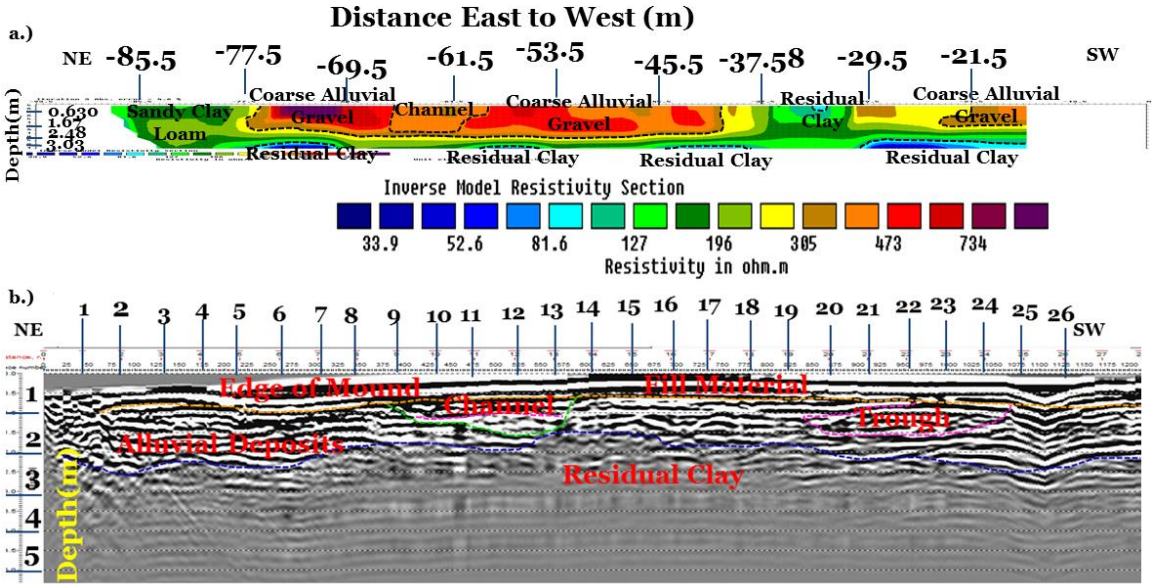

E1: A comparison of interpreted results of a.) the final resistivity model and b.) 250 MHz GPR antenna for transect 2.

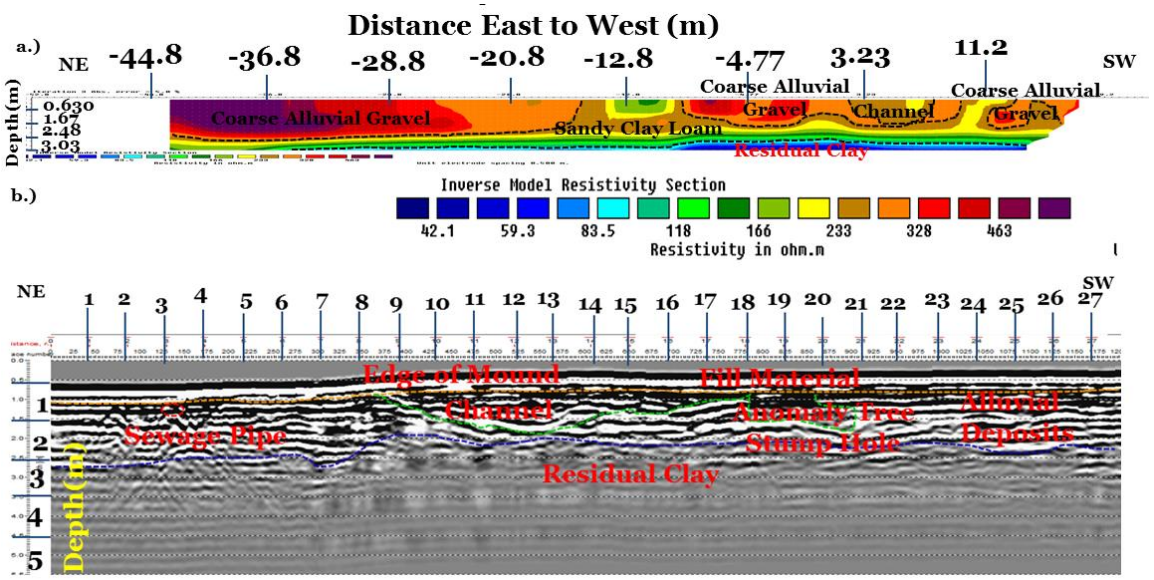

E2: A comparison of interpreted results of a.) the final resistivity model and b.) 250 MHz GPR antenna for transect 3.

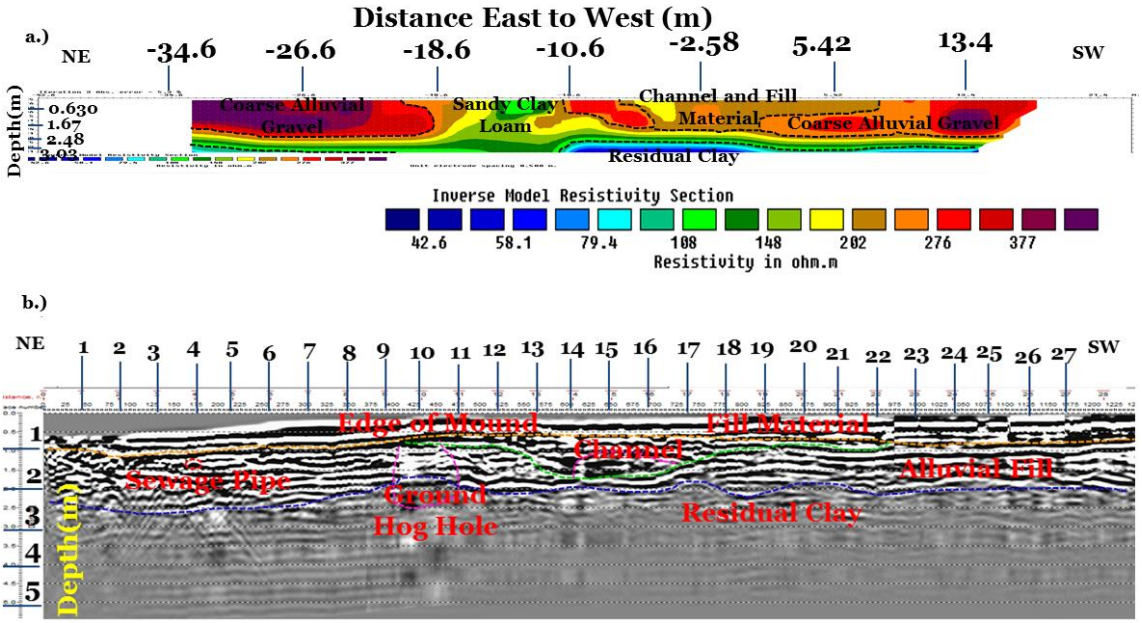

E3: A comparison of interpreted results of a.) the final resistivity model and b.) 250 MHz GPR antenna for transect 4.

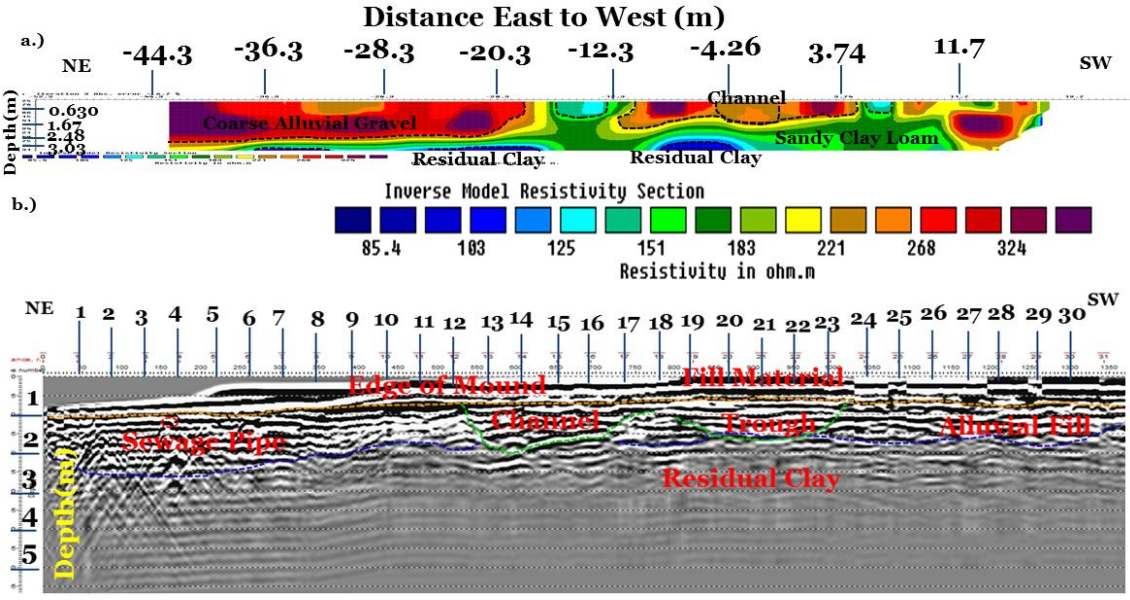

E4: A comparison of interpreted results of a.) the final resistivity model and b.) 250 MHz GPR antenna for transect 5.

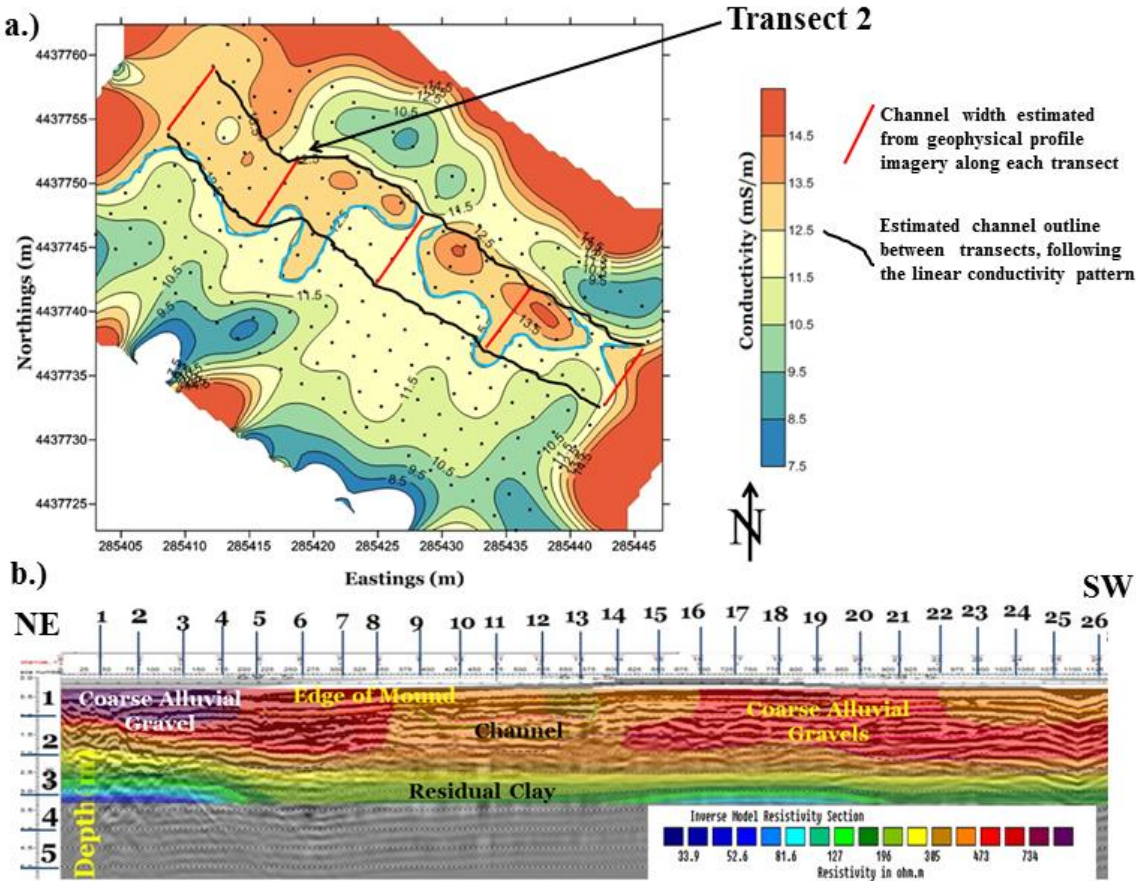

E5: A comparison of the results from a.) EM, and b.) ER and GPR (250 MHz antenna) for transect 2.

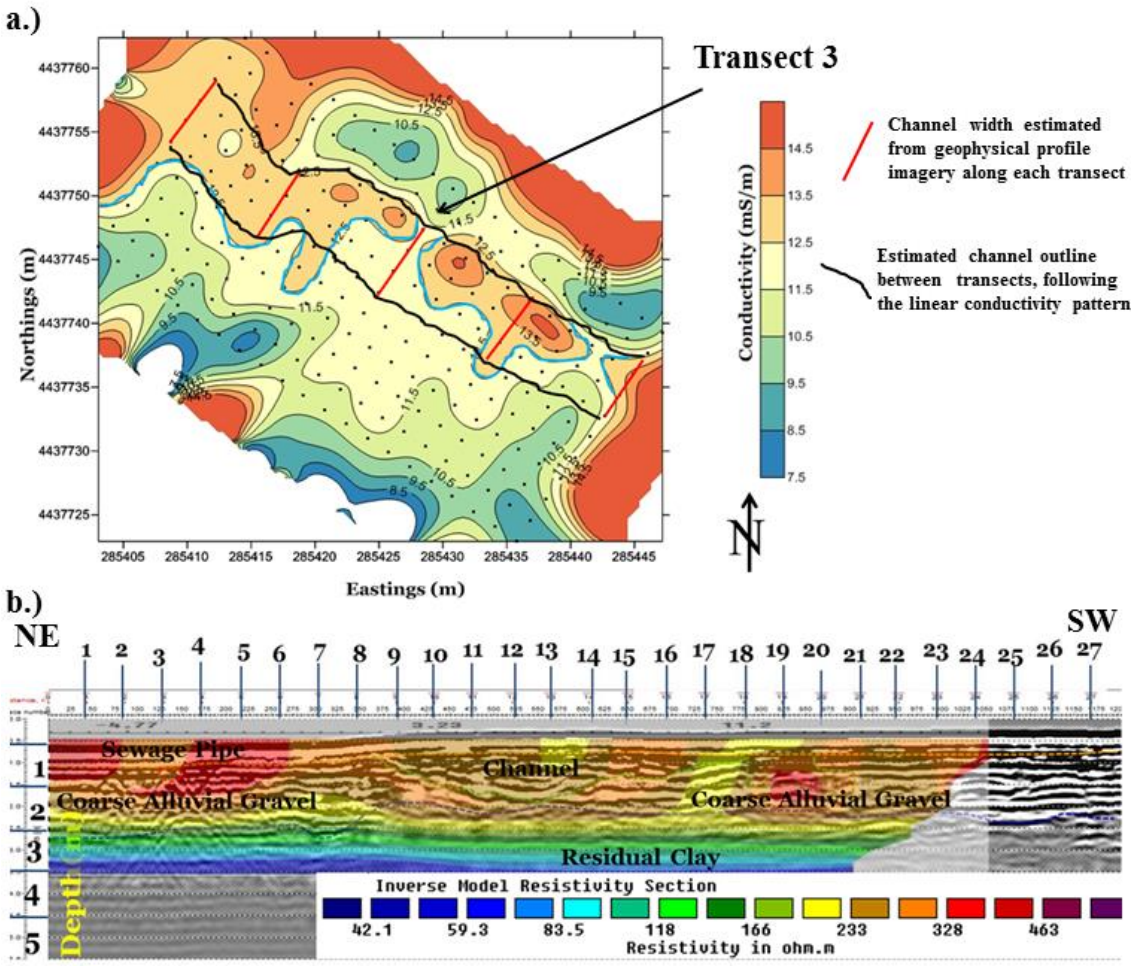

E6: A comparison of the results from a.) EM, and b.) ER and GPR (250 MHz antenna) for transect 3.

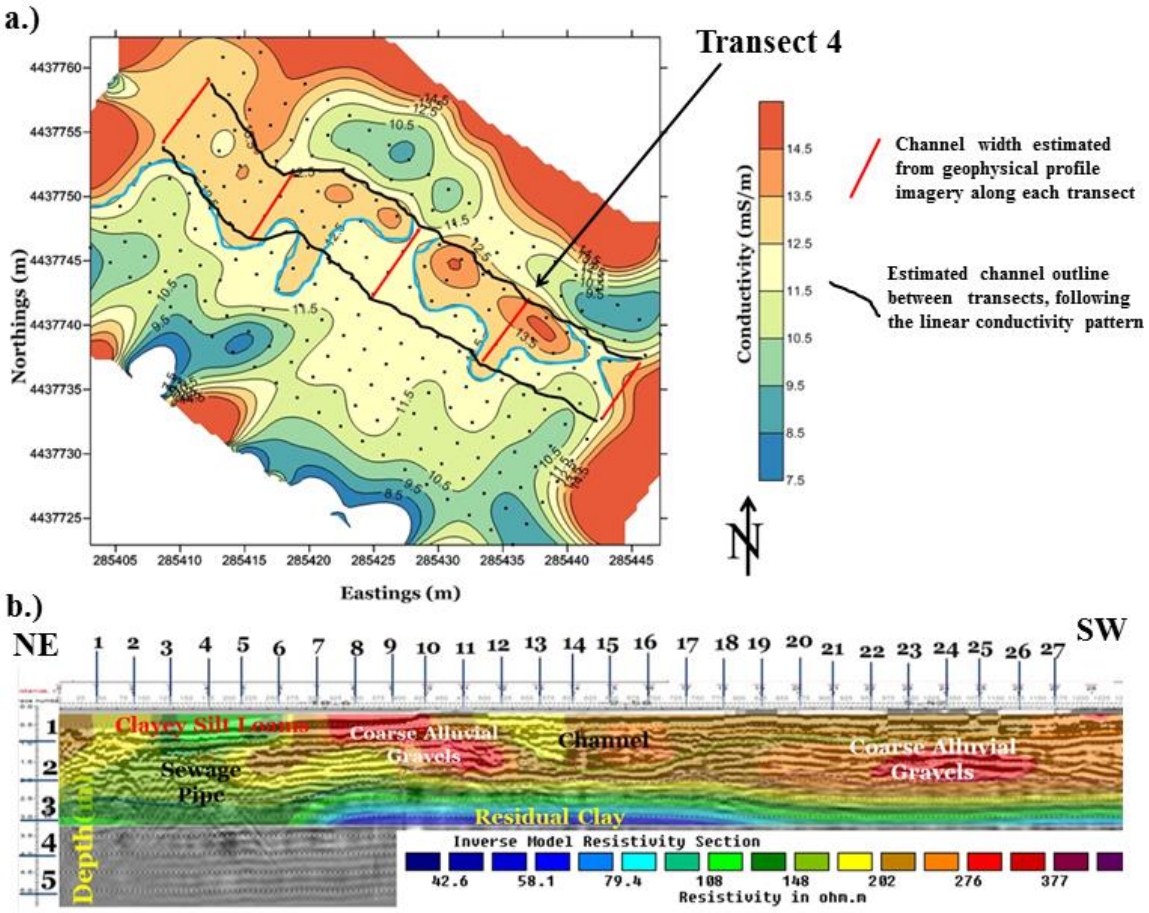

E7: A comparison of the results from a.) EM, and b.) ER and GPR (250 MHz antenna) for transect 4.

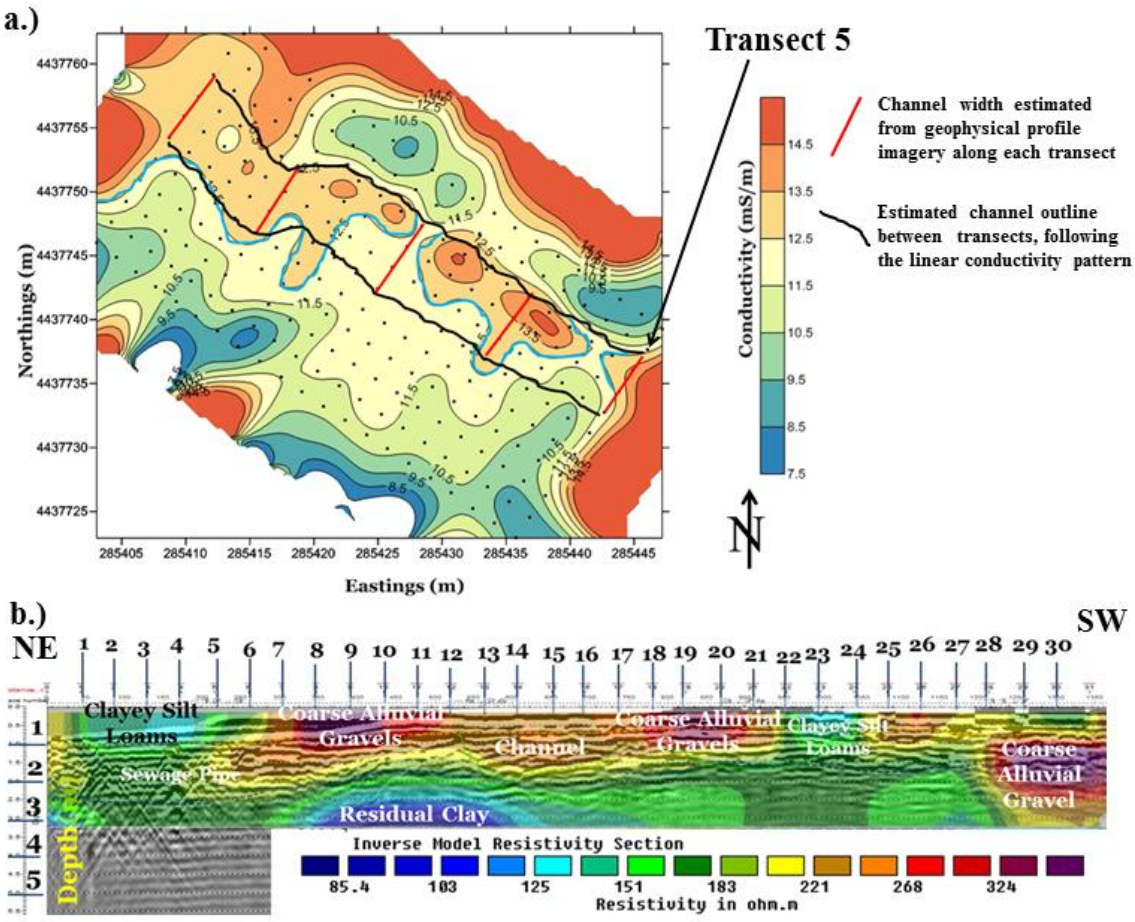

E7: A comparison of the results from a.) EM, and b.) ER and GPR (250 MHz antenna) for transect 4.